Quantum Phases and Phase Transitions In Disordered Low-Dimensional Systems: Thin Film Superconductors, Bilayer Two-dimensional Electron Systems, And One-dimensional Optical Lattices

Thesis by

Yue Zou

In Partial Fulfillment of the Requirements

for the Degree of

Doctor of Philosophy

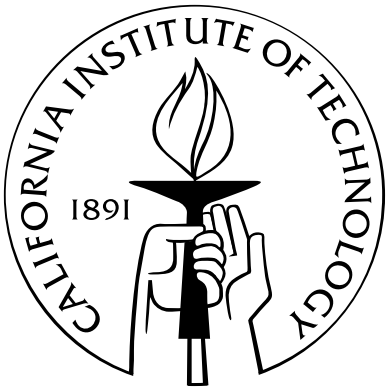

California Institute of Technology

Pasadena, California

2011

(Submitted 2010)

In memory of my grandfather

Acknowledgments

I would like to express my deep gratitude to my advisor Gil Refael. I always consider myself extremely lucky to have him as my advisor, who is more than an advisor but also my role model and personal good friend. I want to thank him for his amazing insights in physics, his encouragement and inspiration, and his patient guidance and support. I would also like to thank many professors I have interactions with: Jim Eisenstein, Ady Stern, and Jongsoo Yoon, for all the exciting and fruitful collaborations; Nai-Chang Yeh and Alexei Kitaev, for many insightful conversations and generous help I received from them; Olexei Motrunich and Matthew Fisher, for many eye-opening discussions and comments. I enjoyed very much working closely with Israel Klich and Ryan Barnett on Chapter 2 and 5 of this thesis during their stay at Caltech. I would also like to thank Waheb Bishara, for being my academic big brother and personal good friend. I also had the privilege to discuss and interact with many great scientists here at Caltech: Jason Alicea, Doron Bergman, Gregory Fiete, Karol Gregor, Oleg Kogan, Tami Pereg-Barnea, Heywood Tam, Jing Xia, and Ke Xu, among others.

I am most grateful to my parents, for their unconditional support for me; and to Zhao, for her consistent love and patience, without which I could not have made it today.

Abstract

The study of various quantum phases and the phase transitions between them in low-dimensional disordered systems has been a central theme of recent developments of condensed matter physics. Examples include disordered thin film superconductors, whose critical temperature and density of states can be affected by a normal metallic layer deposited on top of them; amorphous thin films exhibiting superconductor-insulator transitions (SIT) tuned by disorder or magnetic field; and bilayer two-dimensional electron systems at total filling factor $\nu = 1$, which exhibit interlayer coherent quantum Hall state at small layer separation and have a phase transition tuned by layer separation, parallel magnetic field, density imbalance, or temperature. Although a lot of theoretical and experimental investigations have been done, many properties of these phases and natures of the phase transitions in these systems are still being debated. Here in this thesis, we report our progress towards a better understanding of these systems. For disordered thin film superconductors, we first propose that the experimentally observed lower-than-theory gap-T_c ratio in bilayer superconducting-normal-metal films is due to inhomogeneous couplings. Next, for films demonstrating superconductor-insulator transitions, we propose a new type of experiment, namely the drag resistance measurement, as a method capable of pointing to the correct theory among major candidates such as the quantum vortex picture and the percolation picture. For bilayer two-dimensional electron systems, we propose that a first-order phase transition scenario and the resulting Clausius-Clapeyron equations can describe various transitions observed in experiments quite well. Finally, in one-dimensional optical lattices, we show that one can engineer the long-sought-after random hopping model with only off-diagonal disorder by fast-modulating an

Anderson insulator.

Contents

Acknowledgments **iv**

Abstract **v**

Contents **vii**

1 Introduction **1**

1.1 Superconductivity primer 1

1.2 Phase fluctuations and superconductor-insulator transitions (SITs) . . 4

1.3 Vortex-boson duality 7

1.4 Overview of our work on thin film superconductors 10

1.5 From superconductivity to quantum Hall effect 14

1.6 Bilayer quantum Hall effect: a hidden superfluid 19

1.7 Half-filled Landau level: a hidden Fermi liquid 23

1.8 Overview of our work on bilayer quantum Hall systems 25

1.9 One-dimensional random hopping model 26

1.10 Realizing random hopping model with dynamical localization 28

2 Effect of Inhomogeneous Coupling On BCS Superconductors **31**

2.1 Introduction 31

2.2 The gap equation of a nonuniform film 33

2.3 The case of inhomogeneous pairing 35

2.4 Superconductor-normal-metal (SN) superlattice analogy 49

2.5 Summary and discussion 50

Appendix 2.A Calculation of $\Delta_{(T=0)}$ in the limit $Q\xi \gg 1$ 55

3 Drag Resistance in Thin Film Superconductors 57

3.1 Introduction 57

3.2 Drag resistance in the quantum vortex paradigm 60

3.3 Drag resistance in the percolation picture 72

3.4 Discussion on the drag resistance in the phase glass theory 76

3.5 Summary and discussion 77

Appendix 3.A The determination of the vortex mass 80

Appendix 3.B Field theory derivation of the vortex interaction potentials 86

Appendix 3.C Classical derivation of the vortex interaction potential . . . 90

Appendix 3.D Hard-disc liquid description of the vortex metal phase . . . 93

Appendix 3.E Coulomb Drag for disordered electron glass 97

Appendix 3.F No drag resistance for a genuine superconductor 99

4 First Order Phase Transitions in Bilayer Quantum Hall Systems 102

4.1 Introduction 102

4.2 Spin transition experiments 104

4.3 Finite temperature transition experiments 108

4.4 Density imbalance experiments 112

4.5 Summary and discussion 118

Appendix 4.A Temperature dependence of the incoherent phase free energy 122

Appendix 4.B Density imbalance dependence of the incoherent phase free energy 125

5 Achieving Random Hopping Model In Optical Lattices 129

5.1 Introduction 129

5.2 Computation of the density of states and the localization length . . . 130

5.3 Effective Hamiltonian in the fast oscillation limit 133

5.4 Numerical results 134

5.5 Discussions on experimental feasibility 138

Bibliography **140**

Chapter 1

Introduction

1.1 Superconductivity primer

Superconductivity was first discovered almost 100 years ago by Onnes[1], when he cooled down various metals such as mercury, tin, and lead, and observed that the electric resistance completely disappeared under a certain temperature. Other phenomena of superconductivity, such as perfect diamagnetism, were also observed subsequently[2]. However, the microscopic theory for superconductivity, the BCS theory[3, 4], only emerged half a century later. Based on simple principles, the BCS theory gives a surprisingly good description of various properties of conventional superconductors, and it remains a paradigm in our understandings of various phenomena in condensed matter physics. Modern renormalization group theory has also demonstrated that BCS pairing instability is actually the only instability of a Fermi liquid with non-nesting Fermi surface[5]. The status of the BCS theory is challenged after the discovery of cuprate[6, 7] and iron-based high-temperature superconductors[8], but it still serves as a good starting point to understand these unconventional superconductors.

The intuitive picture of the BCS theory is that in a superconductor, electrons with opposite spins and momenta near the Fermi surface pair up to form an object called "Cooper pair". Formed by two fermions, a Cooper pair is approximately a boson, which can Bose-Einstein condense and flow dissipationlessly. The starting point of

the BCS theory is the following Hamiltonian

$$H = \int_r \sum_{s=\uparrow,\downarrow} \psi_s^\dagger \left(-\frac{\nabla^2}{2m}\right) \psi_s - U\psi_\downarrow^\dagger \psi_\uparrow^\dagger \psi_\uparrow \psi_\downarrow, \tag{1.1}$$

where ψ_s is the electron field operator with spin-s, and $U > 0$ represents an attractive interaction crucial for the pairing of electrons. In conventional s-wave superconductors, this attractive interaction comes from electron-phonon interactions, and renormalization-group analysis shows that this attractive interaction is a relevant perturbation[5], which explains why superconductivity occurs despite the strong Coulomb repulsion between electrons. Conventional BCS theory focuses on the case of a uniform coupling constant U, and in Chapter 2 we will analyze the consequence of an inhomogeneous coupling $U(\vec{r})$ and show that it corresponds to some experimental situations.

The crucial concept in the BCS theory is the identification of the electron pairing order parameter

$$\Delta(x) \equiv UF(x) \equiv U\langle\psi_\uparrow(x)\psi_\downarrow(x)\rangle, \tag{1.2}$$

where $F(x)$ is called the anomalous average or anomalous Green's function, because unlike in the Fermi liquid phase it has nonzero expectation value in the superconducting phase. With this order parameter ansatz, one can decouple the quartic interaction term in the original Hamiltonian, and reduce it to a quadratic mean-field Hamiltonian

$$H_{MF} = \int_r \sum_{s=\uparrow,\downarrow} \psi_s^\dagger \left(-\frac{\nabla^2}{2m}\right) \psi_s - \Delta\psi_\downarrow^\dagger \psi_\uparrow^\dagger - \Delta^* \psi_\uparrow \psi_\downarrow. \tag{1.3}$$

It is simple exercise to diagonalize this mean-field Hamiltonian by defining a new quasiparticle operator which is a coherent superposition of the original particle and hole operators:

$$c_{\uparrow,k} = u_k \psi_{\uparrow,k} + v_k \psi_{\downarrow,k}^\dagger. \tag{1.4}$$

The ground state, a vacuum for the new quasiparticle operators, is simply a conden-

sate for Cooper pairs:

$$|\text{Ground State}\rangle = \prod_k (u_k + c_k \psi^\dagger_{\uparrow,k} \psi^\dagger_{\downarrow,-k})|0\rangle; \tag{1.5}$$

and the quasiparticle excitations have an energy gap Δ, with spectrum

$$E_k = \sqrt{\frac{k^2}{2m} + \Delta^2}. \tag{1.6}$$

To find the value of Δ, one needs to solve the self-consistency equation

$$\Delta(x) = U\langle\psi_\uparrow(x)\psi_\downarrow(x)\rangle. \tag{1.7}$$

The highest temperature T that permits a nonzero solution Δ is the mean-field critical temperature T_c^{MF}. An important result of the BCS self-consistency equation calculation is that the ratio of the zero-T gap (=order parameter in uniform systems) Δ and the T_c^{MF} is a universal number

$$\frac{2E_g}{T_c^{MF}} = 3.52. \tag{1.8}$$

More refined microscopic theory of superconductivity, namely the Eliashberg theory[9], takes into account the phonons explicitly, and 3.52 serves as a lower-bound on the gap-T_c^{MF} ratio albeit not universal. Years of experiments on Bulk conventional superconductors have verified this result[9]. However, we will show in Chapter 2 that if the coupling constant U is non-uniform, this ratio can become lower than the BCS value 3.52 as indeed happened in some experiments.

The most important length scale in the BCS theory is the superconducting coherence length ξ, which characterizes the length scale of spatial variations of the order parameter Δ. For "clean" superconductors with no disorder,

$$\xi = \frac{\hbar v_F}{\Delta}, \tag{1.9}$$

where v_F is the Fermi velocity; for disordered "dirty" superconductors,

$$\xi \sim \sqrt{\frac{\hbar D}{\Delta}}, \tag{1.10}$$

where D is the diffusion constant.

1.2 Phase fluctuations and superconductor-insulator transitions (SITs)

The BCS theory, although extremely successful in describing conventional bulk superconductors, does not provide a satisfactory framework for disordered superconducting films. This is because BCS theory is simply a mean-field theory, while in disordered thin film superconductors, fluctuation effects are much stronger due to the low dimensionality and disorder.

The effect of disorder on superconductivity has been extensively investigated since the pioneering work of Anderson[10] and Abrikosov and Gorkov[11], who found that nonmagnetic impurities have no considerable effect on the thermodynamic properties of s-wave superconductors, including the mean field T_c and the gap; this result is known as the "Anderson theorem" for weakly-disordered dirty superconductors. Nevertheless, the superfluid stiffness is reduced by disorder. For a weakly-disordered superconductor, the superfluid stiffness is given by[12]

$$\rho_s = \frac{\sigma_n \Delta}{2\sigma_Q} \tanh \frac{|\Delta|}{2T}, \tag{1.11}$$

where the effect of disorder enters through the normal state conductivity σ_n, and $\sigma_Q = e^2/h$ is the conductance quantum.

One immediate consequence of the suppression of superfluid density by weak nonmagnetic disorder is that the resistance transition gets widened. Below the mean field transition temperature T_c^{MF}, although the order parameter amplitude $|\Delta|$ is nonzero, phase θ of Δ could fluctuate strongly and destroy long-range phase coherence and

thereby dissipationless supercurrent. In two dimensions, only below the Kosterlitz-Thouless transition[13] temperature T_{KT} is the phase coherence established, and the resistance is truly zero[14, 15]. In weak disorder regime, where BCS theory is still valid, the transition width, i.e., the difference between T_c^{MF} and T_{KT}, can be simply estimated as follows. Near T_c^{MF}, BCS theory gives[16]

$$\ln \frac{T}{T_c^{MF}} = -\frac{7\zeta(3)}{8}\left(\frac{\Delta}{\pi T}\right)^2, \tag{1.12}$$

where $\zeta(3) \approx 1.202$. From (1.11) the superfluid stiffness for a dirty superconductor near T_c^{MF} is

$$\rho_s = \frac{\sigma_n \Delta^2}{4\sigma_Q T}. \tag{1.13}$$

T_{KT} is obtained by self-consistently solving $T_{KT} = \frac{\pi}{2}\rho_s$:

$$\left(\frac{\Delta_{T=T_{KT}}}{T_{KT}}\right)^2 = \frac{8}{\pi}\frac{\sigma_Q}{\sigma_n}, \tag{1.14}$$

and thus

$$\ln \frac{T}{T_c^{MF}} \approx \frac{T_{KT} - T_c^{MF}}{T_c^{MF}} = -\frac{7\zeta(3)}{\pi^3}\frac{\sigma_Q}{\sigma_n}. \tag{1.15}$$

We can see that in more disordered films which are characterized by lower values of the normal state conductance σ_n, the resistive transition is considerably broadened. Naturally, one expects that if the disorder is strong enough, the phase coherence temperature T_{KT} can be driven to zero while T_c^{MF} remains finite (see FIG. 1.1). The nonsuperconducting state in this scenario is expected to be the quantum analog of the Kosterlitz-Thouless vortex proliferated state - the vortex condensed state. In the strongly-disordered regime, vortices are believed to be fairly light and mobile bosons[17], and they could Bose-Einstein condense and destroy the phase coherence. Thus, the insulating (or vacuum) phase for vortices is the superfluid phase for Cooper pairs, and the "superfluid" phase for vortices is the physical insulating phase in which Cooper pairs are localized. The effect of a perpendicular magnetic field is quite similar: it increases the density of vortices, degrades the phase coherence, and eventually

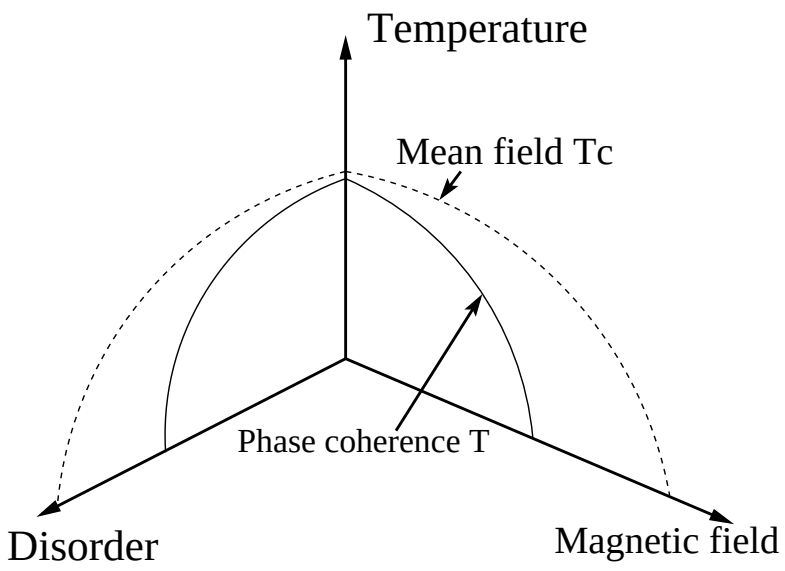

Figure 1.1: Schematic phase diagram of disordered superconducting films. Disorder and magnetic field reduce the phase coherence temperature and eventually drive the system into insulating phase in which Cooper pairs are localized.

the vortices condense and dissipationless supercurrent is lost.

This is one of the major explanations[20, 21, 22, 23, 24, 17] for the superconductor-insulator transitions observed in experiments[18, 25, 26, 27, 28, 29, 30, 31, 32, 33, 34, 35, 19], where an amorphous superconducting film (Bi, MoGe, InO, Ta, TiN, etc.) can be tuned to an insulator by either decreasing its thickness (enhancing disorder) or increasing a perpendicular magnetic field. FIG. 1.2 shows some typical experimental results, where at large thickness or small magnetic field, the resistance drops with decreasing temperature which is characteristic of a superconductor, but at small thickness or high magnetic field, the resistance rises with decreasing temperature which is characteristic of an insulator. In the vortex scenario for superconductor-insulator transitions, the amplitude of the superconducting order parameter remains finite even in the insulating phase, but the Cooper pairs are localized in this phase due to loss of phase coherence. For completeness, we also mention that another school of thoughts tries to explain this phenomenon by attributing the loss of dissipationless state to BCS electron-depairing mechanism and extending BCS theory to strongly disordered regime[36, 37, 38]. In this theory, Cooper pairs are completely destroyed in the insulating phase, and the phase transition is due to order parameter amplitude

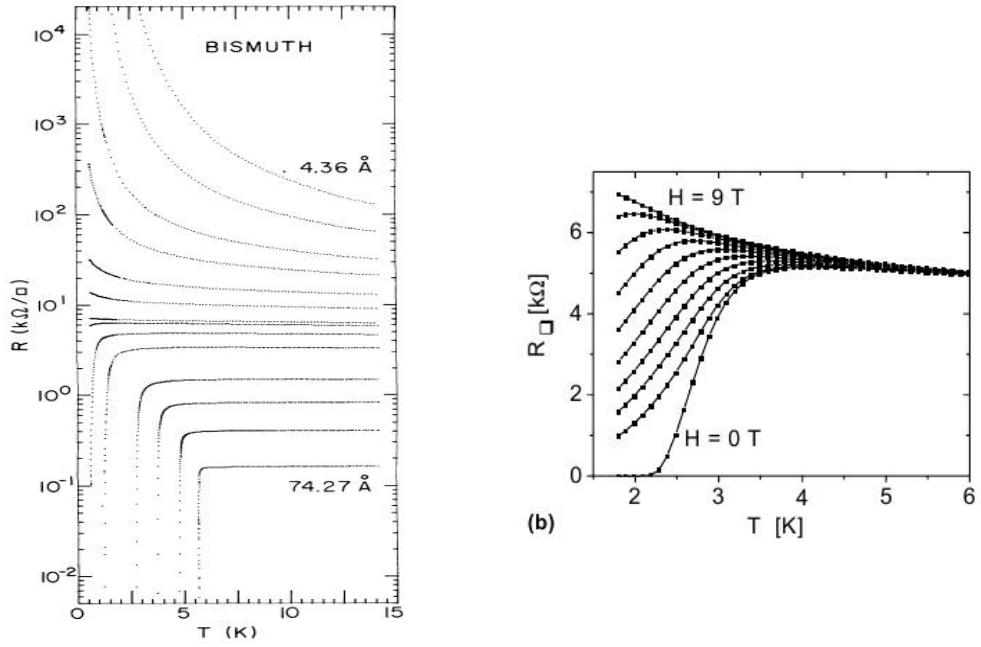

Disorder−tuned SIT, Bi film Magnetic−field−tuned SIT, InO film

Figure 1.2: Resistance vs. temperature traces in typical superconductor-insulator transition (SIT) experiments tuned by disorder (left, taken from Ref. [18]) or perpendicular magnetic field (right, taken from Ref. [19]).

fluctuations.

1.3 Vortex-boson duality

Before diving into more experimental work on superconducting films that motivated our theoretical work, we discuss in more details the vortex picture for superconductor-insulator transitions and introduce the basic idea of the vortex-boson duality[39, 20, 21, 40, 41, 42] which has the power of exposing vortex degrees of freedom from a superfluid. This duality is also referred to as the duality between the XY model and the Abelian Higgs model. This formalism will also be generalized to describe some quantum Hall states in subsequent sections. One starts with the quantum XY model

which is the low energy theory of the BCS theory or the Bogoliobov superfluid theory:

$$\begin{aligned} \mathcal{Z} &= \int \mathcal{D}\theta e^{-\int \mathrm{d}x_\mu \mathcal{L}} \\ \mathcal{L} &= \frac{1}{2}\rho_s(\partial_\mu \theta)^2, \end{aligned} \tag{1.16}$$

where ρ_s is the superfluid stiffness, θ is the phase of the superconductor/superfluid order parameter, and we set the phonon velocity to be 1 (for illustration purposes, we neglect the complication of non-linear dispersing phonons in superconducting films. See Chapter 3 for more details). Next, one introduces the current field j_μ by a Hubbard-Stratonovich transformation:

$$\begin{aligned} \mathcal{Z} &= \int \mathcal{D}\theta \mathcal{D} j_\mu e^{-\int \mathrm{d}x_\mu \mathcal{L}} \\ \mathcal{L} &= \frac{1}{2\rho_s} j_\mu^2 + \mathrm{i} j_\mu \partial^\mu \theta. \end{aligned} \tag{1.17}$$

Then we split the phase field into a smooth part and a vortex part $\theta = \theta_s + \theta_v$, and integrate out the smooth part to obtain the continuity constraint $\partial_\mu j^\mu = 0$:

$$\begin{aligned} \mathcal{Z} &= \int \mathcal{D}\theta_v \mathcal{D} j_\mu \delta(\partial_\mu j^\mu) e^{-\int \mathrm{d}x_\mu \mathcal{L}} \\ \mathcal{L} &= \frac{1}{2\rho_s} j_\mu^2 + \mathrm{i} j_\mu \partial^\mu \theta_v. \end{aligned} \tag{1.18}$$

Now notice that the continuity constraint is automatically satisfied by introducing a gauge field α_μ and parametrizing j_μ as

$$j^\mu = \frac{1}{2\pi}\epsilon^{\mu\nu\rho}\partial_\nu \alpha_\rho. \tag{1.19}$$

Therefore upon integrating by parts, and noting the definition of vortex currents

$$j_\mu^v = \frac{1}{2\pi}\epsilon^{\mu\nu\rho}\partial_\nu \partial_\rho \theta^v, \tag{1.20}$$

the partition function now looks like

$$\begin{aligned} \mathcal{Z} &= \int \mathcal{D}a_\mu \mathcal{D}j^v_\mu e^{-\int \mathrm{d}x_\mu \mathcal{L}} \\ \mathcal{L} &= \frac{1}{8\pi^2\rho_s}(\epsilon^{\mu\nu\rho}\partial_\nu \alpha_\rho)^2 - \mathrm{i}j^v_\mu \alpha_\mu. \end{aligned} \tag{1.21}$$

This dual theory looks just like charges (which are vortices) interacting with a Maxwell gauge field α_μ, and it contains all the physics of the original XY model. For example, phonon excitations in the original XY model now become photons with a Maxwell term; the well-known logarithmic interaction between vortices is represented as two-dimensional "Coulomb" interaction here if one integrates out α_0 in the transverse gauge of α_μ; the supercurrent now becomes the dual "electric field" (rotated by 90 degrees), while the boson density fluctuation becomes the dual "magnetic field", which is easy to understand from (1.19); the Magnus force[43], which is the transverse force exerted by a supercurrent on a vortex, is simply recovered as the electric force in this dual formalism.

Interestingly, the Cooper pair supercurrent acts as the electric field for vortices, and the vortex current also acts as the electric field for Cooper pairs (AC Josephson effect[4]). Consequently the physical conductance is the inverse of the "vortex conductance":

$$\sigma_{physical} = \frac{j}{E} = \frac{E_{vortex}}{j_{vortex}} = \frac{1}{\sigma_{vortex}}. \tag{1.22}$$

Due to this relation, a "vortex superfluid" ($\sigma_{vortex} = 0$) is an insulator ($\sigma_{physical} = \infty$), and vice versa. Alternatively, this correspondence between the phases of the original XY model and those of the dual theory can be also understood by including an external electromagnetic field $A_{ext,\mu}$ from the beginning and integrating out all fluctuating fields of both theories to show that in the superfluid phase of the original theory and in the "insulating phase" of the dual theory,

$$\mathcal{L} \sim \rho_s A^2_{ext,\mu}, \tag{1.23}$$

which gives a superfluid response

$$j_\mu = \frac{\partial \mathcal{L}}{\partial A_{ext,\mu}} \sim \rho_s A_{ext,\mu}, \tag{1.24}$$

while in the insulating phase of the original theory and in the "superfluid phase" of the dual theory

$$\mathcal{L} \sim (\epsilon^{\mu\nu\rho}\partial_\nu A_{ext,\rho})^2 \tag{1.25}$$

which is just the Maxwell theory giving an insulator response.

Since in disordered superconducting films, vortex mobility is $\mu \sim e^2\xi^2/(\hbar^2\sigma_n)$ where σ_n is the normal state conductance, vortices are immobile in less disordered films[15, 14, 17]. Hence, the ground state is an insulating phase for vortices, i.e., physical superfluid phase. On the other hand, in strongly disordered films vortices are mobile, or when there is a strong external magnetic field which would be translated to a large background vortex density, the system is in a "Higgs" phase and vortices "condense". This is an insulator where all excitations are gapped. That completes our discussion of the vortex picture for superconductor-insulator transitions.

1.4 Overview of our work on thin film superconductors

Motivated by the physics of superconductor-insulator transitions in thin-films, more experimental studies have been undertaken in recent years in several different directions. One of them is to focus on the nature of the density of states (DOS) and the quasi-particle energy gap in superconducting thin films[44, 45, 46, 27, 30, 29, 32] and superconductor - normal-metal (SN) bilayers [47, 48, 49]. Interestingly, these studies found a broadening of the BCS peak and also a subgap density of states[45, 27, 30, 29, 32, 48]. Of particular interest to us is the work in Ref. [49], which studied a thin SN bilayer system, and found a surprisingly low value of the ratio of the energy gap to T_c, in contradiction to standard BCS theory, and the theory of proximity[50, 51, 52]

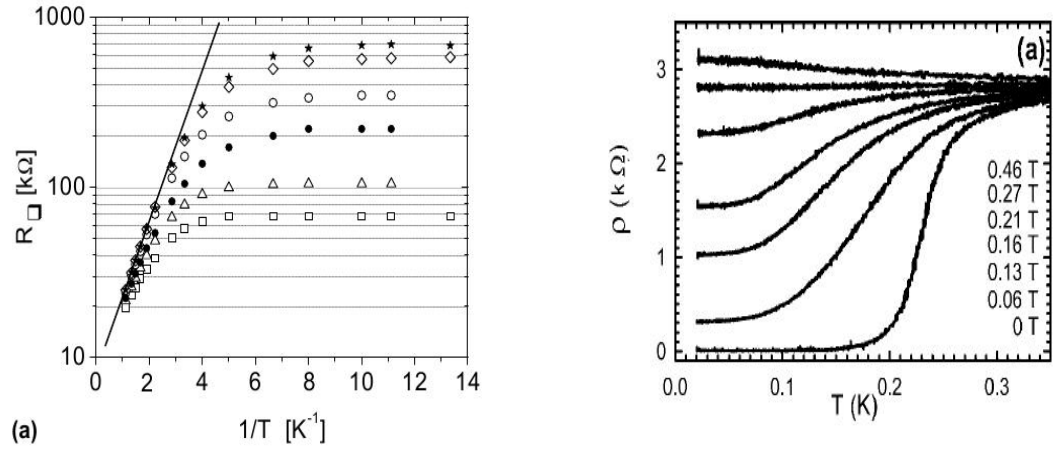

Figure 1.3: The resistance vs. inverse of temperature (left) and resistance vs. temperature (right) in the metallic phase at intermediate values of magnetic field. Left: experiment on InO film, taken from Ref. [19]. Right: experiment on Ta film, taken from Ref. [53].

where it is claimed that the energy gap-T_c ratio should be bounded from below by ~ 3.52. A drop below this bound, $2E_g/T_c < 3.52$, was also observed in amorphous Bi films as it approaches the disorder tuned SIT[27, 30]. Similar trends were also observed in SN bilayers in Ref. [47] and in amorphous tin films in Ref. [46]. In Chapter 2, we show that a reduction of the $2E_g/T_c$ ratio in a dirty superconductor could be explained as a consequence of inhomogeneity in the pairing interaction.

Another direction of recent experimental studies is to investigate the films exhibing magnetic-field-tuned superconductor-insulator transition at lower temperatures (< 100mK) and higher magnetic fields (ranging from 1T to 15T). One puzzling observation is that a metallic phase intervenes between the superconducting and the insulating phases[54, 55, 56, 35, 19, 57, 53, 58] (see FIG. 1.3). Near the "SIT critical point", as temperature is lowered below ~ 100mK, the resistance curve starts to level off, indicating the existence of a novel metallic phase, with a distinct nonlinear $I-V$ characteristics at least in Ta films[57]. Another interesting experimental finding is the nonmonotonic behavior of the magnetoresistance[35, 59, 19, 60]. As one increases magnetic field further from the "SIT point", the resistance climbs up quickly to very large value in InO and TiN films, before plummeting back to the normal state resis-

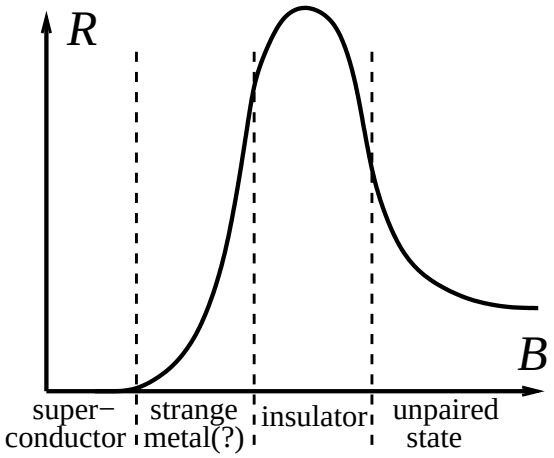

Figure 1.4: A typical magnetoresistance curve of amorphous thin film superconductors. As the magnetic field B increases, the superconducting phase is destroyed, and a possible metallic phase emerges. After which the system enters an insulating phase, where the magnetoresistance reaches its peak. The resistance drops down and approaches normal state value as B is further increased.

tance, as shown in FIG. 1.4. In Ta and MoGe films, as well as some InO films, the resistance peak is not as large, but is still apparent[54, 55, 56, 19, 57, 53].

Two competing paradigms may account for the metallic phase as well as the giant magnetoresistance. On one hand, the quantum vortex pictures [21, 40, 61, 62] attempt to explain these phenomena by extending the original simple superconductor-insulator transition theory as we dicussed in Sec. 1.3. The insulating phase at the peak of the magnetoresistance implies the condensation of quantum vortices as before, but to explain the high field negative magnetoresistance, one needs to explicitly incorporate unpaired electrons into the model and interpret the negative magnetoresistance as the gradual depairing of Cooper pairs and the appearance of a finite electronic density of states at the Fermi level. The intervening metallic phase is described as a delocalzed but yet uncondensed diffusive vortex liquid as described in Ref. [62]. In this picture disorder and charging effects are most important on length scales smaller or of order ξ (the superconducting coherence length, typically of order $10nm$).

On the other hand, the percolation paradigm[64, 65, 63, 66, 67] describes the amorphous film as a mixture of superconductor and normal or insulating puddles, with disorder playing a role at scales larger than ξ. Particularly germane is the pic-

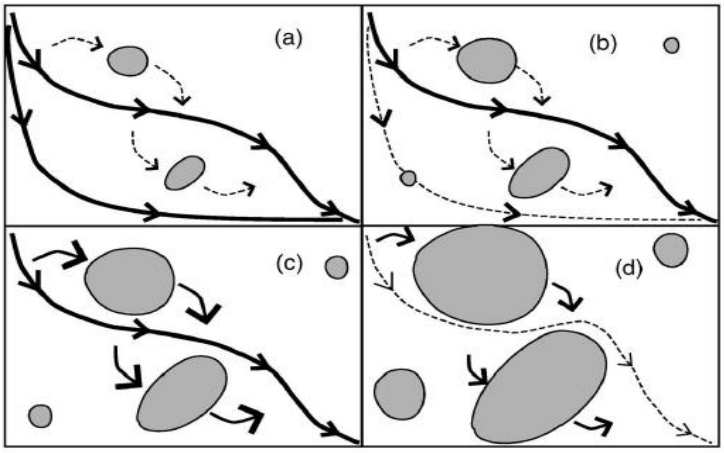

Figure 1.5: Schematic representation of the percolation theory explanantion to the negative magnetoresistance in magnetic-field-tuned superconductor-insulator transitions. Taken from Ref. [63].

ture in Ref. [63] which phenomenologically captures both a metallic phase as well as the strongly insulating phase by assuming superconducting islands exhibit a Coulomb blockade for electrons. This theory also assumes that the major effect of the magnetic field is to decrease the portion of superconducting puddles. This way the peak in the magnetoresistance arises from electron transport through the percolating normal regions consisting of narrow conduction channels. To be more specific (see FIG. 1.5), when the magnetic field is large, superconducting islands are small, charging gap is large for electrons, and therefore conduction is mainly through the normal metal region (FIG. 1.5a). When the magnetic field is slightly lowered (FIG. 1.5b), superconducting islands become larger, but the charging gap is still large enough to penalize electrons trying to enter superconducting islands; however the enlarged superconductors squeeze the conduction path in the normal metal region, and therefore the resistance increases with decreasing magnetic field. When the magnetic field is further lowered (FIG. 1.5c,d), superconducting islands are finally large enough so that tunneling into them becomes energetically favorable, and the resistance is decreased with smaller magnetic fields. Finally, when superconducting islands percolate, the system enters the superconducting phase.

We also note that yet a third theory tries to account for the low field superconductor-

metal transition using a phase glass model [68, 69] (see, however, Ref. [70] which argues against these results), but does not address the full magnetoresistance curve.

Qualitatively, both paradigms above are consistent with magnetoresistance observations, and recent tilted field[71], AC conductance[72], Nernst effect[73], and Scanning Tunneling Spectroscopic[74] measurements cannot distinguish between them. Particularly intriguing is the origin of the metallic phase - is it vortex driven or does it occur due to electronic conduction channels dominating transport through the film? In Chapter 3, we propose a new type of experiments, namely the drag resistance measurement, as a method capable to point to the correct theoretical picture.

1.5 From superconductivity to quantum Hall effect

The classical Hall effect, discovered more than a century ago, is straightforward to understand with classical electromagnetism. When charge carriers move in a perpendicular magnetic field, charge will accumulate in the transverse direction which generates an electric field to balance the Lorentz force exerted by the perpendicular magnetic field. The Hall resistance, namely the transverse voltage drop divided by the longitudinal electric current, is therefore proportional to the magnetic field.

For two-dimensional electron gas (2DEG) in semiconductor heterostructures and later in graphene, when a strong perpendicular magnetic field commensurate with the electron density is applied, a series of remarkable quantum Hall states emerge[76, 77, 78]. What makes these states different from the classical Hall effect is the existence of plateaus in Hall resistance and the simultaneous vanishing of longitudinal resistance near certain integer and fractional filling factors (defined as $\nu \equiv \rho/(B/\phi_0)$, ρ is the carrier density, B is the magnetic field, ϕ_0 is the flux quantum). When the filling factor slightly deviates from these special values, the Hall resistance stays quantized at $R_{xy} = \frac{1}{\nu}\frac{h}{e^2}$ (see FIG. 1.6).

Integer quantum Hall effect (for integer ν) can be understood with non-interacting

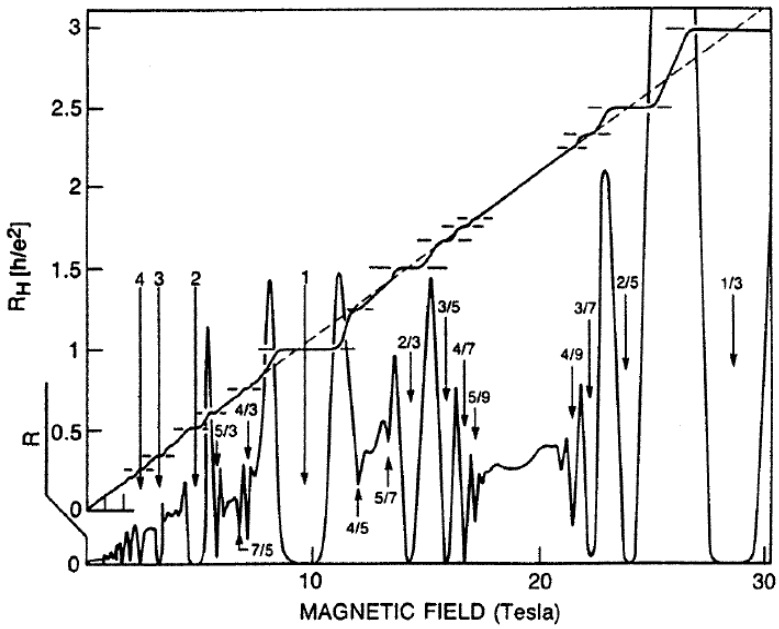

Figure 1.6: Experimental results of the Hall resistance and the longitudinal resistance in 2DEG. Taken from Ref. [75].

electrons by invoking quenched disorder. Disorder is necessary for the existence of this plateau, which can be understood either through a Galilean invariance argument[79] or a vortex argument (see below). For fractional quantum Hall effect, the Coulomb interaction plays a crucial role[79, 80, 81] instead. The fractional quantum Hall effect with odd-integer-denominator filling factor can be understood with Laughlin's wavefunctions[82], and Chern-Simons flux attachment approaches including composite boson[83, 84] and composite fermion approaches[85, 86]. Both integer and fractional quantum Hall effect have a gap for all bulk excitations, but it has been shown that gapless chiral excitaions exist on the edge[81]. In recent years, a lot of interest have been generated by the possibility of non-abelian quantum Hall states in higher Landau levels and their possible applications to topological quantum computations[87, 88].

To lay down the foundation for later sections, we now focus on Laughlin states at $\nu = 1/(2k+1)$. At these filling fractions, in the non-interacting limit, the ground state is highly degenerate due to the flat dispersion of Landau levels. Naturally Coulomb interaction will lift the degeneracy and select the true ground state, and Laughlin's

answer is[82]

$$\psi = \prod_{i<j}(z_i - z_j)^{2k+1} \exp\left[-\sum_i |z_i|^2/(4l^2)\right], \tag{1.26}$$

where l is the magnetic length, and $z_j = x_j + \mathrm{i}y_j$. This wavefunction has almost unity overlap with the exact ground state, and its virtue could be understood by the fact that it has *no wasted zeros*[89, 80], which means the following. Given N electrons and therefore $N(2k+1)$ flux quanta, when we view the Langhlin wavefunction as a wavefunction of z_1 and take this electron around the sample in a loop, the wavefunction should pick up a Aharonov-Bohm phase $2\pi N(2k+1)$, which implies that there have to be $N(2k+1)$ zeros in the wavefunction. Among these zeros, Pauli-exclusion principle only requires N of them to lie on other electrons, however in the Laughlin wavefunction all zeros do lie on other electrons, which is very efficient in keeping electrons apart and lowering the interaction energy.

Next, we proceed to discuss the composite boson theory which carries the features of quantum Hall states in a very compact way. From the Laughlin wave function, we see that in terms of Berry's phase, essentially electrons see each other as a $2\pi(2k+1)$ flux source, in this way they are kept apart and the interaction energy is lowered. In the same spirit, we can trade each electron for $2k+1$ flux quanta and a composite boson, and transform the original Lagrangian for electron ψ

$$\mathcal{L} = \psi^\dagger(\mathrm{i}\partial_t - A_t)\psi + \frac{1}{2m}\psi^\dagger\left(-\mathrm{i}\nabla - \vec{A}_{ext}\right)^2\psi + V(|\psi|), \tag{1.27}$$

where V is the potential energy including the Coulomb interaction and disorder potentials, into the Lagrangian for composite boson ϕ and a Chern-Simons gauge field a_μ:

$$\mathcal{L} = \phi^\dagger(\mathrm{i}\partial_t - a_t - A_t)\phi + \frac{1}{2m}\phi^\dagger\left(-\mathrm{i}\nabla - \vec{a} - \vec{A}_{ext}\right)^2\phi + V(|\phi|) + \frac{1}{4\pi(2k+1)}a_\mu\epsilon^{\mu\nu\rho}\partial_\nu a_\rho. \tag{1.28}$$

One can check that $2k+1$ flux quantum of a_μ is attached to ϕ by minimizing $\mathcal{L}$ with

respect to a_t, which leads to

$$(2k+1)\phi^\dagger\phi = \frac{1}{2\pi}\nabla\times\vec{a}. \tag{1.29}$$

Therefore at the mean-field level, the Chern-Simons flux and the external magnetic field cancel each other, and composite bosons see zero net flux. As bosons, they condense and form a superfluid. Since the total electric field vanishes inside a charged superfluid, we have

$$\vec{e}+\vec{E}_{ext}=0, \tag{1.30}$$

where the "electric field" $\vec{e}\equiv-\partial_t\vec{a}-\nabla a_t$. Minimizing the action with respect to $\vec{a}$, we obtain

$$(2k+1)\vec{j} = \frac{1}{2\pi}\hat{z}\times\vec{e}, \tag{1.31}$$

and hence the defining property of quantum Hall effect

$$\vec{j} = \frac{1}{2\pi(2k+1)}\vec{E}_{ext}\times\hat{z} \text{ at filling fraction } \nu=\frac{1}{2k+1}.$$

Therefore, the quantum Hall effect at filling factor $\nu = 1/(2k+1)$, the so-called Laughlin fraction, can be understood as a condensate of composite bosons which is formed by attaching $(2k+1)$ flux quanta to each electron, and these background fluxes cancel the external magnetic field exactly at these special filling factors. Vortex excitations of this composite boson superfluid are introduced when the filling fraction is slightly moved away from $\nu = 1/(2k+1)$, but similar to the situation of superconductors, vortices will be pinned by quenched disorder, and the conductance remains the same. This explains the Hall plateau. One can also generalize the vortex-boson duality formalism to transform the above Lagrangian to reveal the vortex degrees of freedom explicitly and show that they have fractional charge and statistics. In the low-energy long-wavelength limit, denoting θ the phase of the composite boson, we have

$$\mathcal{L} = \frac{1}{2}\rho(\partial_\mu\theta - A^{ext}_\mu - a_\mu)^2 + \frac{1}{4\pi(2k+1)}a_\mu\epsilon^{\mu\nu\rho}\partial_\nu a_\rho. \tag{1.32}$$

Next, one introduces the composite-boson current field j_μ through the Hubbard-Stratonovich transformation:

$$\mathcal{L} = \frac{1}{2\rho} j_\mu^2 + \mathrm{i} j_\mu \left(\partial^\mu \theta - A_\mu^{ext} - a_\mu \right) + \frac{1}{4\pi(2k+1)} a_\mu \epsilon^{\mu\nu\rho} \partial_\nu a_\rho. \tag{1.33}$$

Again, we split the phase field into a smooth part and a vortex part $\theta = \theta_s + \theta_v$, and integrate out the smooth part to obtain the continuity constraint $\partial_\mu j^\mu = 0$ which is solved by introducing a gauge field $j^\mu = \frac{1}{2\pi} \epsilon^{\mu\nu\rho} \partial_\nu \alpha_\rho$:

$$\mathcal{L} = \frac{1}{8\pi^2 \rho} (\epsilon^{\mu\nu\rho} \partial_\nu \alpha_\rho)^2 + \mathrm{i} \frac{1}{2\pi} \epsilon^{\mu\nu\rho} \partial_\nu \alpha_\rho \left(\partial_\mu \theta^v - A_\mu^{ext} - a_\mu \right) + \frac{1}{4\pi(2k+1)} a_\mu \epsilon^{\mu\nu\rho} \partial_\nu a_\rho. \tag{1.34}$$

Integrating by parts, noting the definition of vortex currents $j_\mu^v = \frac{1}{2\pi} \epsilon^{\mu\nu\rho} \partial_\nu \partial_\rho \theta^v$, and integrating out the Chern-Simons field a_μ, we can rewrite the Lagrangian into the following form:

$$\mathcal{L} = \frac{1}{8\pi^2 \rho} (\epsilon^{\mu\nu\rho} \partial_\nu \alpha_\rho)^2 + \frac{(2k+1)}{4\pi} \alpha_\mu \epsilon^{\mu\nu\rho} \partial_\nu \alpha_\rho - \mathrm{i} \frac{1}{2\pi} \epsilon^{\mu\nu\rho} \partial_\nu \alpha_\rho A_\mu^{ext} - \mathrm{i} j_\mu^v \alpha_\mu. \tag{1.35}$$

Unlike the case of superconductors, the gauge field α_μ which represents the (composite) boson density fluctuation now acquires a Chern-Simons term, which renders it a gap. Therefore the quantum Hall fluid is incompressible at $\nu = 1/(2k+1)$, while superfluid and (1D,2D) superconductors are compressible. The Chern-Simons term for α_μ also indicates that $1/(2k+1)$ flux quantum is attached to each vortex, which explains their fractional statistics. According to the third term in this Lagrangian, A_t^{ext} is coupled to the one flux quantum of α_μ, which means one flux quantum of α_μ has one unit of electric charge. Since each vortex has $1/(2k+1)$ flux quantum, each of them has $1/(2k+1)$ electric charge as well. When vortices are absent, one can also integrate out all fluctuating fields and obtain

$$\mathcal{L} = \frac{1}{4\pi(2k+1)} A_\mu^{ext} \epsilon^{\mu\nu\rho} \partial_\nu A_\rho^{ext}, \tag{1.36}$$

which gives

$$j^\mu = \frac{\delta \mathcal{L}}{\delta A_\mu^{ext}} = \frac{1}{2\pi(2k+1)} \epsilon^{\mu\nu\rho} \partial_\nu A_\rho^{ext}, \tag{1.37}$$

which is again the defining property of the quantum Hall effect at $\nu = 1/(2k+1)$.

1.6 Bilayer quantum Hall effect: a hidden superfluid

In bilayer two-dimensional electron systems with negligible interlayer tunneling and total filling factor $\nu_{tot} = 1$, when the layer separation d is comparable to the magnetic length l, a remarkable bilayer quantum Hall state with interlayer phase coherence emerges due to the interlayer Coulomb interaction[90]. The extra layer index degrees of freedom adds a lot of interesting physics to the system, and many remarkable experimental signatures of this phase predicted by theories have been observed in experiments, including enormous enhancement of zero bias interlayer tunneling[91], linearly dispersing Goldstone mode[92], quantized Hall drag[93], and vanishing resistance in counterflow[94].

There are several equivalent and complimentary ways to understand this bilayer quantum Hall state. In the pseudospin ferromagnet approach[95], one treats the layer index as pseudospin, and by Hund's rule, the ground state is a pseudospin ferromagnet which makes the spatial wavefunction completely anti-symmetric and therefore lowers the interaction energy. In addition, due to the charging energy at nonzero layer separation, the SU(2) symmetry is broken down to the easy-plane U(1) symmetry, and the ground state has a pseudospin lies in the xy-plane. Denoting $\psi_{1,X}$ and $\psi_{2,X}$ the electron field operators at guiding center X in the two layers respectively, we have

$$\langle \psi_{1,X}^\dagger \psi_{2,X} \rangle \sim e^{\mathrm{i}\theta}, \tag{1.38}$$

and the ground state can be written as

$$|\text{Ground State}\rangle \sim \prod_X \left(\psi^\dagger_{1,X} + e^{\mathrm{i}\theta}\psi^\dagger_{2,X}\right)|0\rangle. \tag{1.39}$$

These are what we meant by interlayer phase coherence. Note its remarkable consequence: each electron wavefunction is a coherent superposition of the state in each layer, even though we start with no interlayer tunneling! In addition, since at each guiding center there is only one electron, we have avoided paying for the strong interlayer Coulomb repulsion, which is partly the reason why this state has a low energy. Also note that the ground state wavefunction (1.39) can be written in a BCS form (cf. Eqn. 1.5)

$$|\text{Ground State}\rangle \sim \prod_X \left(1 + e^{\mathrm{i}\theta}\psi^\dagger_{2,X}\psi_{1,X}\right)|G\rangle, \text{ where } |G\rangle \sim \prod_X \psi^\dagger_{1,X}|0\rangle. \tag{1.40}$$

Contrary to the canonical BCS form Eqn. 1.5, $\psi_{1,X}$ is the *hole* creation operator in a filled Landau level. Consequently, the bilayer quantum Hall state can also be viewed as an exciton condensate in which electrons in one layer and holes in the other layer pair up[90]. Since the ground state (1.39) breaks the easy-plane pseudospin U(1) symmetry, a linearly-dispersing Goldstone mode is expected. In addition, the analog of supercurrent in exciton condensate is easily seen to be currents flowing in opposite directions, i.e., the counterflow in this state is expected to be dissipationless. Furthermore, if one puts a bias voltage between the two layers, it is easy to see in the exciton picture that the tunneling conductance will be huge near zero bias, because an electron is perfectly correlated with a hole in the other layer, and when it tunnels into the other layer, it rarely bumps into other electrons. These fascinating predictions have been observed in experiments [91, 92, 93, 94] (see FIG. 1.7). However, there are still important discrepancies between theories and experiments. For example, the height of the interlayer tunneling conductance is observed to be finite[91], while theories predict it to be infinite[96, 95]. Also, transport in counterflow experiments should be completely dissipationless under a critical temperature for phase coherence,

but in experiments dissipationless counterflow is only seen in the zero-temperature limit[94]. The effect of quenched disorder is believed to be crucial to reconcile these discrepancies[97, 98, 99], although a quantitative understanding is still lacking. Using the pseudospin analogy, one can also deduce the actions for various excitations including spin waves, skyrmions, merons, etc., and estimate the parameters in these effective actions using microscopic parameters[95].

Next, we briefly introduce the composite boson formalism[96, 95], which gives the same results in an elegant way. The basic physical picture is the same as those in the pseudospin ferromagnet picture and the exciton condensate picture: since the interlayer distance between electrons d is comparable to the intralayer distance ($\sim$ magnetic length l), both interlayer and intralayer Coulomb interactions are strong, and electrons tend to get as far as possible from other electrons both in the same layer and in the other layer. Now we formulate this idea by following the previous section's idea that when electrons avoid each other, they see each other as an odd integer number of flux quanta. Here, because of the total filling factor $\nu_{tot} = 1$ and because the strong interlayer interaction, each electron see those both in their own layer and those in the other layer as 2π flux source (equivalently, one zero in their wavefunction). Thus, each electron is traded for one composite boson and one flux quantum, and this background flux cancels the external magnetic field due to the total filling factor $\nu_{tot} = 1$. Generalizing the formalism of the previous section, in the low-energy long-wavelength limit, the Lagrangian for composite bosons is

$$\mathcal{L} = \frac{1}{2}\rho(\partial_\mu\theta_1 - a_\mu - A_\mu^{ext})^2 + \frac{1}{2}\rho(\partial_\mu\theta_2 - a_\mu - A_\mu^{ext})^2 + \frac{1}{4\pi}a_\mu\epsilon^{\mu\nu\rho}\partial_\nu a_\rho, \tag{1.41}$$

where $\theta_{1,2}$ are the phases of the composite boson fields of each layer due to the flux attachment transformation. Performing the same duality transformation as in the previous section, and defining

$$\alpha_{\pm\mu} = \alpha_{1\mu} \pm \alpha_{2\mu}, \qquad j_{\pm\mu} = j_{1\mu} \pm j_{2\mu} \tag{1.42}$$

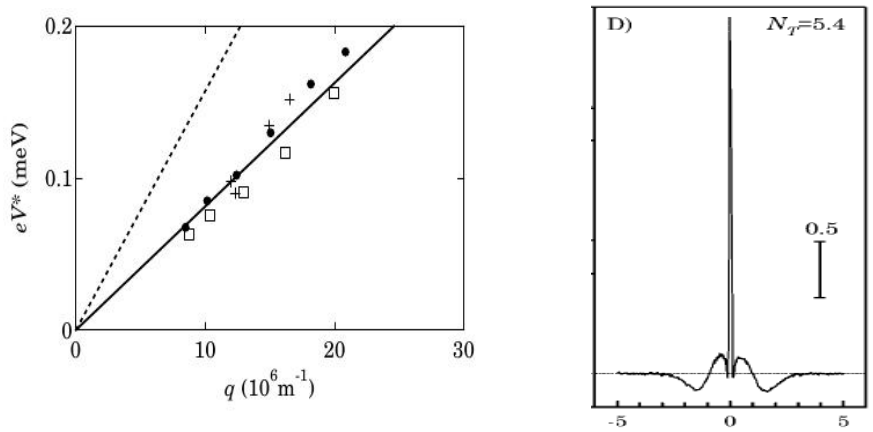

Figure 1.7: Experimental evidence of the interlayer coherent bilayer quantum Hall state at $\nu = 1$. Left: excitation energy vs. wavevector - evidence for a linearly-dispersing Goldstone mode. Taken from Ref. [92]. Right: interlayer tunneling conductance vs. bias voltage - evidence for the Josephson-like interlayer tunneling. Taken from Ref. [91].

where $\alpha_{1,2}$ and $j_{1,2}$ are the gauge fields introduced in the duality transformation and the composite boson currents in the two layers, respectively, we can rewrite the Lagrangian as

$$\begin{aligned} \mathcal{L} &= \mathcal{L}_+ + \mathcal{L}_-, \\ \mathcal{L}_+ &= \frac{1}{16\pi^2\rho}(\epsilon^{\mu\nu\rho}\partial_\nu\alpha_{+\rho})^2 + \frac{1}{4\pi}\alpha_{+\mu}\epsilon^{\mu\nu\rho}\partial_\nu\alpha_{+\rho} - \mathrm{i}\frac{1}{2\pi}\epsilon^{\mu\nu\rho}\partial_\nu\alpha_{+\rho}A^{ext}_\mu; \\ \mathcal{L}_- &= \frac{1}{16\pi^2\rho}(\epsilon^{\mu\nu\rho}\partial_\nu\alpha_{-\rho})^2 \end{aligned} \tag{1.43}$$

when vortices are absent. Apparently, the transport property of the "+" sector corresponds to treating the bilayer system as a whole. In this sector, one can neglect the less relevant Maxwell term and integrate out the fluctuating gauge field α_μ to obtain

$$\mathcal{L}_+ = \frac{1}{4\pi}A^{ext}_\mu\epsilon^{\mu\nu\rho}\partial_\nu A^{ext}_\rho, \tag{1.44}$$

which is again the defining property of a $\nu = 1$ quantum Hall state.

On the other hand, the transport property of the "-" sector corresponds to counterflow, i.e., currents flowing in opposite directions in two layers. What is unique for

this state is that its "-" sector has no Chern-Simons term! It looks exactly the same as the dual representation of a superfluid [cf. Eqn. (1.21)]. Immediately this leads to the prediction of dissipationless counterflow, a linearly dispersing mode which is represented as "photons" here, and the analog of Josephson tunneling, as we discussed earlier.

1.7 Half-filled Landau level: a hidden Fermi liquid

This interlayer coherent quantum Hall state only survives when the ratio of layer separation d and the magnetic length l is relatively small. In the opposite limit $d/l \to \infty$, two layers are decoupled, and each layer is at half-filling. Surprisingly, a half-filled Landau level behaves as a Fermi liquid, and much progress has been made in understanding this "composite fermion" Fermi liquid phase using the Chern-Simons approach[100, 101, 102, 103, 104] and the dipolar quasiparticle approach[105, 106, 107, 108, 109, 80].

The basic idea for this composite fermion Fermi liquid phase is quite simple to illustrate using flux attachment. At half-filling, if we try to trade electrons for composite particles and flux quanta to cancel the background flux as we did in previous sections, we have to attach two flux quanta to each electron. Therefore when two electrons are interchanged, we obtain an additional 2π phase instead of a π phase for Laughlin states or bilayer $\nu_{tot} = 1$ state. Hence, what we have obtained are composite fermions instead of composite bosons. Consequently, electrons at half-filling is equivalent to composite fermions with no magnetic field, which is naturally in a Fermi liquid state. However, due to the strong coupling of composite fermions with fluctuating Chern-Simons gauge fields, the composite Fermi liquid is much more complicated than conventional ones.

Halperin *et al.*[100] was the first who seriously pursued this picture and studied various properties of this composite fermion Fermi liquid phase in detail. Many interesting predictions were made. For example, if the filling factor ν deviates from half-filling and $\nu = p/(2p+1)$, composite fermions will see a magnetic field, and it is

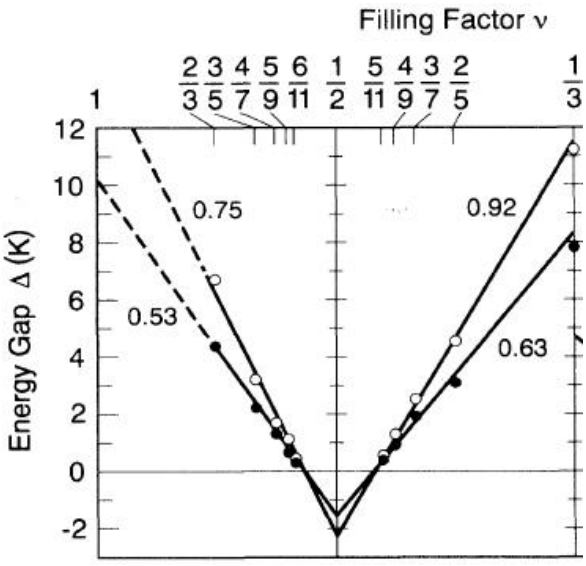

Figure 1.8: Activation gap of quantum Hall states $\nu = p/(2p+1)$ as a function of the filling factor ν, measured in Ref. [110]. The linear relation supports the composite fermion picture, and the slope is inversely proportional to the composite fermion mass.

easy to see that ($\hbar = e = 1$):

$$\Delta B \equiv B - B_{1/2} = 2\pi\frac{\rho}{p}, \qquad \text{with } B_{1/2} \equiv 4\pi\rho, \tag{1.45}$$

where ρ is the electron density. Thus, the composite fermions are in an integer quantum Hall state with p Landau levels filled. In other words, the fractional quantum Hall effect at $\nu = p/(2p+1)$ can be understood as integer quantum Hall effect of composite fermions, and the activation gap in these states can be identified as the cyclotron gap of composite fermions:

$$E_g = \frac{\Delta B}{m_*} = \frac{2\pi\rho}{pm_*}, \tag{1.46}$$

m_* being the composite fermion mass, which can be determined by fitting measured gap values near $\nu = 1/2$. Experiments have indeed confirmed the linear relation between the gap E_g and ΔB (see FIG. 1.8), which gives strong support for the composite fermion picture.

Many other experimental works have been undertaken to detect composite fermions

in half-filled Landau levels, and typically there are at least qualitative agreements with composite fermion theories, although it is often difficult to find very good quantitative agreements (see review articles by Refs. [111, 104, 80]). These efforts include measuring surface-acoustic-wave velocity shift[111], cyclotron orbit radius[112, 113], NMR relaxation rate T_1^{-1}[114], specific heat which is expected to be linear in T but with logarithmic corrections[115], Coulomb drag resistance which is expected to scale as $T^{4/3}$[116], etc.

1.8 Overview of our work on bilayer quantum Hall systems

Although we understand well both the coherent phase at $d/l \to 0$ and the composite Fermi liquid state at $d/l \to \infty$, the transition between them has been shrouded in mystery. There have been many experimental[117, 118, 119, 120, 121, 122, 123, 124, 125, 126, 127, 128, 129, 130] and theoretical[131, 132, 133, 134, 135, 136, 137, 138, 139, 140, 141, 142, 143] studies regarding the nature of this transition. While some of these theoretical works point to a direct transition between the two limiting phases, either continuous[140] or of first order[137, 138], some other works predict the existence of various types of exotic intermediate phases, including translational symmetry broken phase[131, 132, 133, 141], composite fermion paired state[134, 135, 142], phase of coexisting composite fermions and composite bosons[139, 143, 144], and quantum disordered phases[136], etc.

These theoretical works typically assume that the physical spin is fully polarized and hence irrelevant across the transition. However, recent experiments have shown that spin plays an important role in the transition. Ref. [121] has found that by applying a NMR pulse or heat pulse to depolarize the nuclei and hence increasing the effective magnetic field coupled to the spin, the coherent phase is strengthened, and the phase boundary shifts to higher value of d/l. Similar behavior has also been observed by applying a parallel magnetic field[125]. These experimental results

indicate that at least one of the phases involved in the transition is not fully polarized, and that the polarization changes significantly across the transition. The most likely possibility is that the incoherent composite Fermi liquid phase at large d/l is only partially polarized, as shown by other experiments on single layer at $\nu = 1/2$[114, 145]. If the transition between the coherent phase and the *less polarized* incoherent phase is a thermodynamic phase transition, it must be of first order: The magnetization is discontinuous across the transition, and, as the experiments of Ref. [121] found, the transition can be tuned using a Zeeman field which is conjugate to the magnetization. These two facts together imply the first order nature of the transition. An alternative to the thermodynamic transition scenario is a singularity-free quantum crossover as was suggested recently in Refs. [142, 143].

In Chapter 4, we assume that the transition tuned by d/l is a thermodynamic first-order transition between spin-polarized coherent $\nu_{tot} = 1$ quantum Hall state and partially-polarized composite Fermi liquid state, and derive the Clausius-Clapeyron relations for this system. The Clausius-Clapeyron relations will allow us to obtain the phase boundary shapes for the transition; a comparison of these boundaries with experiments presents a stringent consistency test of the first order transition scenario.

1.9 One-dimensional random hopping model

In this section, we switch from two-dimensional systems to one-dimensional cases. Being particularly interesting to us is the one-dimensional non-interacting random hopping model, namely tight-binding model with off-diagonal disorder:

$$H = -\sum_n J_n c_n^\dagger c_{n+1} + h.c., \tag{1.47}$$

where n is the site index, and the hopping amplitude J_n is random. This model has been investigated theoretically using various techniques for many years, and it is also known to be equivalent to many other models, such as quantum particles connected by random strength strings, spin 1/2 random XX chains, random quantum

Ising chains in transverse field, and random mass Dirac fermions. This model exhibits many surprising features. Early theoretical works[146, 147, 148, 149] focus on properties derivable from the mean local Green's function, notably the typical localization length and the mean density of states. For example, the state with zero energy is a delocalized state[148]. To illustrate this, we start with the Schrodinger equation of this system

$$-J_n\psi_{n+1} - J_{n-1}\psi_{n-1} = E\psi_n, \tag{1.48}$$

where ψ_n is the wavefunction at site n. For zero energy, this equation gives

$$\frac{\psi_{n+1}}{\psi_{n-1}} = -\frac{J_{n-1}}{J_n}. \tag{1.49}$$

Thus,

$$\frac{\psi_{2n+1}}{\psi_1} = \left(-\frac{J_{2n-1}}{J_{2n}}\right)\left(-\frac{J_{2n-3}}{J_{2n-2}}\right)...\left(-\frac{J_1}{J_2}\right). \tag{1.50}$$

Using the definition of localization length λ [147]

$$\frac{1}{\lambda} = -\lim_{n\to\infty}\frac{1}{2n}\ln\left|\frac{\psi_{2n+1}}{\psi_1}\right| \tag{1.51}$$

and the central limit theorem, one readily sees that the inverse of the localization length vanishes. Therefore this state has infinite localization length. More detailed analysis[149] shows that the localization length diverges as $\sim \ln|E|$ near the band-center, and the mean density of states (DOS) also diverges as $\sim 1/|E(\ln E^2)^3|$ as energy E approaches band-center. These behaviors are very different from Anderson insulators in which case disorder comes into diagonal terms and there are no singularities in the spectrum of the localization length or the density of states (see FIG. 1.9).

Recent work have studied this model using real space renormalization group method[150] and supersymmetry method[151] and have uncovered more interesting results, most importanly a different length scale - mean localization length which diverges as $\sim \ln^2|E|$. More recently, the effect of random hopping amplitude on in-

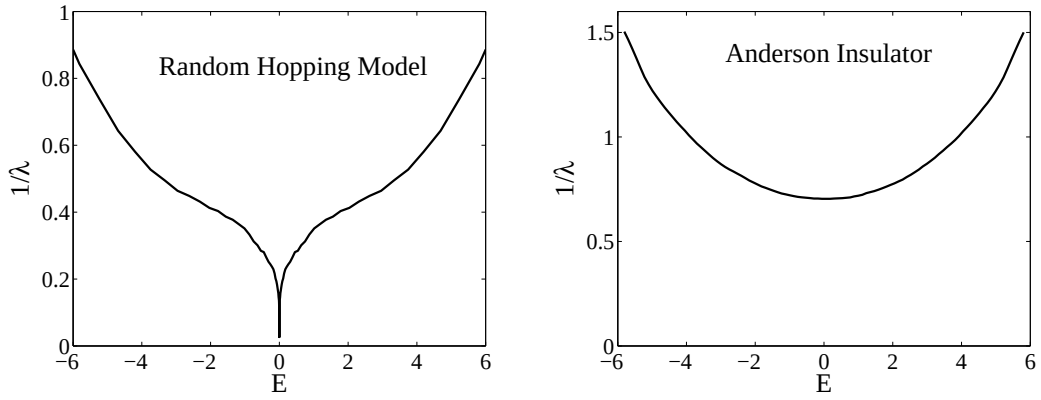

Figure 1.9: Comparison of the inverse of the localization length vs. energy in (left) random hopping model and (right) Anderson insulator.

teracting fermion and boson systems have also been investigated. In fermion case[152], it has been shown that random hopping amplitude could lead to a novel type of instability; in boson case[153, 154], novel "Mott glass" phase has been predicted in addition to usual Mott insulating and superfluid phases.

Nevertheless, pure random hopping model behavior is extremely difficult to engineer experimentally. This is mainly because diagonal disorder inevitably comes in, and any amount of diagonal disorder would break the particle-hole symmetry of the random hopping model and thereby destroy the interesting properties near the band-center. Hence, it is highly desirable to find a feasible and robust way to experimentally realize a random hopping model.

1.10 Realizing random hopping model with dynamical localization

In Chapter 5, we propose that a pure random hopping model can be realized in optical lattices by first creating an Anderson insulator and then modulate the disordered on-site potential energy periodically. Our idea is closely connected to recent work on the phenomena dubbed "Dynmaical Localization" or "Coherent Destruction of Tunneling" in double wells and optical lattices[155, 156, 157, 158, 159, 160, 161, 162,

163, 164, 165, 166, 167, 168, 169]. The basic idea of Dynamical Localization is the following. Consider a double well with a tunneling amplitude $J/2$ and a potential energy difference oscillating at frequency ω:

$$H = -\frac{J}{2}(a^\dagger b + b^\dagger a) + \frac{V}{2}\cos(\omega t)(a^\dagger a - b^\dagger b). \tag{1.52}$$

Switching to spin representation

$$S_x = \frac{1}{2}(a^\dagger b + b^\dagger a), \qquad S_z = \frac{1}{2}(a^\dagger a - b^\dagger b), \tag{1.53}$$

we have

$$H = -JS_x + V\cos(\omega t)S_z. \tag{1.54}$$

By performing a unitary transformation with

$$\psi = U\tilde{\psi}, \qquad U = e^{-\mathrm{i}\frac{V}{\omega}\sin(\omega t)S_z}, \tag{1.55}$$

one transforms the original Schrodinger equation $\mathrm{i}\partial_t\psi = H\psi$ into

$$\mathrm{i}\partial_t\tilde{\psi} = H_{eff}\tilde{\psi}, \tag{1.56}$$

where

$$\begin{aligned} H_{eff} &= U^\dagger H U - U^\dagger(\mathrm{i}\partial_t U) \\ &= -Je^{\mathrm{i}\frac{V}{\omega}\sin(\omega t)S_z}S_x e^{-\mathrm{i}\frac{V}{\omega}\sin(\omega t)S_z} \\ &= -J\left[S_x\cos\left(\frac{V}{\omega}\sin\omega t\right) - S_y\sin\left(\frac{V}{\omega}\sin\omega t\right)\right], \end{aligned} \tag{1.57}$$

which can be expanded as a series of Bessel functions. In the limit of fast oscillation, the leading order term is

$$H_{eff} \approx -J\mathcal{J}_0\left(\frac{V}{\omega}\right)S_x = -\frac{J}{2}\mathcal{J}_0\left(\frac{V}{\omega}\right)(a^\dagger b + b^\dagger a), \tag{1.58}$$

where $\mathcal{J}_0$ is the zeroth Bessel function. Thus one can see that the effect of oscillating potential energy is simply to renormalize the tunneling amplitude J in the large-ω limit. This "Dynamical Localization" phenomena has been observed in experiments[165, 166], and it has been proposed to be used as a method to tune interacting bosons through superfluid-insulator transition[159, 161], to observe the analog of photon-assisted tunneling[160], etc. For our purpose, it suffices to notice that the original potential energy V now resides in the renormalization factor of the hopping amplitude. Thus, if one modulates an Anderson insulator in a one-dimensional lattice instead, one expects that the randomness in the onsite energy should be transferred into the randomness of hopping amplitude in the same way. In other words, one obtains the random hopping model by fast-modulating the disordered potential energies of an Anderson insulator. We will demonstrate these ideas in detail in Chapter 5.

Chapter 2

Effect of Inhomogeneous Coupling On BCS Superconductors

2.1 Introduction

As discussed in Chapter 1, motivated by the thin-film physics, the experimental work in Ref. [49] studied a thin SN bilayer system, and found a surprisingly low value of the ratio of the energy gap to T_c, in contradiction to standard BCS theory, and the theory of proximity [50, 51, 52] where it is claimed that the energy gap-T_c ratio should be bounded from below by ~ 3.52. A drop below this bound, $2E_g/T_c < 3.52$, was also observed in amorphous Bi films as it approaches the disorder tuned SIT [27, 30]. Similar trends were also observed in SN bilayers in Ref. [47] and in amorphous tin films in Ref. [46].

In this Chapter we show that a reduction of the $2E_g/T_c$ ratio in a dirty superconductor could be explained as a consequence of inhomogeneity in the pairing interaction. In SN bilayer thin films, thickness fluctuations of either layer result in effective pairing inhomogeneity (in thin SN bilayers the effective pairing is the volume averaged one, c.f., Ref. [51, 52] and Sec. 2.4). Such inhomogeneities in other systems occur due to grain boundaries, dislocations, or compositional heterogeneity in alloys[170]. For simplicity we will assume in our analysis that the pairing coupling constant takes a one-dimensional modulating form:

$$U(\vec{r}) = \bar{U} + U_Q \cos(Qx). \tag{2.1}$$

In bilayer SN films, the effect of localization and Coulomb interaction is minor compared to proximity effect, and therefore we will neglect these complications in this chapter.

In our results, the ratio between the inhomogeneity length, $L \equiv 1/Q$, and the superconducting coherence length ξ, plays a crucial role. When $Q\xi \gg 1$, the superconducting properties are determined by an effective coupling $\bar{U} \lesssim U_{eff} < \bar{U} + U_Q$ [171]. In this limit, the ratio $2E_g/T_c$ is preserved at the standard BCS value ~ 3.52. Small corrections are obtained when $1/(Q\xi)$ is finite. In the opposite limit, $Q\xi \ll 1$, the system tends to be determined by the local value of $U(x)$. Within mean field theory, the ratio $2E_g/T_c$ is generally suppressed from the BCS value 3.52; in 2d, however, when one includes the thermal phase fluctuation and studies the Kosterlitz-Thouless temperature, T_{KT}, the ratio $2E_g/T_{KT}$ can be larger than the usual BCS value. These results on $2E_g/T_c$ are summarized in FIG. 2.6.

Our analysis is inspired by similar previously studied models. Particularly, the T_c of the clean case of this model has been analyzed in Ref. [171]. Here we extend the study of non-uniform pairing to both T_c and zero-temperature properties of disordered films, in the regime where the electron mean free path l obeys $1/k_F \ll l \ll \xi_0 \sim \frac{\hbar v_F}{T_c}$, which is relevant to the experiments of Long et al.[48, 49]. Note that while Anderson theorem states that the critical temperature and gap of a homogenous superconductor do not depend on disorder[10], in an inhomogeneous system the theorem does not hold. Indeed, we find that the results of Ref. [171], are modified in the dirty case. In another related work, a system with a Gaussian distribution of the inverse pairing interaction was studied [172, 173]. It was shown that an exponentially decaying subgap density of states appears due to mesoscopic fluctuations which lie beyond the mean field picture. Finally, inhomogeneous coupling in the attractive Hubbard model [174, 175] and lattice XY model [176] were also analyzed, with relevance to High-T_c materials.

This chapter is adapted from our published work Ref. [177], and it is organized as follows. In Sec. 2.2 we review the quasiclassical Green's function formalism which we use, and briefly demonstrate how it works for the usual dirty superconductors

with spatially uniform coupling constant. Then, in Sec. 2.3 we discuss the cases with nonuniform coupling classified by the competition of two length scales: the coherence length ξ and the length scale associated with the variation of the coupling constant $L = 1/Q$. We will also discuss the effect of other types of inhomogeneities briefly. In section 2.4 we provide a useful analogy with superconductor-normal metal superlattice to provide more physical intuition about our results on the energy gaps. In section 2.5 we will summarize our analysis and discuss the connection with experimental results.

2.2 The gap equation of a nonuniform film

The starting point of our analysis is the standard s-wave BCS Hamiltonian:

$$\begin{aligned} H &= H_0 + H_{int} + H_{imp}, \\ H_0 &= \sum_\sigma \psi^\dagger_\sigma(\vec{r})\hat{\xi}\psi(\vec{r})_\sigma, \\ H_{int} &= -U(\vec{r})\psi^\dagger_\downarrow(\vec{r})\psi^\dagger_\uparrow(\vec{r})\psi_\uparrow(\vec{r})\psi_\downarrow(\vec{r}), \end{aligned} \tag{2.2}$$

where $\hat{\xi} \equiv -\frac{\nabla^2}{2m} - \mu$, and $U(\vec{r}) > 0$ is the attractive coupling constant between electrons, and H_{imp} includes scattering with nonmagnetic impurities. When the pairing interaction, $U(\vec{r})$, is nonuniform, so is the order parameter in this system. A standard technique to tackle this non-uniform superconductivity problem is the quasiclassical Green's functions [178, 12, 179]. In the dirty limit $\ell \ll \xi_0 \sim \frac{\hbar v_F}{T_c}$, the quasiclassical Green's functions obey a simple form of the Usadel equation, which in the absence of a phase gradient is:

$$\frac{D}{2}\left(-\nabla^2\theta\right) = \Delta\cos\theta - \omega_n \sin\theta, \tag{2.3}$$

where $D = \frac{1}{d}v_F l$ is the diffusion constant, l is the mean free path, d is the spatial dimension, and Δ is the superconducting order parameter. θ is a real function of space and Matsubara frequencies ω_n and is a parametrization of the quasiclassical

Green functions g and f:

$$g = \cos\theta, f = f^{\dagger} = -i\sin\theta. \tag{2.4}$$

Also, we list the relation between the integrated quasiclassical Green's function and Gor'kov's Green's function G and F:

$$g(\vec{r}) = \int \frac{d\Omega_p}{4\pi} \int \frac{d\xi_p}{i\pi} G(\vec{r},\vec{p}) = \frac{1}{i\pi N_F} \int \frac{d^3p}{(2\pi)^3} G(\vec{r},\vec{p}),$$

$$f(\vec{r}) = \int \frac{d\Omega_p}{4\pi} \int \frac{d\xi_p}{i\pi} F(\vec{r},\vec{p}) = \frac{1}{i\pi N_F} \int \frac{d^3p}{(2\pi)^3} F(\vec{r},\vec{p}),$$

where $\vec{r}$ is the center of mass coordinate, and $\vec{p}$ is momentum corresponding to the relative coordinate; Ω_p is the angle of momentum $\vec{p}$ and N_F is the density of states (per spin) of the normal state at the Fermi energy. The self-consistency equation reads:

$$\Delta(\vec{r}) = U(\vec{r}) N_F \pi T \sum_n i f_{\omega_n}(\vec{r}). \tag{2.5}$$

For simplicity we assume the pairing is as given in Eq. (2.1),

$$U(\vec{r}) = \bar{U} + U_Q \cos(Qx).$$

2.2.1 The uniform pairing case

Before analyzing the inhomogeneous pairing problem, let us briefly review the calculation of T_c, the superconducting order parameter $\Delta(T=0)$, and the DOS $\nu(E)$ of a dirty superconductor with a spatially uniform coupling constant U, using quasiclassical Green's functions. In this case Eqs. (2.3) and (2.5) admit a uniform solution for both θ and Δ:

$$\theta = \arctan\left(\frac{\Delta}{\omega_n}\right). \tag{2.6}$$

Using (2.5), we obtain the standard BCS self-consistency equation:

$$1 = UN_F\pi T\sum_n \frac{1}{\sqrt{\Delta^2+\omega_n^2}}. \tag{2.7}$$

T_c and $\Delta(T=0)$ are easily obtained from (2.7):

$$T_c = \frac{2C}{\pi}\omega_D e^{-\frac{1}{UN_F}}, \Delta_{(T=0)} = 2\omega_D e^{-\frac{1}{UN_F}}.$$

where $C = e^\gamma \approx 1.78$, with $\gamma = 0.5772\ldots$ the Euler constant, and ω_D the Debye frequency. The DOS can be obtained from the retarded quasiclassical Green's function: $\nu(E) = \mathrm{Re}\{g^R(E)\}$, which can be obtained from $g(\omega_n) = \cos(\theta_n)$ by analytical continuation $i\omega \to E + i0^+$:

$$\nu(E) = \mathrm{Re}\frac{-iE}{\sqrt{\Delta^2-(E+i0^+)^2}} = \begin{cases} \frac{E}{\sqrt{E^2-\Delta^2}}, & \text{if } E>\Delta \\ 0, & \text{if } E<\Delta \end{cases}.$$

Thus there exists a gap in the excitation spectrum $E_g = \Delta$, and its ratio with T_c is a universal number $\pi/C \approx 1.76$. As expected, these results for dirty superconductors are exactly the same as those of clean superconductors, thus explicitly illustrating Anderson theorem.

2.3 The case of inhomogeneous pairing

Using the formalism reviewed in the previous section, we now discuss the non-uniform superconducting film. Our discussion will concentrate on the limits of fast and slow pairing modulations, i.e., large and small $Q\xi$ respectively (ξ is the zero temperature coherence length in the dirty limit: $\xi = \sqrt{\hbar D/\bar{\Delta}_{T=0}} \sim \sqrt{\hbar D/T_c}$, where $\bar{\Delta}$ is the spatially averaged $\Delta(x)$).

2.3.1 Fast pairing modulation: proximity enhanced superconductivity

With a nonuniform coupling $U(x)$, uniform solution of either $\theta(x)$ or $\Delta(x)$ no longer exists. When fast pairing modulation are present, the angle θ is dominated by its $k = 0$ Fourier component, θ_0, since it can not respond faster than its characteristic length scale ξ. Corrections to the uniform solution are of the form $\theta_1 \cos(Qx)$, and are suppressed by powers of $\frac{1}{Q\xi}$. From Eq. (2.5), we see that in contrast to θ, the order parameter $\Delta(x)$ has a factor of $U(x)$ in its definition, and therefore it can fluctuate with the fast modulation of $U(x)$. The modulating component of $\Delta(x)$ is thus only suppressed by $U_Q/\bar{U}$, while the modulating part of $\theta(x)$ is suppressed by both $U_Q/\bar{U}$ and $1/(Q\xi)$. Keeping both $1/Q\xi \ll 1$ and expanding in $U_Q/\bar{U}$, we can perturbatively solve Eqs. (2.3) and (2.5). Starting with:

$$\Delta(x) = \Delta_0 + \Delta_1 \cos(Qx), \theta(x) = \theta_0 + \theta_1 \cos(Qx); \tag{2.8}$$

Eq. (2.3) can be solved order by order:

$$\begin{aligned} \theta_0 &= \arctan\left(\frac{\Delta_0}{\omega_n}\right), \\ \theta_1 &= \Delta_1 \frac{\omega_n}{\frac{D}{2}Q^2\sqrt{\omega_n^2+\Delta_0^2}+\omega_n^2+\Delta_0^2}. \end{aligned} \tag{2.9}$$

The self-consistency equation (2.5) can be Fourier transformed:

$$\begin{aligned} \Delta_0 &= N_F \pi T \sum_{\omega_n} \left(\bar{U}\sin\theta_0 + 2\frac{U_Q}{2}\frac{\cos\theta_0}{2}\theta_1\right), \\ \frac{\Delta_1}{2} &= N_F \pi T \sum_{\omega_n} \left(\bar{U}\frac{\cos\theta_0}{2}\theta_1 + \frac{U_Q}{2}\sin\theta_0\right), \end{aligned} \tag{2.10}$$

where the ω_n index of θ_0 and θ_1 is implicit.

When $T \to T_c$, we can linearize θ_0 and θ_1 with respect to Δ_0 and Δ_1, respectively:

$$\sin\theta_0 \approx \frac{\Delta_0}{|\omega_n|}, \quad \theta_1(\cos\theta_0) \approx \frac{\Delta_1}{|\omega_n| + \frac{DQ^2}{2}}.$$

Note that

$$\sum_{n=0}^{N_0} \frac{1}{n+1/2} \approx \ln N_0 + 2\ln 2 + \gamma \text{ for } N_0 \gg 1, \tag{2.11}$$

where γ is the Euler constant, we have approximately

$$\begin{aligned} 2\pi T \sum_{\omega_n=0}^{\frac{\omega_D}{2\pi T}} \frac{1}{\omega_n} &\approx \ln(2C\omega_D/\pi T), \\ 2\pi T \sum_{\omega_n=0}^{\frac{\omega_D}{2\pi T}} \frac{1}{\omega_n + DQ^2/2} &\approx \ln\left(1 + \frac{\omega_D}{DQ^2/2}\right), \end{aligned} \tag{2.12}$$

where, as before, $C = e^\gamma \approx 1.78$ and ω_D is the Debye frequency. Defining

$$K_0 = \bar{U} N_F \ln(2C\omega_D/\pi T), \quad K_1 = \bar{U} N_F \ln\left(1 + \frac{2\omega_D}{DQ^2}\right), \tag{2.13}$$

we get

$$\begin{aligned} \Delta_0 &= K_0\Delta_0 + \frac{1}{2}\frac{U_Q}{\bar{U}} K_1 \Delta_1, \\ \Delta_1 &= \frac{U_Q}{\bar{U}} K_0 \Delta_0 + K_1 \Delta_1. \end{aligned}$$

T_c is the temperature at which this equation admits a nonzero solution:

$$T_c = \frac{2C}{\pi}\omega_D \exp\left(-\frac{1}{U_{eff} N_F}\right), \tag{2.14}$$

where the effective pairing strength is:

$$U_{eff} = \bar{U}\left(1 + \left(\frac{U_Q}{\bar{U}}\right)^2 \frac{K_1}{2(1-K_1)}\right). \tag{2.15}$$

This is the dirty case analogue of the result obtained by Ref. [171].

Next we turn to the order parameter. At $T = 0$ the sums in the self-consistency

equations (2.10) become integrals, which can be performed (see also Appendix 2.A):

$$\begin{aligned}\Delta_0 &= N_F\bar{U}\Delta_0 \ln\left(\frac{2\omega_D}{\Delta_0}\right) + \frac{1}{2}\frac{U_Q}{\bar{U}}K_1\Delta_1, \\ \frac{\Delta_1}{2} &= \frac{K_1\Delta_1}{2} + \frac{N_F U_Q}{2}\Delta_0 \ln\left(\frac{2\omega_D}{\Delta_0}\right),\end{aligned} \tag{2.16}$$

thus giving the solution

$$\begin{aligned}\Delta_{0(T=0)} &= 2\omega_D \exp\left(-\frac{1}{U_{eff}N_F}\right), \\ \Delta_{1(T=0)} &= \Delta_{0(T=0)}\frac{U_Q}{U_{eff}}\frac{1}{1-K_1}.\end{aligned}$$

with the same U_{eff} defined in (2.15). Noting that Δ_0 is the spatially averaged value of the order parameter $\bar{\Delta}$, we arrive at the conclusion that in the limit $Q\xi \gg 1$, the ratio

$$\frac{2\bar{\Delta}}{T_c} = \frac{2\Delta_{0(T=0)}}{T_c} = \frac{2\pi}{C} \tag{2.17}$$

is preserved.

The modification of the gap, however, must be addressed separately. Although the gap and the order parameter coincide for a uniform BCS superconductor, this is not generally true in a nonuniform superconductor. To obtain the DOS and the gap one has to rephrase the problem in a real-time formalism and calculate the retarded Green's function which is parameterized by a complex $\theta(x,E) = \theta'(x,E) + i\theta''(x,E)$ with both θ', θ'' real, and then compute the DOS via $\nu(x,E) = \mathrm{Re}g^R(x,E) = \mathrm{Re}\cos\theta(x,E) = \cos\theta'\cosh\theta''$[12, 179]. Naively one can perform the prescription $i\omega \to E + i0^+$ in the imaginary time Green's functions to obtain the retarded ones, but our perturbative solution will break down as E approaches Δ_0, since θ_1 diverges faster than θ_0. Therefore to analyze the gap one has to re-solve the real time counterpart of equation (2.3) with $\Delta(x)$ given above. Note that our solution of $\Delta(x)$ is still valid, sparing us the need to solve the self-consistency equation.

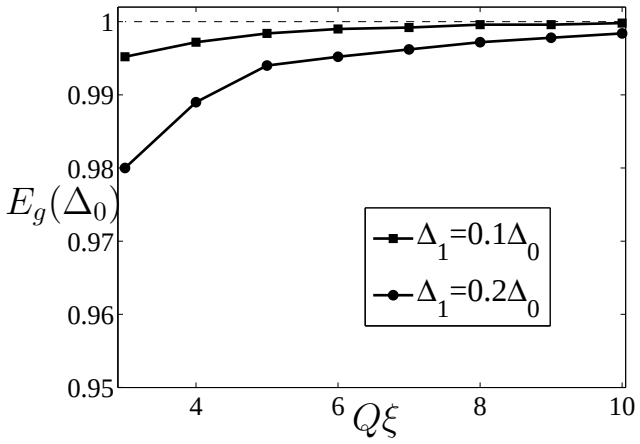

Figure 2.1: The energy gap, E_g, measured in units of Δ_0, vs. $Q\xi$ for $Q\xi \gg 1$. The two curves are for $\Delta_1/\Delta_0 = 0.1$ and 0.2, respectively. Here, Δ_0 and Δ_1 are the uniform and oscillating components of the order parameter, respectively. Q is the modulating wavevector of the inhomogeneous coupling constant; ξ is the superconducting coherence length. The estimated numerical error of E_g/Δ_0 is about 0.01. The deviation of E_g from Δ_0 is small, but it increases with larger Δ_1/Δ_0 or smaller $Q\xi$.

In real time, Eq. (2.3) becomes:

$$\begin{aligned} -\frac{D}{2}\partial_x^2\theta' &= \cos\theta'(\Delta\cosh\theta'' - E\sinh\theta''), \\ \frac{D}{2}\partial_x^2\theta'' &= \sin\theta'(\Delta\sinh\theta'' - E\cosh\theta''). \end{aligned} \tag{2.18}$$

We numerically solved these coupled equations with periodic boundary condition on $[0, 2\pi/Q]$, and computed the DOS $\nu(E) = \cos\theta_1 \cosh\theta_2$, and thereby obtained the gap. We find that despite the fluctuating $\Delta(x)$, the energy gap, E_g, is spatially uniform. Fig. 2.1 shows a graph of E_g vs. $Q\xi$ for $\Delta_1/\Delta_0 = 0.1$ and 0.2. Again, in the plot we define the coherence length ξ to be $\sqrt{\hbar D/\bar{\Delta}_{T=0}} = \sqrt{\hbar D/\Delta_{0,T=0}}$. One can see that in the limit $Q\xi \to \infty$ E_g coincides with Δ_0, and nonzero $1/(Q\xi)$ brings about only small corrections to make the gap slightly smaller than Δ_0. These corrections increase with smaller $Q\xi$ or larger $U_Q/\bar{U}$ (i.e., Δ_1/Δ_0). Thus we find that for $Q\xi \gg 1$ case

$$\frac{2E_{g(T=0)}}{T_c} \lesssim \frac{2\Delta_{0(T=0)}}{T_c} = \frac{2\pi}{C} = 3.52. \tag{2.19}$$

It is easy to understand the uniformity of E_g, since the wave function of a quasiparticle excitation should be extended on a length scale $1/Q \ll \xi$. Some intuition for the fact that $E_g \approx \Delta_0$ is provided in Sec. 2.4.

2.3.2 Slow pairing fluctuations: WKB-like local superconductivity

When the pairing strength fluctuates slowly, i.e., over a large distance, both the Green's functions and the order parameter $\Delta(x)$ can vary on the length scale of $1/Q$, and we can approximate the zeroth order solution by a 'local solution':

$$\theta_0(x) = \arctan\left(\frac{\Delta(x)}{\omega_n}\right), \tag{2.20}$$

where $\Delta(x)$ is to be solved from the self-consistency equation. This 'local' property of the system implies a large spatial variation of both $\Delta(x)$ and $\theta(x)$, in contrast to the $Q\xi \gg 1$ case. To improve the zeroth order solution, we write $\theta(x) = \theta_0(x) + \theta_1(x)$. Neglecting the small gradient term of θ_1, one can solve for θ_1 from Usadel's equation (2.3) :

$$\theta_1 = \frac{D}{2}\left(\frac{\omega_n \partial_x^2 \Delta}{(\Delta^2+\omega_n^2)^{3/2}} - \frac{2\Delta\omega_n(\partial_x\Delta)^2}{(\Delta^2+\omega_n^2)^{5/2}}\right), \tag{2.21}$$

thus the self-consistency equation (2.5) becomes

$$\Delta(x) = U(x)N_F 2\pi T \sum_{n=0}^{\frac{\omega_D}{2\pi T}} \left(\frac{\Delta}{\sqrt{\Delta^2+\omega_n^2}} + \frac{\omega_n}{\sqrt{\Delta^2+\omega_n^2}}\theta_1\right). \tag{2.22}$$

In the Ginzburg-Landau regime, one is justified in keeping lowest order terms in (2.22):

$$\Delta(x) = U(x)N_F\left\{\Delta(x)\ln\left(\frac{2C\omega_D}{\pi T}\right) - \frac{7\zeta(3)}{8\pi^2T^2}\Delta^3(x) + \frac{\pi\hbar D}{8T}\partial_x^2\Delta(x)\right\}, \tag{2.23}$$

where $\zeta(n)$ is the Riemann ζ function. Remarkably, equation (2.23) is nothing but the Ginzburg-Landau equation for a modulating coupling constant $U(x)$ with $Q\xi \ll 1$, and is precisely the dirty case analogue of equation (9) in Ref. [171], with ξ replaced by the dirty limit expression $\tilde{\xi}^2 = \hbar\pi D/8T$ ($\tilde{\xi}$ is slightly different from the coherence length defined in this work $\xi \equiv \sqrt{\hbar D/\bar{\Delta}_{T=0}}$, where $\bar{\Delta}$ is the spatially averaged $\Delta(x)$). In the limit $Q\xi \to 0$, $\Delta(x)$ would be determined only by the local value of $U(x)$, and the mean field transition temperature would be given by $T_{c,max} = 2C\omega_D/\pi \exp(-1/(\bar{U}+U_Q))$. A small but nonzero $Q\xi$ leads to a weak coupling between spatial regions, hence slightly reducing the mean field T_c. Following the analysis of Ref. [171], one obtains the mean field transition temperature:

$$T_c^{MF} \approx \frac{2C\omega_D}{\pi} e^{-1/N_F(\bar{U}+U_Q)} e^{-\tilde{\xi}QA/\sqrt{2}}, \tag{2.24}$$

where $A \equiv \sqrt{U_Q/(N_F\bar{U}^2)}$.

Although the inhomogeneous $U(x)$ largely increases the mean field T_c, it also makes the system more susceptible to phase fluctuations. This effect will be more pronounced in a two-dimensional superconductor, which we will focus on now. A film becomes superconducting through a Kosterlitz-Thouless transition. To determine the Kosterlitz-Thouless transition temperature, T_{KT}, we note that the Ginzburg-Landau free energy corresponding to (2.23) is

$$\begin{aligned} F(\Delta(x)) &= N_F \int d^3x \{\alpha(x)\Delta^2(x) + \frac{\beta}{2}\Delta^4(x) \\ &+ \gamma(\partial_x\Delta)^2)\}, \\ \alpha(x) &= \frac{1}{N_F U(x)} - \ln\left(\frac{2\times 1.78\omega_D}{\pi T}\right), \\ \beta &= \frac{7\zeta(3)}{8\pi^2 T^2}, \gamma = \frac{\pi\hbar D}{8T}. \end{aligned} \tag{2.25}$$

As a functional of $\Delta(x)$, F can be minimized numerically, thus giving a solution of $\Delta(x)$. The free energy cost for phase fluctuations is approximately $F =$

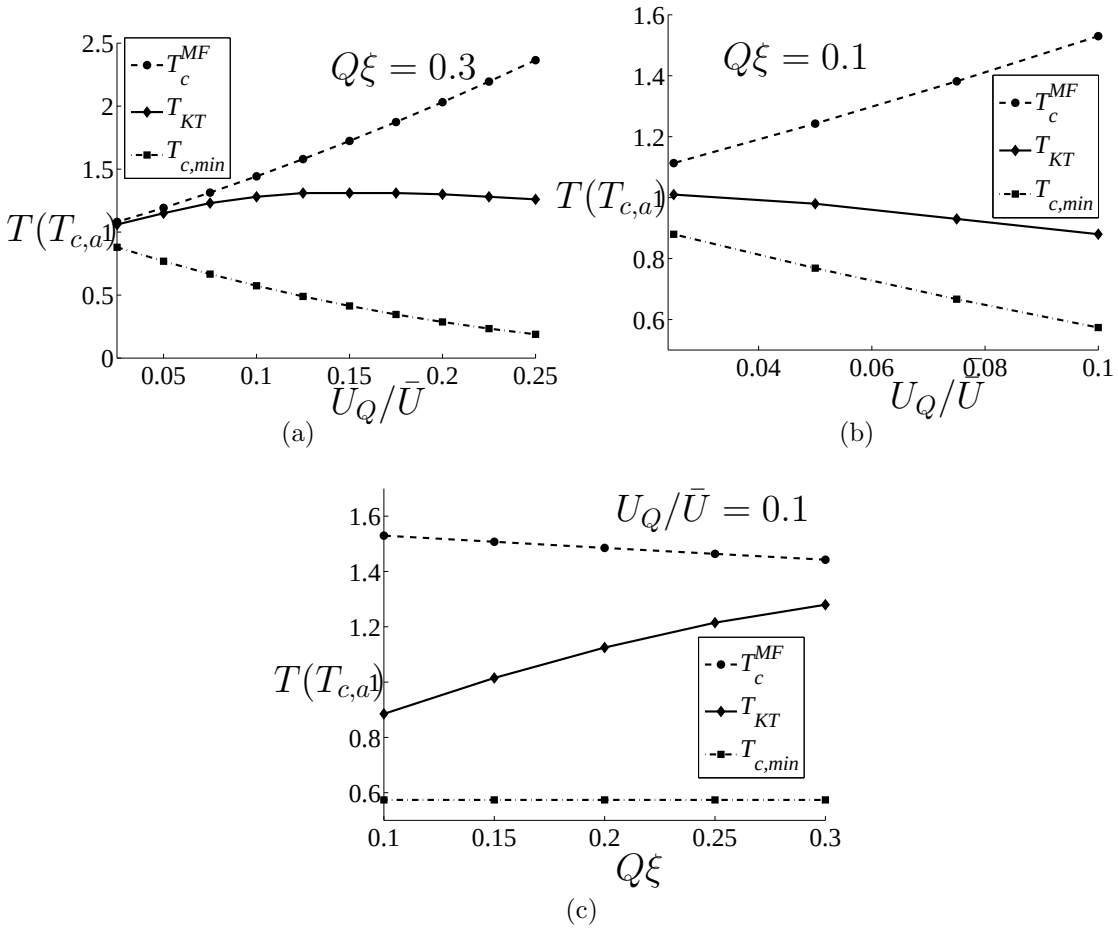

Figure 2.2: The mean field transition temperature T_c^{MF}, the Kosterlitz-Thouless temperature T_{KT}, and the minimum mean field transition temperature $T_{c,min} = \frac{2C}{\pi}\omega_D e^{-1/N_F(\bar{U}-|U_Q|)}$ (a) vs. $U_Q/\bar{U}$ with $Q\xi = 0.3$; (b) vs. $U_Q/\bar{U}$ with $Q\xi = 0.1$; (c) vs. $Q\xi$ with $U_Q/\bar{U} = 0.1$. In all cases $\bar{U}N_F = 0.2$. T is in units of $T_{c,a} \equiv \frac{2C}{\pi}\omega_D e^{-1/N_F\bar{U}}$. Here, $\bar{U}$ and U_Q are the uniform and oscillating components of the coupling constant, respectively. N_F is the density of states of the normal state; Q is the modulating wavevector of the inhomogeneous coupling constant; ξ is the superconducting coherence length. The estimated numerical error of $T_{KT}/T_{c,a}$ is about 0.01.

$\frac{1}{2}\int d^2x J(x)(\nabla\theta)^2$. For quasi-2d films,

$$J(x) = 2N_\perp N_F^{2d}\tilde{\xi}^2|\Delta_{MF}(x)|^2, \tag{2.26}$$

where N_F^{2d} is the 2d electron DOS, $N_\perp$ is the number of channels, $\tilde{\xi} \equiv \sqrt{\frac{\pi\hbar D}{8T}}$, and Δ_{MF} is the mean field solution of (2.25). To explain the bilayer thin film experiments investigated by Long et al.[48, 49], we use the measured value of the diffusion constant $D = 5\times10^{-3}m^2s^{-1}$ (see Ref. [48]), and estimate $N_\perp = k_F d/\pi \approx 50$, where the film thickness $d \approx 10 \sim 20$nm[48, 49], and the Fermi wave vector $k_F \sim 1 Angstrom^{-1}$. As in Ref. [171], one can estimate T_{KT} self-consistently from

$$T_{KT} = \frac{\pi}{2}\sqrt{\overline{J(x)}(\overline{1/J(x)})^{-1}}, \tag{2.27}$$

since $\overline{J(x)}$ is the stiffness along the "stripes", while $(\overline{1/J(x)})^{-1}$ perpendicular to the "stripes". Although our estimation of $N_\perp$ is crude, the value of T_{KT} is very insensitive to it. This is because T_{KT} is solved self-consistently from (2.27). If one attempts to use a larger $N_\perp$ in (2.26), the enhancement of T_{KT} is limited by $J(x)$ which itself is suppressed as temperature increases. Typical solutions of T_{KT} are shown in FIG. 2.2. One can see that the phase fluctuation region, i.e. the difference between T_c^{MF} and T_{KT}, increases with stronger inhomogeneity (FIG. 2.2(a) and (b)). Also for longer wave length modulation T_{KT} is reduced more strongly (FIG. 2.2(c)). Heuristically, this is because for smaller $Q\xi$ the superconducting stripes become farther apart, and therefore it is more difficult for them to achieve phase coherence.

Moving our focus to the zero-temperature order parameter and gap, we note that at $T = 0$ the integrals in equation (2.22) can be done:

$$\frac{\Delta(x)}{U(x)N_F} = \Delta(x)\ln\left(\frac{2\omega_D}{\Delta(x)}\right) + \frac{\pi D\partial_x^2\Delta}{8\Delta(x)} - \frac{\pi D(\partial_x\Delta)^2}{16\Delta^2(x)},$$

This can be approximately solved by:

$$\begin{aligned} \Delta(x) &\approx \Delta_0(x)e^{-\eta(x)}, \\ \Delta_0(x) &= 2\omega_D e^{-\frac{1}{N_F \bar{U}(x)}}, \\ \eta(x) &= \frac{\pi D}{8\Delta_0(x)} Q^2 A^2 \left(\cos(Qx) - \frac{1}{2}A^2 \sin^2(Qx)\right). \end{aligned} \tag{2.28}$$

Note that $\partial_x \Delta(x) \approx -A^2 Q \sin(Qx)\Delta(x)$ [with A defined under Eq. (2.24)], for our WKB analysis to be self-consistent, we need to require the that $A \lesssim \mathcal{O}(1)$, thus $U_Q/\bar{U}$ needs to be small. Also, when this is satisfied, $\eta(x)$ leads to a slight averaging between $\Delta(x)$, which is a manifestation of proximity effect.

To analyze the gap, we must switch to a real time formalism again, since our perturbative solution for the Green's function becomes invalid as $E \to \Delta(x)$. Thus we have to solve the real time Usadel equation (2.18) with $\Delta(x)$ obtained above. Using the same numerical code as in Sec. 2.3.1, we have obtained the local gap $E_g(x)$, which is plotted vs. x in FIG. 2.3 for half a period of modulation. One can see that in general $E_g(x)$ is lower than $\Delta(x)$, and when $Q\xi = 0.3$, $E_g(x)$ is largely set by the region with weakest coupling; but when $Q\xi \to 0$, $E_g(x)$ tends to follow much closer to $\Delta(x)$ as expected. In addition, the minimum of $E_g(x)$ is always slightly higher than the minimum of $\Delta(x)$ by an amount that also diminishes upon $Q\xi \to 0$. This behavior will be further clarified in the next section.

The ratio $\bar{E}_g/\bar{\Delta}$ vs. $U_Q/\bar{U}$ or $Q\xi$ is plotted in FIG. 2.4. The suppression of the gap strengthens when either the inhomogeneity becomes stronger ($U_Q/\bar{U}$ is large) or its length scale $L \sim 1/Q$ becomes smaller, consistent the results in FIG. 2.3. The $\bar{E}_g$ suppression relative to $\bar{\Delta}$, together with the fact the T_c^{MF} is largely determined by strongest-coupling region, implies that the ratio $2\bar{E}_g/T_c^{MF}$ is generically reduced. The ratios $2\bar{E}_g/T_c^{MF}$ and $2\bar{E}_g/T_{KT}$ are plotted in FIG. 2.5 for several representative cases. As expected, there is always a strong suppression of the ratio $2\bar{E}_g/T_c^{MF}$ from 3.52; for a two-dimensional system, however, the ratios with T_{KT} are more subtle: for very small $Q\xi$ the ratio $2\bar{E}_g/T_{KT}$ might be enhanced due to the large deviation of T_{KT} from T_c^{MF} (see also FIG. 2.2(c)), while for larger value of $Q\xi$ the phase fluctuation

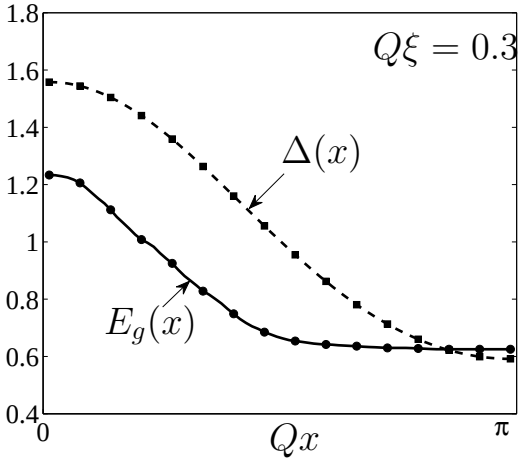

(a)

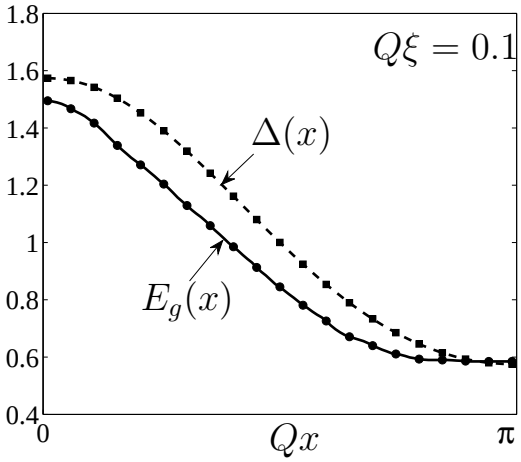

(b)

Figure 2.3: The local order parameter $\Delta(x)$ and the local gap $E_g(x)$ (in units of $\Delta(U_Q = 0) = 2\omega_D e^{-1/\bar{U}N_F}$) vs. spatial coordinate $x \in [0, \pi/Q]$. $Q\xi = 0.3$ and 0.1 in subfigure (a) and (b), respectively. $\bar{U}N_F = 0.2$, $U_Q N_F = 0.02$. Here, $\bar{U}$ and U_Q are the uniform and oscillating components of the coupling constant, respectively. N_F is the density of states of the normal state; Q is the modulating wavevector of the inhomogeneous coupling constant; ξ is the superconducting coherence length. The estimated numerical error of $E_g(x)$ is about 0.01.

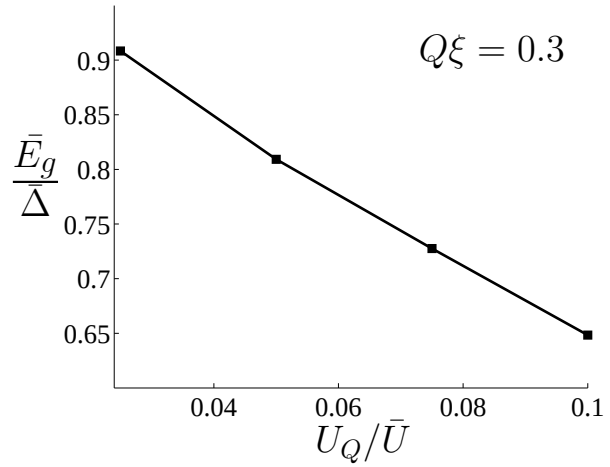

(a)

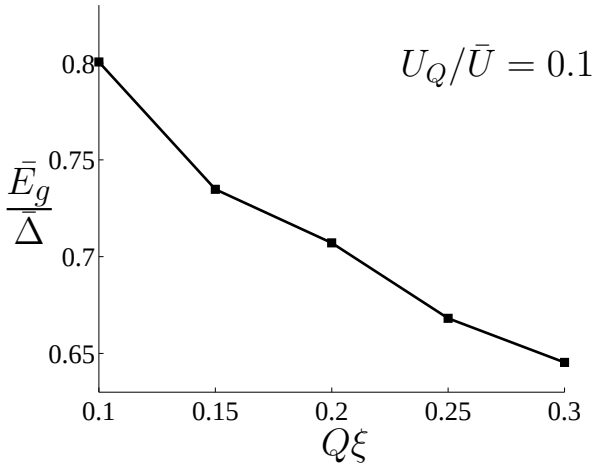

(b)

Figure 2.4: The ratios of the spatially averaged gap $\bar{E}_g$ to the spatially averaged $\bar{\Delta}$ (a) vs. $U_Q/\bar{U}$ with $Q\xi = 0.3$; (b) vs. $Q\xi$ with $U_Q/\bar{U} = 0.1$. $\bar{U}N_F = 0.2$ in all cases. Here, $\bar{U}$ and U_Q are the uniform and oscillating components of the coupling constant, respectively. N_F is the density of states of the normal state; Q is the modulating wavevector of the inhomogeneous coupling constant; ξ is the superconducting coherence length. The estimated numerical error is about 0.01.

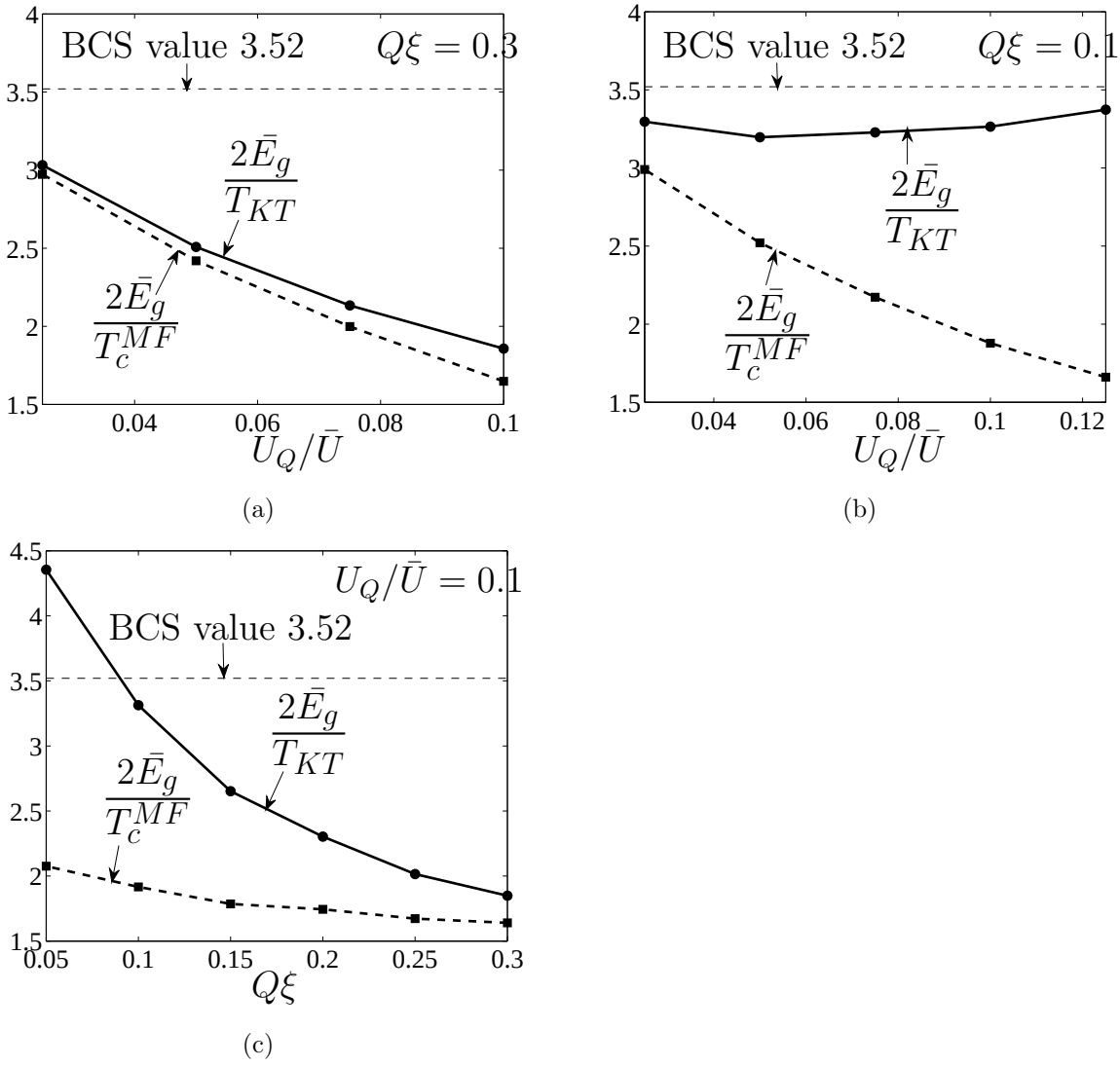

Figure 2.5: The ratios of the spatially averaged gap $\bar{E}_g$ to T_c^{MF} or T_{KT} (a)vs. $U_Q/\bar{U}$, $Q\xi = 0.3$; (b) vs. $U_Q/\bar{U}$, $Q\xi = 0.1$; (c) vs. $Q\xi$, $U_Q/\bar{U} = 0.1$. In all cases $\bar{U}N_F = 0.2$. Here, $\bar{U}$ and U_Q are the uniform and oscillating components of the coupling constant, respectively. N_F is the density of states of the normal state; Q is the modulating wavevector of the inhomogeneous coupling constant; ξ is the superconducting coherence length. The estimated numerical error is about 0.02.

region is narrow(see also FIG. 2.2(a)), and $2\bar{E}_g/T_{KT}$ is reduced from 3.52.

For the purpose of comparison with the thin film experiments, a comment on the determination of T_c^{MF} and T_{KT} is in order. Due to disorder and phase fluctuations, the resistive transition curve can be significantly broadened. T_c^{MF} can be estimated as the temperature at which the resistance drops to half of its normal state value, while T_{KT} can be defined as the temperature at which the resistance drops below the measurement threshold (see, for example, Ref. [32]). Alternatively, one can extract T_c^{MF} from fitting the fluctuation resistance to Aslamazov-Larkin theory[180], and obtain T_{KT} from nonlinear I-V characteristics or from fitting the resistance below T_c^{MF} to Halperin-Nelson form[181] (see, e.g., Refs. [182, 14]). Thus both T_c^{MF} and T_{KT} in principle can be measured from experiments, and can be used for comparison with our theoretical results here.

2.3.3 Additional inhomogeneities

Apart from modulation of the coupling U, one may also be interested in a simultaneous modulation of other properties. For example, in the small $Q\xi$ limit, one may expect the periodicity of U to be accompanied by a periodicity of the local density of states at the fermi level, or the mean free path. Another possible modulation, that of a periodic potential, is suggested in [171], and in practice is equivalent to local modulation of U. Indeed, one may use an effective description of the self consistency equation (2.5), taking $N_F \to N_F + N_Q \cos(Qx)$ to lowest order in the amplitude N_Q of the local DOS in the form:

$$\Delta(\vec{r}) = N_F U_{mod}(\vec{r}) \pi T \sum_n i f_{\omega_n}(\vec{r}). \tag{2.29}$$

where $U_{mod} = \overline{U} + \frac{N_Q \overline{U} + \overline{N_F} U_Q}{\overline{N_F}} \cos(Qx)$, and N_F is the spatially averaged DOS. Formally this is exactly the same as Eq. (2.1), and can be treated similarly, taking

$$U_Q \to \frac{N_Q \overline{U} + N_F U_Q}{N_F} \tag{2.30}$$

In practice, a local periodic potential may be imposed on the system externally by either acoustic means or an electromagnetic field. Thus it might be interesting to check the change in T_C of a superconductor in the presence of an acoustic wave experimentally.

Another possibility of interest is that along with U the electron mean-free path is modulated in the system. This can be naturally occurring if the periodicity in U is a consequence of spatial variation in the properties of the material used. Alternatively, one may obtain this case by a periodic doping of the superconductor.

In this case we may describe the system effectively by modification of the Usadel equation (2.3) to:

$$-\frac{1}{2}\nabla\cdot(D\nabla\theta) = \Delta\cos\theta - \omega_n\sin\theta, \tag{2.31}$$

and taking the diffusion coefficient D to be spatially dependent. Choosing $D = \overline{D} + D_Q\cos(Qx)$ and repeating the treatment above, we find that D_Q does not change the values of the Green's functions θ_0, θ_1 above (It however appears at higher orders of the equation), and so doesn't change the results of this chapter within this order.

2.4 Superconductor-normal-metal (SN) superlattice analogy

Some insight into the nature of the lowest-lying excitations for both large and small $Q\xi$ cases can be gained by considering a simplified system: superconductor-normal-metal-superconductor (SNS) junctions. First, consider a single SNS junction with length $L = 2\pi/Q$, and $\Delta(x) = \Delta$, 0 in the S, N part respectively. Andreev bound states will form in the normal metal, and the energy of these states can be obtained by solving Bogoliubov-de Gennes (BdG) equations for the clean case, or Usadel equations for the dirty case. In the limit $L \to 0$, the energy of the lowest-lying state is Δ, while in the opposite limit $L \gg \xi$, the (mini)gap is much smaller than Δ: in the clean case $E_g \sim v_F/L \sim (Q\xi)\Delta$ and in the dirty case the gap equals the Thouless energy $D/L^2 \sim (Q\xi)^2\Delta$ [51, 183, 184]. These states exponentially decay into the

superconductors for a distance $\sim \xi$.

Based on a single SNS junction, one can build an SN superlattice with alternating superconductor and normal metal, each with length $L = 2\pi/Q$, and $\Delta(x) = \Delta$, 0 in the S, N part respectively. If $L \gg \xi$, Andreev bound states remain localized in the normal regions with the gap much smaller than Δ. On the other hand if $L \ll \xi$, these states strongly mix with each other, and they form a tight-binding band. Therefore the gap, namely the lower band edge, is lower than Δ, and in the limit $Q\xi \to \infty$ it is precisely at $\Delta/2$, the averaged $\Delta(x)$ (see the analytical calculation by Ref. [185]). The SN superlattice thus allows a qualitative understanding of the gap's behavior in the problem we addressed above: if $Q\xi \gg 1$, all excitations are extended in space, with the uniform gap $E_g \approx \bar{\Delta}$; if $Q\xi \ll 1$, the lowest-lying excitations are localized in the weakest coupling regions whose gap is close to the minimum of $\Delta(x)$. This analogy also elucidates the features in FIG. 2.3: given a point in space x_0, $E_g(x_0)$ is generally lower than $\Delta(x_0)$, because the wave function of the low-lying excitations originating at a nearby region (within $\sim \xi$) with smaller $\Delta(x)$ are exponentially suppressed at x_0, and when ξ is smaller this effect is reduced; thus $E_g(x)$ follows closer to $\Delta(x)$ in the limit $Q\xi \to 0$. Finally, the difference between the minimum of $E_g(x)$ and the minimum of $\Delta(x)$ resembles the minigap in SN superlattice $\sim v_F/L$ or D/L^2, which approaches zero as $Q\xi \to 0$.

2.5 Summary and discussion

In this chapter we investigated the properties of dirty BCS superconductors with a fluctuating pairing coupling constant $U(x) = \bar{U} + U_Q \cos(Qx)$. Particularly, we analyzed the change in the mean field T_c, the zero-temperature order parameter $\Delta(x)$, and the energy gap in quasiparticle excitation $E_g(x)$ using the Usadel equation for quasiclassical Green's functions. In addition, we estimated the Kosterlitz-Thouless transition temperature T_{KT}. Our analysis found four different regimes:

(1) $Q\xi \to \infty$. In this case the mean field T_c and the spatially averaged order parameter $\bar{\Delta}$ are determined by the effective coupling constant $U_{eff} \gtrsim \bar{U}$ [see Eq. (2.15)].

Moreover, since in this regime any quasiparticle wavefunction is extended over the length scale $L = 1/Q$, the local energy gap E_g is uniform in space, and we found it to coincide with the spatially averaged $\bar{\Delta}$. The ratios $2\bar{\Delta}/T_c = 2E_g/T_c = 3.52$ maintain their universal BCS value.

(2) $Q\xi \gtrsim 1$. In this regime the physics is qualitatively the same as that of the previous case. The gap E_g, however, is smaller than $\bar{\Delta}$ by an amount that grows with decreasing $Q\xi$ or increasing $U_Q/\bar{U}$. Therefore $2\bar{E}_g/T_c \lesssim 3.52$ (see FIG. 2.1).

(3) $Q\xi \lesssim 1$. The system tends to divide into regions which behave according to the the local value of $U(x)$. Thus the mean field T_c is determined by the first formation of local superconductivity upon lowering temperature, and therefore T_c^{MF} is close to highest 'local T_c'. In contrast, the global energy gap or the spatially averaged local gap is largely determined by the region with smallest $U(x)$. Consequently, in this regime the ratio $2\bar{E}_g/T_c^{MF}$ is always suppressed from the universal BCS value, 3.52 (see FIG. 2.5a). Moreover, although the system is affected by phase fluctuations, in this regime T_{KT} is close to T_c^{MF} for small values of U_Q (see FIG. 2.2a). Thus $2\bar{E}_g/T_{KT}$ is also smaller than 3.52 (see FIG. 2.5a).

(4) $Q\xi \to 0$. As opposed to the previous regime, here phase fluctuations lead to a large suppression of T_{KT} relative to T_c^{MF} (see FIG. 2.2b). Although $2\bar{E}_g/T_c^{MF}$ is still below 3.52, the ratios $2\bar{E}_g/T_{KT}$ is close to or larger than 3.52 (see FIG. 2.5c).

The value of $2\bar{E}_g/T_c^{MF}$ and $2\bar{E}_g/T_{KT}$ vs. the entire range of $Q\xi$ is plotted schematically in FIG. 2.6, with regimes 1-4 explicitly labeled in the graph. Schematic results of T_c^{MF} and T_{KT} vs. $Q\xi$ are summarized in FIG. 2.7.

Finally, we discuss connections with thin film experiments [48, 49]. A straightforward realization of inhomogeneous coupling is in disordered superconductor-normal-metal (SN) bilayer thin films. In a homogeneous bilayer SN with thickness smaller than the coherence length ξ, mean field analysis yields that T_c and the energy gap E_g of the system are determined by the averaged coupling constant [50, 51, 52]

$$U_{eff} = \frac{d_S N_S}{d_S N_S + d_N N_N} U, \tag{2.32}$$

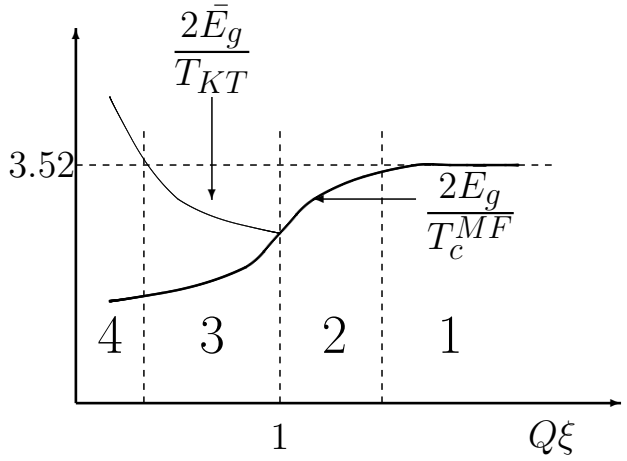

Figure 2.6: Schematic plot of the ratios $2\bar{E}_g/T_c^{MF}$ and $2\bar{E}_g/T_{KT}$ vs. $Q\xi$. Here $\bar{E}_g$ is the spatially averaged gap in local DOS; T_c^{MF} is the mean field T_c; T_{KT} is the Kosterlitz-Thouless transition temperature in 2d; Q is the modulating wavevector of the inhomogeneous coupling constant; ξ is the superconducting coherence length. 1,2,3, and 4 are labels of different regimes described in the text.

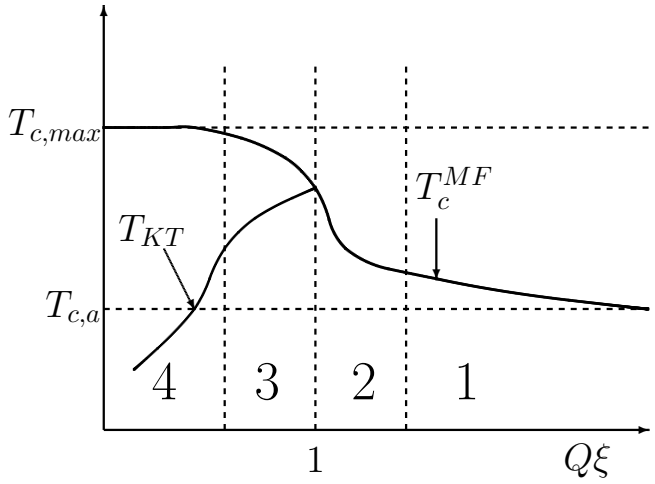

Figure 2.7: Schematic plot of the mean field transition temperature T_c^{MF} and the Kosterlitz-Thouless temperature T_{KT} vs. $Q\xi$, where Q is the modulating wavevector of the inhomogeneous coupling constant; ξ is the superconducting coherence length; $T_{c,max} = \frac{2C}{\pi}\omega_D e^{-1/N_F(\bar{U}+U_Q)}$ is the maximum T_c^{MF}; $T_{c,a} \equiv \frac{2C}{\pi}\omega_D e^{-1/N_F\bar{U}}$ is the mean field T_c for a uniform coupling $\bar{U}$. 1,2,3, and 4 are labels of different regimes described in the text. The qualitative feature of these results on T_c are similar to those of Ref. [171] on clean superconductors.

where U is the pairing coupling in the superconducting layer, d is the thickness, N is the DOS at the Fermi energy, and the subscripts S and N denote the superconductor and normal metal layers respectively. Thus the ratio $2E_{g(T=0)}/T_c$ is expected to remain at the BCS value $2\pi/C \approx 3.52$ in a homogeneous SN bilayers. Nevertheless, from (2.32) one observes that a spatially inhomogeneous thickness $d_{S,N}(x)$ (which is also consistent with the granular morphology of the sample[186]) leads to a nonuniform coupling $U(x)$ even if the original coupling U is homogeneous. Therefore thickness variation generically leads to a superconductor with inhomogeneous pairing coupling. According to our results, a deviation of $2E_g/T_c$ from 3.52 is expected in such a system.

Indeed our study was motivated by such observations. In Refs. [48, 49] Long et al. report measurements of recently fabricated a series of Pb-Ag bilayer thin films, with thickness $d_{Pb} = 4$nm and d_{Ag} increases from 6.7nm to 19.3nm. They observed a significant reduction of $2\bar{E}_g/T_c^{MF}$ from the expected value ~ 3.52, where $\bar{E}_g$ is the spatially averaged gap extracted from tunneling measurement of the DOS, and T_c^{MF} is measured as the temperature at which $R(T)$ drops to half of its normal state value, and the resistive transition is sharp and well-defined. This suppression of $2\bar{E}_g/T_c^{MF}$ is more pronounced in systems with thicker Ag thereby lower T_c^{MF}. In these samples with T_c^{MF} decreasing from 2.55K to 0.72K with increasing d_{Ag}, the ratio $2\bar{E}_g/T_c^{MF}$ decreases from ~ 3.6 to ~ 2.6 (see FIG 3(b) of Ref. [49]).

These results can be qualitatively well understood by our study. The reduction of $2E_g/T_c^{MF}$ from 3.52, together with the observed fact that the resistive transition is sharp and well-defined[48], implies that the experimental systems are in the regime (2) or (3) of our theoretical results summarized above (see FIG. 2.6). In these regimes both $2\bar{E}_g/T_c^{MF}$ and $2\bar{E}_g/T_{KT}$ are lower than 3.52, and the phase fluctuation is either absent or small enough to keep T_{KT} close to T_c^{MF}, explaining the sharp resistive transition. For samples with lower T_c, $\bar{U}$ is smaller. Therefore, if we assume roughly the same amount of U_Q for all samples, the effect of inhomogeneity will be stronger for samples with lower T_c samples, and, consequently, the gap-to-T_c ratio is even smaller for them. To make a rough comparison, we have calculated the gap-T_c ratio vs. $\bar{U}$ for fixed U_Q and plotted the results in FIG. 2.8. Although not claiming more

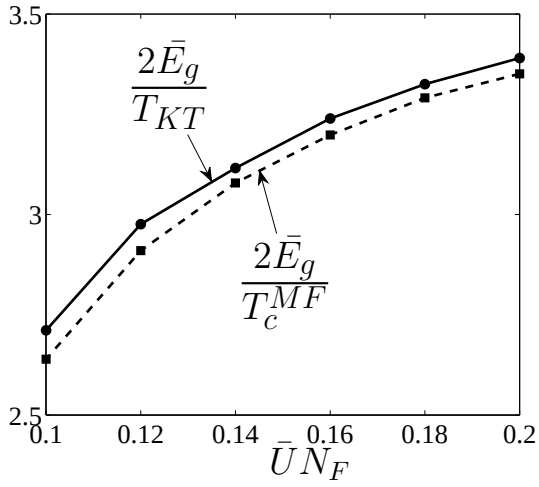

Figure 2.8: The ratios of the spatially averaged gap $\bar{E}_g$ to the mean field transition temperature T_c^{MF} or the Kosterlitz-Thouless transition temperature T_{KT} vs. $\bar{U}N_F$. $U_Q N_F = 0.002$, $Q\xi = 0.3$. Here, $\bar{U}$ and U_Q are the uniform and oscillating components of the coupling constant, respectively. N_F is the density of states of the normal state; Q is the modulating wavevector of the inhomogeneous coupling constant; ξ is the superconducting coherence length. Since T_c^{MF} monotonically increases with $\bar{U}$, this result resembles the experimental data of Ref. [49] (see FIG. 2.9 below for comparison), which shows that the lower the measured T_c of a thin-film bilayer is, the smaller the ratio $2E_g/T_c$.The estimated numerical error is about 0.02.

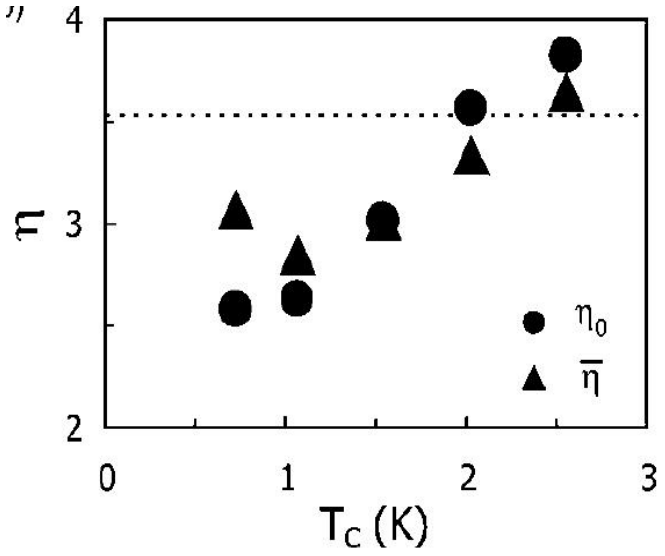

Figure 2.9: Experimentally measured gap-T_c ratio vs. T_c in Ref. [49]. Taken from Ref. [49].

than a qualitative explanation of the bilayer measurements, we note that our FIG. 2.8 resembles FIG. 3(b) of Ref. [49].

An interesting venue for future research, which may extend to more 2d superconducting systems, is to consider a general fluctuation of the pairing interaction, not restricted to a particular wave number, but rather having a particular correlation length. In addition, aside from the low gap-T_c ratio, Ref. [48] has also reported an unexpected subgap density of states of quasiparticles in the same bilayer materials. Although our current model does not produce this behavior, one expects that it could be explained by including large spatial fluctuations of the pairing interaction (e.g. $\frac{U_Q}{\bar{U}} \sim 1$), which strongly suppress the gap, and the effect of mesoscopic fluctuations which tend to produce subgap states[173].

2.A Calculation of $\Delta_{(T=0)}$ in the limit $Q\xi \gg 1$

Here we show some calculation details in deriving equation (2.16). At $T = 0$ the self-consistency equations are

$$\Delta_0 = N_F \bar{U} \left(\int_0^{\omega_D} d\omega \sin\theta_0 \right) + \frac{N_F U_Q}{2} \left(\int_0^{\omega_D} d\omega \theta_1 \cos\theta_0 \right);$$

$$\frac{\Delta_1}{2} = \frac{N_F \bar{U}}{2} \left(\int_0^{\omega_D} d\omega \theta_1 \cos\theta_0 \right) + \frac{N_F U_Q}{2} \left(\int_0^{\omega_D} d\omega \sin\theta_0 \right).$$

The evaluation of the integrals gives (define $a = \frac{DQ^2/2}{\Delta_0}$ and $x_0 = \omega_D/\Delta_0$):

$$\int_0^{\omega_D} d\omega \sin\theta_0 = \Delta_0 \operatorname{arcsinh}\left(\frac{\omega_D}{\Delta_0}\right) \approx \Delta_0 \ln\left(\frac{2\omega_D}{\Delta_0}\right);$$

$$\begin{aligned}\int_0^{\omega_D} d\omega\theta_1\cos\theta_0 &= \frac{\Delta_1}{2a}\{-2\arctan(x_0)+2a\,\mathrm{arcsinh}(x_0)\\ &- \sqrt{a^2-1}\left[\mathrm{arctanh}\left(\frac{x_0\sqrt{a^2-1}+1}{a\sqrt{x_0^2+1}}\right)\right.\\ &+ \mathrm{arctanh}\left(\frac{x_0\sqrt{a^2-1}-1}{a\sqrt{x_0^2+1}}\right)\\ &- \left.2\,\mathrm{arctanh}\left(\frac{x_0}{\sqrt{a^2-1}}\right)\right]\Big\}. \qquad (2.33)\end{aligned}$$

We take the limit $x_0=\frac{\omega_D}{\Delta_0}\gg 1$ and $a=(Q\xi)^2\gg 1$ simultaneously, but their relative ratio might be either large or small. Also using $\mathrm{arctanh}(z)=1/2\ln(|1+z|/|1-z|)$, one can show that in this limit the above integral equals

$$\begin{aligned}&= \frac{\Delta_1}{2a}\left\{2a\ln(2x_0)-a\left[\frac{1}{2}\ln\left(\frac{2x_0a}{\frac{a}{2x_0}+\frac{x_0}{2a}-1}\right)\right.\right.\\ &+ \left.\left.\frac{1}{2}\ln\left(\frac{2x_0a}{\frac{a}{2x_0}+\frac{x_0}{2a}+1}\right)+\ln\left(\frac{|x_0-a|}{x_0+a}\right)\right]\right\}\\ &= \frac{\Delta_1}{2}\left\{2\ln(2x_0)-\left[\ln\left(\frac{2x_0a}{|\frac{x_0}{2a}-\frac{a}{2x_0}|}\right)+\ln\left(\frac{|x_0-a|}{x_0+a}\right)\right]\right\}\\ &= \Delta_1\ln\left(1+\frac{x_0}{a}\right)=\Delta_1\ln\left(1+\frac{2\omega_D}{DQ^2}\right)=\frac{\Delta_1}{\bar{U}N_F}K_1,\end{aligned}$$

where K_1 has exactly the same form as defined in (2.13).

Chapter 3

Drag Resistance in Thin Film Superconductors

3.1 Introduction

As discussed in Chapter 1, recent experiments on amorphous thin films have revealed surprising results, including a metallic phase intervening the superconducting and the insulating phase[54, 55, 56, 35, 19, 57, 53, 58], and a huge peak in the magnetoresistance[35, 59, 19, 60, 54, 55, 56, 19, 57, 53]. Most theoretical work regarding these phenomena can be classified into two categories: quantum vortex picture [21, 40, 61, 62], where the insulating phase at the peak of the magnetoresistance implies the condensation of quantum vortices, and the high field negative magnetoresistance indicates the gradual depairing of Cooper pairs and the appearance of a finite electronic density of states at the Fermi level, while intervening metallic phase is described as a delocalized but yet uncondensed diffusive vortex liquid as described in Ref. [62]; the percolation paradigm[64, 65, 63, 66, 67], where the amorphous film is decribed as a mixture of superconductor and normal or insulating puddles, and the peak in the magnetoresistance arises from electron transport though the percolating normal regions consisting of narrow conduction channels.

Given the similarity in the predictions of the distinct vortex-condensation and percolation paradigms, an experiment that distinguishes between them would be highly desirable. We propose that a thin film "Giaever transformer"[187] experiment (FIG.

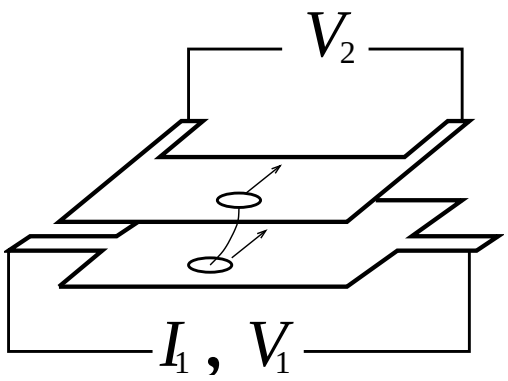

Figure 3.1: Our proposed bilayer setup for the drag resistance measurement. A current bias I_1 is applied in one layer, and a voltage V_2 is measured in the other layer. The drag resistance R_D is defined as $R_D = V_2/I_1$.

3.1) can qualitatively distinguish between these two paradigms. The original design of a Giaever transformer consists of two type-II superconductors separated by an insulating layer in perpendicular magnetic fields. A current in one layer moves the vortex lattice in the entire junction, yielding the same DC voltage in both layers. Determining the drag resistance $R_D = V_2/I_1$ in a similar bilayer structure of two amorphous superconducting thin films should qualitatively distinguish between the two paradigms (see also Refs. [188, 189]): within the vortex paradigm, vortices in one layer drag the vortices in the other, but within the percolation picture, the drag resistance is solely due to interlayer "Coulomb drag", as studied in semiconductor heterostructures [190].

The first qualitative difference between vortex drag and Coulomb drag is the sign of the drag voltage V_2. Denoting the voltage drop in the driving layer as V_1, it is easy to see that V_1 and V_2 have the same sign if they are produced by vortex motion, because vortices in the two layers move in the same direction transverse to the current bias I_1. This would induce a current in the opposite direction in the secondary layer, since no outside voltage source balances the EMF produced by the vortex motion. On the other hand, V_1 and V_2 would have opposite signs if they are due to electron Coulomb drag, because V_2 has to balance the drag force to ensure the open circuit condition in the second layer. In other words, Coulomb drag would try to produce current in the same direction in the primary and secondary layer.

More importantly, we have found that in the vortex scenario, the drag resistance is expected to be several orders of magnitude larger than that in other models. Partially this is expected because in these films, the sheet carrier density $\sim 10^{16}\text{cm}^{-2}$ is much larger than the vortex density $\sim B/\Phi_0 \sim 10^{10}\text{cm}^{-2}$, and the drag effect is typically smaller for larger densities. For example, two identical films as in FIG. 2(b) of Ref. [35] with 25nm center-to-center layer separation at 0.07K would produce a drag resistance $\sim 10^{-4}\Omega$ according the vortex theory (see FIG. 3.2), but only $\sim 10^{-12}\Omega$ for the percolation theory (see FIG. 3.3). But as we shall show below, the large vortex drag effect is also a consequence of the extremely high magneto-resistance slope, which has different implications for the vortex condensation and percolation pictures. The strength of the thin-film Giaever tranformer experiment would therefore be in the transition region where the metallic phase transforms into the insulating phase, and the magneto-resistance is at a maximum.

We believe that these qualitative differences between the drags in the two paradigms are quite general for each paradigm, and does not depend the various microscopic assumptions made in various flavors of these phenomenological pictures. We will support these claims by analyzing the drag resistance between two identical thin films within a representative theoretical framework in the vortex [62] and percolation paradigms [63]. We will restrict ourselves to the standard drag measuring geometry assuming zero tunneling between the layers. We expect that allowing small tunneling will stregthen the effect; we will pursue this possiblity in future work.

This Chapter is based on our published work Ref. [191] and unpublished work Ref. [192], and it is organized as follows. In Sec. 3.2, we extend the quantum vortex formalism to bilayers, and then we calculate the drag resistance in the insulating and the metallic regime, respectively. The effect of unpaired electrons on the drag resistance is also studied. In Sec. 3.3, we review the percolation theory of Ref. [63], and then extend this theory to bilayers as well, in order to calculate the drag resistance. In Sec. 3.4, we briefly discuss the drag resistance behavior within the phase glass model of Refs. [68, 69]. Finally, we summarize and discuss our results in Sec. 3.5. Some details are provided in appendices.

3.2 Drag resistance in the quantum vortex paradigm

3.2.1 The vortex description of double-layer amorphous films

Within the quantum vortex paradigm, the insulating phase has been explained as a superfluid of vortices by the "dirty boson" model of Ref. [21], while the metallic phase is expected to be an uncondensed vortex liquid (see also Ref. [40]). This picture has been pursued by Ref. [62] which argues that vortices form a Fermi liquid for a range of magnetic field, thereby explaining the metallic phase. At larger fields, where the insulating phase breaks down, it is claimed that gapless bogolubov quasi particles nicknamed spinons, i.e., unpaired fermions with finite density of states at the Fermi energy, become mobile, impede vortex motions, destroy the insulating phase, and suppress the resistance down to normal metallic values.

We will concentrate on the case where no interlayer Josephson coupling exists, and the vortex drag comes from the magnetic coupling between vortices in different layers which tends to align themselves vertically to minimize the magnetic energy. To calculate the drag resistance in a bilayer setup, it is crucial to derive the vortex interaction potential due to the current-current magnetic coupling between the layers, which is captured by the B^2 term in the Maxwell action. We achieve this by both a field theory formalism and a classical calculation. The classical calculation is relegated to Appendix 3.C.

Let us next derive the vortex action. Treating the superconducting film as a Cooper pair liquid, we have the following partition function

$$\mathcal{Z} = \int \mathcal{D}\rho_1 \mathcal{D}\rho_2 \mathcal{D}\theta_1 \mathcal{D}\theta_2 \mathcal{D}\vec{A} e^{-S}, \tag{3.1}$$

where

$$\begin{aligned} S &= \int_0^\beta \mathrm{d}\tau \left\{ \int \mathrm{d}^2 r \sum_{n=1,2} \hbar \rho_n \partial_\tau \theta_n + H_0 + H_{int} \right\}, \\ H_0 &= \int \mathrm{d}^2 r \sum_{n=1,2} \frac{\rho_s}{2\hbar^2} \left(\hbar \nabla \theta_n - \frac{2e}{c} \vec{A}_{ext} - \frac{2e}{c} \vec{A} \right)^2 \\ &+ \frac{1}{4\pi} \int \mathrm{d}^3 r \vec{B}^2, \\ H_{int} &= \int \mathrm{d}^2 r \int \mathrm{d}^2 r' \frac{1}{2} \sum_{n=1,2} \rho_n(r) V_i(r-r') \rho_n(r') \\ &+ \rho_1(r) V_e(r-r') \rho_2(r'), \end{aligned}$$

where a is the (center-to-center) layer-separation, ρ_n and θ_n are the 2d density and phase fluctuation of the $n-$th layer Cooper pair field, respectively, A and A_{ext} are the fluctuating and external part of the electromagnetic field, respectively. The intralayer Coulomb interaction $V_i(r) = (2e)^2/r$ (whose 2d Fourier transform would be $2\pi(2e)^2/q$), and the interlayer Coulomb interaction $V_e(r) = (2e)^2/\sqrt{r^2+a^2}$ (whose 2d Fourier transform is $2\pi(2e)^2/qe^{-qa}$). ρ_s is the superfluid phase stiffness of each layer, which can be determined approximately from the Kosterlitz-Thouless temperature T_{KT}:

$$T_{KT} = \frac{\pi}{2} \rho_s. \tag{3.2}$$

Next, we follow a procedure of vortex-boson duality transformation taking into account the B^2 term (which will be the origin of the interlayer vortex interaction), and obtain the following dual action for the vortex field ψ_{vn} of the n-th layer and two

U(1) gauge fields α_μ and β_μ (see Appendix 3.B for details):

$$\begin{aligned} S = \sum_{\vec{q},\omega} \Bigg\{ \sum_{n=1,2} \Bigg[& -i\hbar\delta\rho_{vn}\omega\phi_n + \frac{1}{2}\delta\rho_{vn}U_i\delta\rho_{vn} \\ & + \frac{1}{2m_v}\left(\left(\hbar\vec{q} - e_1^*\frac{\vec{\alpha}}{c_1^*} + (-1)^n e_2^*\frac{\vec{\beta}}{c_2^*}\right)\psi_{vn}\right)^2\Bigg] \\ & + \delta\rho_{v1}U_e\delta\rho_{v2} + \frac{1}{4\pi}(\omega^2 - c_{*1}^2q^2)\left(\frac{\vec{\alpha}}{c_1^*}\right)^2 \\ & + \frac{1}{4\pi}(\omega^2 - c_{*2}^2q^2)\left(\frac{\vec{\beta}}{c_2^*}\right)^2\Bigg\}, \end{aligned} \tag{3.3}$$

where $\delta\rho_{vn} = \rho_{vn} - B/\Phi_0$, Φ_0 is the flux quantum, $\rho_{vn} = \psi_{vn}^\dagger\psi_{vn}$, ϕ_n is the phase of the vortex field ψ_{vn}, and m_v is the vortex mass. Since there is still controversy over the theoretical value of m_v, we chose to determine the vortex mass from experiments. As discussed in Appendix 3.A, for the InO film of Ref. [35], we obtain $m_v \approx 19m_e$ where m_e is the bare electron mass.

α_ν and β_ν are gauge fields which mediate the symmetric and antisymmetric part of the vortex-vortex interaction. They are related to the Cooper pair currents $j_{n\mu}$ in the $n-$the layer by

$$\begin{aligned} j_{1\mu} + j_{2\mu} &= \frac{e_1^*}{\pi\hbar}\epsilon_{\mu\nu\eta}\partial_\nu\alpha_\eta, \\ j_{1\mu} - j_{2\mu} &= \frac{e_2^*}{\pi\hbar}\epsilon_{\mu\nu\eta}\partial_\nu\beta_\eta. \end{aligned} \tag{3.4}$$

For $\nu = 1, 2$, the dual charges and the dual "light speeds" are

$$e_\nu^* = \sqrt{\pi\rho_s}\sqrt{\frac{q}{q + q_c(1-(-1)^n e^{-qa})}}, \tag{3.5}$$

$$c_\nu^* = c\sqrt{\frac{q_c(1-(-1)^n e^{-qa})}{q + q_c(1-(-1)^n e^{-qa})}}, \tag{3.6}$$

where q_c is the inverse of the 2d Pearl screening length[193], which can be estimated

from the value of T_{KT}:

$$q_c = \frac{d}{2\lambda^2} = \frac{2\pi\rho_s(2e)^2}{\hbar^2c^2} = \frac{16e^2T_{KT}}{\hbar^2c^2}. \tag{3.7}$$

For example, the film in Ref. [35] has T_{KT} around 0.5K. This corresponds to $q_c \approx (4\text{cm})^{-1}$, and it is much smaller than the inverse of typical sample size $1/L \sim 1\text{mm}^{-1}$.

In (3.3), we have chosen the transverse gauge for the gauge fields α_μ and β_μ and integrated out α_0 and β_0 to obtain the vortex interaction potentials. The intralayer vortex interaction potential

$$U_i(q) = \frac{\Phi_0^2 q_c}{2\pi} \frac{q + q_c}{q(q^2 + 2q_c q + q_c^2(1 - e^{-2qa}))}, \tag{3.8}$$

and the interlayer vortex interaction potential

$$U_e(q) = -\frac{q_c}{q + q_c} e^{-qa} U_i. \tag{3.9}$$

When $r < 1/q_c$, $U_i(r)$ gives the familiar log interaction; for $r > 1/q_c$, i.e., beyond the Pearl screening length, $U_i(r)$ is still logarithmic but with half of the magnitude [194], in contrast to the $1/r$ behavior of the single layer case (which is Eq. (3.8) with $a \to \infty$). The interlayer interaction U_e is purely due to the magnetic coupling, i.e., vortices in different layers tend to align to minimize the energy cost in the B^2 term. As expected, the interaction between two vortices with the same vorticity in different layers is attractive, although its strength is suppressed with increasing distance a and decreasing q_c. U_i and U_e can also be derived classically by solving London equations and Maxwell's equations, which we will show in Appendix 3.C. In addition, the form of U_e is equivalent to those derived in Ref. [195, 196].

Following Ref. [40], one can examine the strength of the interaction between vortices and transverse gauge field modes by looking at the dimensionless coupling constant

$$\alpha_T \equiv \frac{e_{*1,2}^2}{m_v c_{*1,2}^2} \sim \frac{\rho_s}{m_v c^2} \cdot \frac{q}{q_c(1 \pm e^{-qa})} \leq 10^{-5} \tag{3.10}$$

for the entire range $0 \leq q \leq 1/\xi$, $\xi \sim 10$nm being the coherence length. Thus, the transverse gauge field excitations can be neglected. For a comparison, the dimensionless parameter for the strength of the longitudinal interactions U_i and U_e is

$$\alpha_L \equiv \frac{e_{*1,2}^2 m_v}{\hbar^2 n_v} \sim \frac{\rho_s m_v}{\hbar^2 n_v} \cdot \frac{q}{q + q_c(1 \pm e^{-qa})} \leq \frac{\rho_s m_v}{\hbar^2 n_v} \sim 1. \tag{3.11}$$

With these simplification, we now rewrite the action for the bilayer system as

$$\begin{aligned} S = \sum_{\vec{q},\omega} [& -\delta\rho_{v1} i\hbar\omega\phi_1 - \delta\rho_{v2} i\hbar\omega\phi_2 \\ & + \frac{1}{2}\delta\rho_{v1} U_i \delta\rho_{v1} + \frac{1}{2}\delta\rho_{v2} U_i \delta\rho_{v2} + \delta\rho_{v1} U_e \delta\rho_{v2} \\ & + \frac{1}{2m_v}\left(\hbar\vec{q}\psi_{v1}\right)^2 + \frac{1}{2m_v}\left(\hbar\vec{q}\psi_{v2}\right)^2 \Big] . \end{aligned} \tag{3.12}$$

As the magnetic fields increases, α_L gets suppressed, and therefore the vortex system goes from a interaction-dominated localized phase (Cooper-pair superfluid phase, i.e., superconducting) to a kinetic-energy-dominated superfluid phase (Cooper-pair insulating phase), possibly through a metallic phase. Finally, when the applied magnetic field is large enough that unpaired electrons ("spinons" in Ref. [62]) are delocalized, they impede vortex motion through their statistical interaction with vortices and therefore suppress the resistance down to values consistent with a normal state in the absence of pairing (see Ref. [62]).

3.2.2 Drag resistance in the vortex metal regime

As explained in the introduction, essentially all films undergoing a magnetic field driven SIT also exhibit the saturation of their resistance at the transition. Within the vortex picture, the intervening metallic phase is interpreted as a liquid of uncondensed vortices [62], and the vortices are diffusive, and have dissipative dynamics. At intermediate fields and low temperatures, where the intermediate metallic phase appears, the vortices are delocalized but uncondensed. In this phase one can derive the following form of the the drag *conductance* σ_D (which for the vortices is the

equivalent through duality to the drag resistance of charges) using either the Boltzman equation or diagrammatic techniques, irrespective of the effective statistics of vortices[190, 197, 198, 199, 200, 201, 202]:

$$\sigma_D = \frac{\hbar^2}{8\pi^2 T}\frac{\partial\sigma_1}{\partial n_1}\frac{\partial\sigma_2}{\partial n_2}\int_0^\infty q^3 \mathrm{d}q \int_0^\infty \mathrm{d}\omega \frac{|U|^2 \,\mathrm{Im}\,\chi_1 \,\mathrm{Im}\,\chi_2}{\sinh^2\left(\frac{\hbar\omega}{2T}\right)}, \tag{3.13}$$

where σ_i, n_i, and χ_i are the *conductance*, density, and the density response function of the vortices in the $i-$th layer. In addition,

$$U = \frac{U_e}{(1+U_i\chi_1)(1+U_i\chi_2) - U_e^2\chi_1\chi_2} \tag{3.14}$$

is the screened interlayer interaction, U_e is the bare interlayer interaction, and U_i is the intralayer interaction, and T is the temperature. $\partial\sigma_v/\partial n_v$ appears since R_D is related to the single layer rectification function, Γ, defined as $\vec{j}_v = \Gamma\phi^2$, with ϕ being the vortex potential field. Γ is generally proportional to $\partial\sigma_v/\partial n_v$ (see Ref. [201]). Combining the vortex density expression $n_i = B/\Phi_0$ and the relation between physical resistance and the vortex conductance $R = (\frac{h}{2e})^2\sigma_v$ with (3.13), one obtains the drag resistance

$$R_D = \frac{e^2\Phi_0^2}{8\pi^4 T}\frac{\partial R_1}{\partial B}\frac{\partial R_2}{\partial B}\int_0^\infty q^3 \mathrm{d}q \int_0^\infty \mathrm{d}\omega |U|^2 \frac{\mathrm{Im}\,\chi_1 \,\mathrm{Im}\,\chi_2}{\sinh^2\left(\frac{\hbar\omega}{2T}\right)}. \tag{3.15}$$

Remarkably, the drag resistance is proportional to $\partial R_{1,2}/\partial B$, and thus R_D peaks when the MR attains its biggest slope. This is one of the most important results of our analysis. Intuitively, the dependence of the drag on $\partial\sigma_V/\partial n_V = \partial R_{1,2}/\partial B$ arises since the drag effect is the result of the nonuniformity of the relevant particle density; how this nonuniformity affects the voltage drop in the medium both in the primary and secondary layers is exactly the origin of the square of the magneto-resistance slope.

The only model-dependent input is the density response functions $\chi_{1,2}$. As one choice of $\chi_{1,2}$, we follow the vortex Fermi liquid description for the metallic phase of Ref. [62] and use the Hubbard approximation form for $\chi_{1,2}$ considering the short-range

repulsion between vortices and also the low density of this vortex Fermi liquid[202, 203]:

$$\chi(\vec{q},\omega) = \frac{\chi_0(\vec{q},\omega)}{1 - U_i(\vec{q})\chi_0(\vec{q},\omega)G(\vec{q})}, \tag{3.16}$$

where $G(\vec{q}) = q^2/(q^2 + k_F^2)$, and k_F of the vortex Fermi liquid can be easily calculated from the vortex density:

$$k_F = \sqrt{4\pi n_v} = \sqrt{4\pi \frac{B}{\Phi_0}}. \tag{3.17}$$

One can define the mean free path l and the transport collision time τ for vortex Fermi liquid. Their value can be estimated by combining the expression for vortex conductivity $\sigma_v = n_v\tau/m_v$ and the relation between the physical resistance and the vortex conductance $R = (\frac{h}{2e})^2\sigma_v$:

$$\begin{aligned} \tau &= R\frac{m_v}{n_v}\left(\frac{2e}{h}\right)^2, \\ l &= \frac{R}{\pi^2\hbar/e^2}\sqrt{\frac{4\pi}{n_v}}. \end{aligned} \tag{3.18}$$

When $ql > 1$ or $\omega\tau > 1$ we approximate χ_0 by the noninteracting ballistic fermion result[204]:

$$\chi_0 = \nu\left(1 - C_+\sqrt{|s_+|} - C_-\sqrt{|s_-|}\right), \tag{3.19}$$

where

$$\begin{aligned} s_+ &\equiv \left(\frac{k_F}{q}\right)^2 - \left(\frac{m_v\omega + q^2/2}{q^2}\right)^2; \\ s_- &\equiv \left(\frac{k_F}{q}\right)^2 - \left(\frac{m_v\omega - q^2/2}{q^2}\right)^2, \end{aligned} \tag{3.20}$$

and

$$\begin{aligned} C_\pm &= \mathrm{sgn}\left(\frac{q^2}{2m_v} \pm \omega\right), \text{ if } s_\pm < 0, \\ C_\pm &= \pm i, \text{ if } s_\pm > 0. \end{aligned} \tag{3.21}$$

For $ql < 1$ and $\omega\tau < 1$, we use the diffusive Fermi liquid result:

$$\chi_0 = \nu \frac{Dq^2}{Dq^2 - i\omega} \tag{3.22}$$

Plugging (3.16) into (3.15), one can numerically compute the drag resistance. The result is given in Sec. 3.2.5.

Note that this result does not crucially depend on choice of fermionic density response function above. As stated earlier, as long as vortices form an uncondensed liquid, (3.15) remains valid. We have also computed R_D by modeling the metallic phase as a classical hard-disk liquid of vortices[205, 206], and putting the corresponding density response function into (3.15). The resulting magnitude and the behavior of R_D are extremely close to the results we obtained above within the vortex Fermi liquid frameworks (see Appendix 3.D). This demonstrates the universality of our results.

3.2.3 Drag resistance in the insulating (vortex superfluid) regime

According to the vortex theory, the insulating phase is a superfluid of bosonic vortices. In this regime, the vortex dynamics is presumably nondissipative. A mechanism of nondisspative supercurrent drag between bilayer bosonic superfluid systems has been studied by Ref. [207, 208, 209]. Here, we apply this approach to the superfluid of vortices in the insulating regime. In the absence of current bias, we have the following action from (3.12) deep in the insulating phase:

$$\begin{aligned} S = \sum_{\vec{q},\omega} \Big\{ & -i\delta\rho_1\phi_1\omega + \frac{n_v}{2m_v}(-q^2\phi_1^2) \\ & - i\delta\rho_2\phi_2\omega + \frac{n_v}{2m_v}(-q^2\phi_2^2) \\ & + \frac{1}{2}U_i(\delta\rho_1)^2 + \frac{1}{2}U_i(\delta\rho_2)^2 + U_e\delta\rho_1\delta\rho_2 \Big\}. \end{aligned} \tag{3.23}$$

Switching to the canonical quantization formalism and using mean field approxi-

mation for the quartic interaction term[208], the above action (3.23) corresponds to the following Hamiltonian for bilayer interacting bosons:

$$H = \sum_{s=\pm} \sum_{\vec{q}} \left\{ \frac{q^2}{2m_v} a_s^\dagger(\vec{q}) a_s(\vec{q}) + \frac{n_v}{2}[U_i(q) + sU_e(q)] \right.$$
$$\left. \times \left[a_s^\dagger(\vec{q}) a_s^\dagger(-\vec{q}) + a_s(-\vec{q}) a_s(\vec{q}) \right] \right\}, \tag{3.24}$$

where

$$a_\pm(\vec{q}) = \frac{1}{\sqrt{2}}[\psi_{v1}(\vec{q}) \pm \psi_{v2}(\vec{q})], \tag{3.25}$$

ψ_{v1} and ψ_{v2} are the bosonic vortex field operators for the first and second layer, respectively. (3.24) can be diagonalized using Bogoliubov transformations:

$$a_\pm(\vec{q}) = u_\pm(\vec{q}) b_\pm(\vec{q}) + v_\pm(\vec{q}) b_\pm^\dagger(-\vec{q}), \tag{3.26}$$

where in the long wavelength limit

$$u_\pm^2(\vec{q}) = \frac{1}{2}\left\{ \frac{n_v[U_i \pm U_e]}{\omega_\pm(q)} + 1 \right\},$$
$$v_\pm^2(\vec{q}) = \frac{1}{2}\left\{ \frac{n_v[U_i \pm U_e]}{\omega_\pm(q)} - 1 \right\},$$
$$\omega_\pm(\vec{q}) = \sqrt{\frac{q^2 n_v}{m_v}[U_i(q) \pm U_e(q)]}. \tag{3.27}$$

A vortex current bias $\vec{v_1}$ in layer 1 (the driving layer) is represented by a perturbation term H_1 in our Hamiltonian:

$$H_1 = \sum_{\vec{q}} m_v \vec{j_1} \cdot \vec{v_1}. \tag{3.28}$$

The drag current in the second layer can be calculated using standard perturbation theory. The new ground state to the first order in v_1 is given by

$$|\Omega\rangle = |0\rangle - \sum_{n \neq 0} \frac{|n\rangle\langle n|H_1|0\rangle}{E_n - E_0}, \tag{3.29}$$

where $|0\rangle$ is the vacuum state of $b_{\pm}^{\dagger}$, and $|n\rangle$ represents all possible states obtained by acting $b_{\pm}^{\dagger}$ on $|0\rangle$. Thus, at this order,

$$\begin{aligned}\langle\vec{j}_2\rangle = \langle 0|\vec{j}_2|0\rangle - \sum_{n\neq 0}\frac{\langle 0|H_1|n\rangle\langle n|\vec{j}_2|0\rangle}{E_n - E_0} \\ - \sum_{n\neq 0}\frac{\langle 0|\vec{j}_2|n\rangle\langle n|H_1|0\rangle}{E_n - E_0}.\end{aligned} \tag{3.30}$$

It is straightforward to check that the only excited states $|n\rangle$ that contribute to the sum are of the form $b_{+}^{\dagger}(\vec{q})b_{-}^{\dagger}(-\vec{q})|0\rangle$. One thus obtains

$$\begin{aligned}\langle\vec{j}_2\rangle &= \frac{\vec{v_1}}{4m_v}\sum_{\vec{q}} q^2\frac{[v_+(\vec{q})u_-(\vec{q}) - v_-(\vec{q})u_+(\vec{q})]^2}{\omega_+(\vec{q}) + \omega_-(\vec{q})} \\ &= \frac{\vec{v_1}}{16m_v}\sum_{\vec{q}} q^2\frac{[\omega_+^2(\vec{q}) - \omega_-^2(\vec{q})]^2}{\omega_+(\vec{q})\omega_-(\vec{q})[\omega_+(\vec{q}) + \omega_-(\vec{q})]^3}.\end{aligned} \tag{3.31}$$

Now, plugging (3.27) into (3.31), to the second order in interlayer interaction U_e we have

$$\langle\vec{j}_2\rangle \;=\; \vec{v_1}\frac{\hbar}{128a^2\Phi_0}\sqrt{\frac{q_c^3}{2\pi n_v m_v}}.$$

Divding this result by $\langle\vec{j}_1\rangle = n_v\vec{v_1}$ and recalling that the resistance is proportional to the vortex current, one is ready to obtain the drag resistance,

$$\frac{R_D}{R} = \frac{\langle j_2\rangle}{\langle j_1\rangle} = \frac{\hbar}{128a^2\Phi_0}\sqrt{\frac{q_c^3}{2\pi m_v n_v^3}}. \tag{3.32}$$

When spinons are mobile, they will suppress the drag resistance, as we will show in section 3.2.4.

3.2.4 The effect of mobile spinons

The discussions in previous sections apply to the case where no mobile unpaired electrons, i.e. spinons in Ref. [62], exist in the system. However when the magnetic

field is strong enough to pull apart Cooper pairs and delocalize spinons, as is signaled by the downturn of the magnetoresistance, the drag resistance is modified by the spinons. In this subsection, we analyze how mobile spinons affect our drag resistance results above.

We follow the semiclassical Drude formalism as in Ref. [62] which takes into account the statistical interaction between Cooper pairs, vortices, and spinons. Vortices and spinons see each other as π-flux source, while electric current exerts Magnus force on vortices. Denoting the electric current, vortex current, and the spinon current in the $n-$th layer as $\vec{J}_n$, $\vec{j}_{v,n}$, $\vec{j}_{s,n}$, we have the following equations for the first (driving) layer (see Ref. [62]):

$$\vec{j}_{v1} = \sigma_v \hat{z} \times (\vec{j}_{s1} - \vec{J}_1),$$
$$\vec{j}_{s1} = \sigma_s \hat{z} \times \vec{j}_{v1}.$$

Similarly, denoting the vortex drag conductance without spinons as σ_D, we incorporate the drag effect in the following way in the equations of the second (passive) layer:

$$\vec{j}_{v2} = \frac{\sigma_D}{\sigma_v} \vec{j}_{v1} + \sigma_v \hat{z} \times \vec{j}_{s2},$$
$$\vec{j}_{s2} = \sigma_s \hat{z} \times \vec{j}_{v2}.$$

This set of equations is a consequence of the absence of electric current but the presence of vortex drag effect in the second layer. We can solve these two sets of equations, and obtain the effective vortex drag conductance:

$$\sigma_D^{eff} = \frac{j_{v2}}{J_1} = \frac{\sigma_D}{(1 + \sigma_v \sigma_s)^2}. \tag{3.33}$$

Since the physical resistance $R = (h/(2e))^2 \sigma_v$, we have

$$R_D^{eff} = \frac{R_D}{(1 + R_v/R_s)^2}. \tag{3.34}$$

where R_D is the drag resistance if spinons are localized, $R_v = (h/2e)^2\sigma_v$ is the vortex contribution to the resistance, and $R_s = \sigma_s^{-1}$ is the spinon contribution to the resistance. Thus, we see that when $R_s \ll R_v$, the drag resistance is quickly suppressed to unmeasurably small as spinon mobility increases.

3.2.5 Results of the drag resistance in the vortex theory

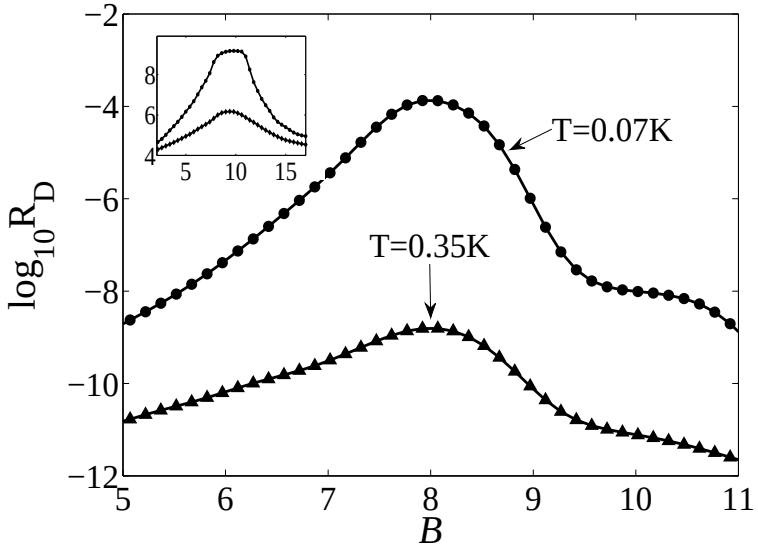

Figure 3.2: Drag resistance R_D (in Ohms) between two identical films as in FIG. 2b of Ref. [35] vs. magnetic field B, according to the vortex picture[62] (log scale); . The drag resistance has been smoothened to avoid discontinuity at the boundary between the metallic and the insulating phase. Center-to-center layer separation $a = 25$nm, temperature $T = 0.07$K and 0.35K. Insets: single layer magnetoresistance (magnetoresistance, log scale) reproduced according to the quantum vortex theory.. The parameters are tuned to make the magnetoresistance resemble the experimental data in FIG. 2b of Ref. [35]. R_D has a peak at the steepest point ($\sim$ 8T) of the magnetoresistance, which is due to the fact that R_D is proportional to the square of the slope of the magnetoresistance in the small magnetic field side of the peak. Also, R_D is larger at lower temperature, because the magnetoresistance curve is then much steeper. Carrying out the experiments at even lower temperatures may further enhance the vortex drag effect.

Collecting the above results and the value of the vortex mass m_v discussed in Appendix 3.2.1, tuning the value of the vortex (spinon) contributions to the resistance R_v (R_s) so that $R = R_v R_s/(R_v + R_s)$ (see Ref. [62]) resembles the resistance observed

in the experiment of Ref. [35], and setting temperature to be 0.07K and 0.35K, we have calculated the drag resistance between two identical films with single layer resistance given by the inset of FIG.3.2, and with center-to-center layer separation 25nm. We assume that vortices form a Fermi liquid (thus (3.15) is applicable; however see also Appendix 3.D) when $B < 9$T, and a bosonic superfluid (thus (3.32) is used) when $B > 9$T. We smoothen the drag resistance curve by convoluting it with a Gaussian function to avoid discontinuity across the phase boundary between the metallic phase and the insulating phase.

The results of vortex drag are summarized in FIG.3.2. One can see that The drag resistance has a peak at the steepest point (~ 8T) of the magnetoresistance. This is due to the fact that in the vortex metal regime, the drag resistance is proportional to the square of the slope of the magnetoresistance. Also, the drag resistance is larger at lower temperature. This is because the magnetoresistance curve is much steeper as one approaches zero temperature(see (3.15)). For the film of Ref. [35], the *sheet* drag resistance is about 10^{-1} mΩ at its maximum, which is measurable despite challenging. We suggest to carry out experiments to even lower temperature, which should leads to a larger drag resistance. Using a Hall-bar shape sample would also amplify the result.

3.3 Drag resistance in the percolation picture

3.3.1 Review of the percolation picture of the magnetoresistance

Within the percolation picture of Ref. [63], it is argued that the non-monotonic magnetoresistance arises from the film breaking down to superconducting and normal regions (described as localized electron glass) [63]. As the magnetic field increases, the superconducting region shrinks, and a percolation transition occurs. Once the normal regions percolate, electrons must try to enter a superconducting island in pairs, and therefore encounter a large Coulomb blockade absent in normal puddles.

The magnetoresistance peak thus reflect the competition between electron transport though narrow normal regions, and the tunneling through superconducting islands.

This picture is captured using a resistor network description. Each site of the network has a probability p to be normal, and $1-p$ to be superconducting; each link is assigned a resistance from the three values R_{NN}, R_{SS}, R_{SN}, that reflect whether the sites the link connects are normal (N), or superconducting (S). An increase of the magnetic field is assumed to only cause p to increase. Since the normal region is described as disordered electron glass, R_{NN}, the resistance between two normal sites, is assumed to be of the form of hopping conduction:

$$R_{ij} \sim R_{N0} \exp\left(\frac{2}{\xi_{loc}} + \frac{|\epsilon_i| + |\epsilon_j| + |\epsilon_i + \epsilon_j|}{k_B T}\right), \tag{3.35}$$

where ξ_{loc} is the localization length, and ϵ_i is the energy of the $i-$th site measured from the chemical potential (taken from a uniform distribution $[-W/2, W/2]$), and for simplicity we allow only nearest neighbor hopping. The resistance between two superconducting sites, R_{SS}, is taken to be very small, but still nonzero, and vanishes as $T \sim T^{\alpha} \to 0$. Most importantly, the resistance between one normal site and a neighboring superconducting site, R_{SN}, is assumed activated:

$$R_{SN} \sim R_{SN0} \exp\left(\frac{E_c}{k_B T}\right) \tag{3.36}$$

to model the charging energy electrons need to pay to enter a superconducting island.

We have reproduced the work of Ref. [63] where the parameters of this model are chosen to reproduce the magneto-resistance curves and temperature dependence observed in the strong-insulator InO sample [35]. The total resistance vs. the probability of normal metal (assumed to increase with increasing magnetic field) is shown in the inset of FIG.3.3. Indeed, the peak of the magnetoresistance can be explained by this theory. However, as we demonstrate now, this theory predicts a very different behavior for the drag resistance.

3.3.2 Calculation of drag resistance within the percolation picture

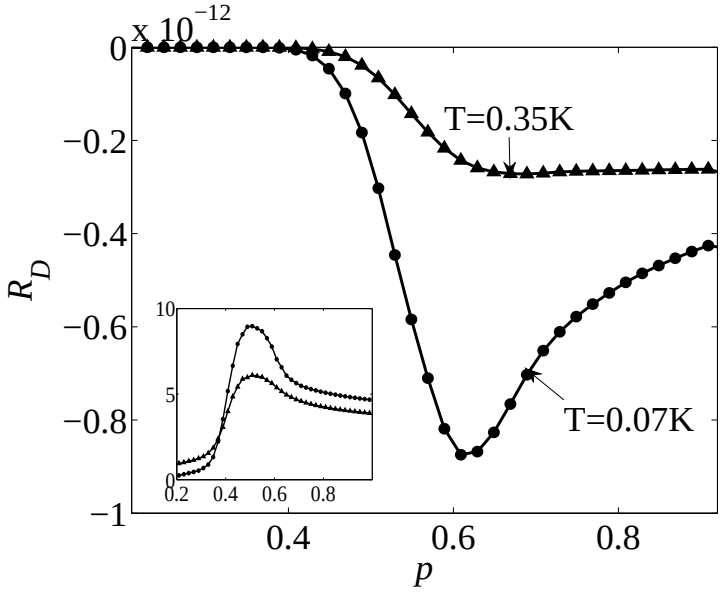

Figure 3.3: Drag resistance R_D (in Ohms) between two identical films as in FIG. 2b of Ref. [35] vs. normal metal percentage p (corresponding to normal magnetic field), according to the percolation picture[63]. Center-to-center layer separation $a = 25$nm, temperature $T = 0.07K$ and $0.35K$. Insets: single layer magnetoresistance (magnetoresistance, log scale) reproduced according to the percolation theory. The parameters are tuned to make the magnetoresistance resemble the experimental data in FIG. 2b of Ref. [35]. The sign of the voltage drop of the passive layer is opposite to that of the driving layer, and the maximum magnitude value of R_D is much smaller, $\sim 10^{-12}\Omega$.

To calculate R_D, we first follow Ref. [63] and tune the parameters to make the single layer resistance resemble the experimental data in FIG. 2(b) of Ref. [35]: $\xi_{loc} = 0.1$, $W = 0.4$K, $E_c = 0.6$K, $R_{SN0} \sim 10^6\Omega$, and $R_{N0} \sim 10^{-5}\Omega$. Next, we place one such network (active layer) on top of another one (passive layer). Each link is treated as a subsystem, which might induce a drag voltage (an emf) $\varepsilon = IR_D$ in the link under it in the passive layer. When a link is between two normal (or superconducting) sites, it is treated as a disorder localized electron glass (or superconductor). In Appendix

3.E, we find R_D between two localized electron glass separated by vacuum is:

$$R_D \approx \frac{1}{96\pi^2}\frac{R_1 R_2}{\hbar/e^2}\frac{T^2}{(e^2 nad)^2}\ln\frac{1}{2x_0}. \tag{3.37}$$

Here, $n \approx 5\times 10^{20}\text{cm}^{-3}$ is the typical carrier density of InO[19], $d = 20$nm is the film thickness, $a = 25$nm is the center-to-center layer separation, $R_{1,2}$ are the resistances of the two normal-normal(NN) links, $x_0 = a/(2\pi e^2 \nu d\xi^2)$ where ν is the density of states and $\xi \approx 1$nm is the localization length. The value of the localization length ξ is estimated by following Ref. [63] to take $\xi \sim 0.1\times$ plaquette size (reflecting the fact that it is a disordered insulator), and we estimate the plaquette size as the superconducting coherence length ~ 10nm. Although this estimation of localization length is crude, the drag resistance R_D has only logarithmic dependence on it in (3.37). Setting $T = 0.07$K, and $R_1 = R_2 = 10^5\Omega$, we can estimate $R_D \sim 10^{-12}\Omega$.

On the other hand, we will show in Appendix 3.F that a genuine (i.e., without mobile vortices) superconductor has no drag effect at all in a resistor network, either when it is aligned with another superconductor link or a normal link. Thus, drag effects associated with a superconducting link can only come from vortices. However, The small resistance for the superconducting islands in this theory implies that vortices in the superconducting islands, if any, have very low mobility. If two superconducting links are vertically aligned, we can estimate the drag resistance due to mobile vortices using our vortex drag result (3.15): roughly $R_D \propto R^2$, for $R \sim 10^9\Omega$ we obtained $R_D \sim 10^{-4}\Omega$, therefore for $R \sim 1\Omega$ we have $R_D \sim 10^{-20}\Omega$, which is negligible compared to the Coulomb drag resistance between two NN links $\sim 10^{-12}\Omega$. Finally, Ref. [210] has shown that a current off the plane where vortices reside does not exert any force on vortices. By Newton's third law or equivalently the Kubo formula for the drag conductance, this also implies that moving vortices does not exert any DC emf in another layer. Therefore, there is no drag effect when a NN link is aligned with a SS link. Consequently, the Coulomb drag between two vertically aligned NN links (Eqn. (3.37)) dominates the drag effect.

Thus, we solve the Kirchoff's equations for the two layers, and obtain the voltage

drop and thereby the drag resistance. The results are shown in FIG. 3.3, with $T =$ 0.07K and 0.35K, film-thickness 20nm, and the center-to-center interlayer distance 25nm. We observe that the sign of the voltage drop of the passive layer is opposite to that of the driving layer (not shown in the Figure), as expected and explained in the introduction, and the maximum magnitude of the drag resistance is around $10^{-12}\Omega$, indeed much smaller than that in the vortex paradigm.

3.4 Discussion on the drag resistance in the phase glass theory

A third theory, namely the phase glass theory[68, 69], focuses on the nature of the metallic phase intervening the superconducting and insulating state. In this theory, the system is described as interacting bosons (Cooper pairs), but it is argued that the glassy phase is in fact a Bose metal, due to the coupling to the glassy landscape.

Specifically, Ref. [68] has studied the quantum rotor model

$$H = -E_c \sum_i \left(\frac{\partial}{\partial \theta_i}\right)^2 - \sum_{\langle i,j \rangle} J_{ij} \cos(\theta_i - \theta_j), \tag{3.38}$$

where the Josephson coupling J_{ij} obeys a Gaussian distribution with nonzero mean. This model is appears to exhibit three phases: superconducting phase, phase glass phase, and a Mott insulator phase. Ref. [68] has employed replica trick to obtain the Landau theory of the the phase glass phase near the glass-superconductor-transition critical point, and has calculated the conductance in this regime. It was found that in this regime the DC conductance is actually finite at zero temperature. For completeness, we note that Ref. [70] argued against these results and obtained infinite conductance instead.

This analysis has recently been extended to include the external perpendicular magnetic field[69], which is more relevant to the experiments on the magnetic field tuned transition. However, Ref.[69] has only studied the regime of small magnetic field

where one just enters the resistive glassy phase and left out issues such as the peak in the magnetoresistance. Therefore, we leave a complete analysis to future work and simply observe that according to this theory, the resistive state is a glassy phase where phase variables θ_i's of the bosons are ordered locally. In other words, there are no mobile vortices moving around. Consequently, the current coupling as we considered in the vortex drag should is absent, and the Coulomb interaction should dominate the drag effect. Therefore, we expect that the sign of the drag voltage is opposite to the voltage drop of the driving layer, as we discussed in the introduction to be a general feature of the Coulomb drag, and the magnitude of the drag resistance should be small. This is in part because for a bosonic system, the phase space available for excitations is much smaller than fermionic systems due to the absence of a Fermi surface.

3.5 Summary and discussion

One of the most exciting possiblities is that the SIT in amorphous thin films realizes the vortex condensation scenario [20, 21, 62]. The amorphous-films Giaver transformer experiment [191], would be able to measure a distinct signature of mobile vortices, which is a drag resistance opposite in its direction to that of coulomb drag. Therefore such a measurement would able to disclose whether the vortex paradigm is suitable for explaining the complex phase diagram of amorphous films in a normal manetic field, or whether the percolation paradigm is indeed more appropriate. We provide a detailed computation of the drag resistance according to the vortex theories of Ref. [21, 62] and the percolation theory of Ref. [63]. The drag resistance implied by the phase glass model[68, 69] is also briefly discussed. We find that vortex picture predicts a drag resistance orders of magnitude stronger than non-vortex pictures. In addition, the drag resistance and the single layer resistance have the same sign according to the vortex picture, but the opposite sign for non-vortex pictures. Therefore, drag resistance measurement are indeed able to distinguish different theoretical paradigms qualitatively.

We considered specifically a bilayer device which will contain two identical films as in Ref. [35] with 25nm layer separation and at 0.07K. A calculation within the vortex paradigm yields a drag resistance $R_D \sim 10^{-4}\Omega$ at its maximum value. This drag arises solely from the attractive interaction of the demagnetizing currents of vortices. The value we find is probably near the limit of measurability; we suggest, however, to carry out experiments at even lower temperature, in which case the single layer magnetoresistance is even steeper, and the drag resistance should be larger. Within the percolation picture of Ref. [63], the dominating drag effect is the drag between two vertically aligned normal regions in the different layers. For two identical films as in Ref. [35] with 25nm layer separation at 0.07K, we find the drag resistance $R_D \sim 10^{-12}\Omega$ at its maximum value, which is indeed orders of magnitude smaller than the drag resistance predicted by the vortex picture. Also, we find the sign of the drag resistance is the opposite of that of the single layer resistance, as expected.

The answer we find should not depend crucially on the details of the microscopic picture which we use. If vortices are not responsible for the inhibitive resistance which the films display, then drag effects will appear primarlily due to Coulomb repulsion of single electrons. This drag effect will be low because of the relatively high electronic density in the films. On the other hands, if vortices are responsible for the large resistance in the intermediate magnetic fields leading to the insulating phase, then they will produce a drag opposite in its direction to the Coulomb drag. To carry out the vortex drag calculation in the metallic phase intervening between the superconducting and insulating phase we used the picture of Ref. [62], which treats the vortices as fermionic diffusive particles. This picture is justified due to the strong long-ranged interactions within the vortex liquid, which render the question of statistics secondary, intuitively, since vortices rarely encircle each other. Nevertheless, to demonstrate the universality of our results, we also carried out the drag calculation in the metalic phase assuming that the vortices are hard core disks, and obtained essentially the same answer (c.f. App. 3.D).

Indeed our strongest results are obtained in the intermediate-field metallic phase. The controversy surrounding this phase requires some special attention. First, we

note that all experiments of thin amorphous films exhibit a saturation of the resistance at temperature below about 100mK at intermediate resistances. This is clearly seen in, e.g, the resistance vs. field traces which overlap at subsequent temperature sweeps as in Fig.2b of Ref. [35]. Second, there are reasons to believe that this saturation is not the result of failure to cool electrons. Resistances that are too low or too high continue to change as the temperature is lowered. But the two heating mechanisms most likely are current heating, with power $\sim I^2R$, and therefore affecting the highest temperatures, and ambient RF heating, which would have a voltage-biased power $\sim V^2/R$, and therefore most effective in the lowest resistances. Neither mechanism explains resistance saturation at intermediate temperatures. Furthermore, experiments on Tantalum films show distinct signatures in the metallic regime which disappear in the insulating and superconducting regimes, and also distinguish it from the thermally-destroyed superconducting phase[53]. Third, even if the metallic behavior of the films is a finite temperature phenomena, within the vortex paradigm, the resistance still arises due to vortex motion. Therefore the drag calculated within this paradigm using a diffusive vortex model should still be adequate, and our results do not depend crucially on the existence of a zero-temperature intervening metallic state.

The signatures we expect to find in the proposed magnetic and Coulomb drag measurements are not large. Incorporating interlayer electron and Josephson tunneling will increase both the vortex-drag effect and the competing Coloumb drag effects. As we point out here, the drag signature of vortex motion, or single electrons or Cooper-pairs motion will have opposite signs. Quite possibly, allowing interlayer tunneling will render both drag effects measurable. Indeed, such a setup will be a deviation from standard drag measurements where charge transfer between layers is forbidden. Nevertheless, a careful choice of tunneling strength and sample geometry will make such experiments plausible and useful. We intend to analyze the vortex and Coloumb drag in the presence of interlayer tunneling in future work.

3.A The determination of the vortex mass

In this appendix, we demonstrate in detail the derivation of the vortex-boson duality for a single layer and discuss the value of the vortex mass. Our starting point is the following partition function for Cooper pairs:

$$\mathcal{Z} = \int \mathcal{D}\rho\mathcal{D}\theta\mathcal{D}\vec{A}e^{-S}, \tag{3.39}$$

where the action S is

$$\begin{aligned} S &= \int_0^\beta \mathrm{d}\tau \left\{ \int \mathrm{d}^2 r(\hbar\rho\partial_\tau\theta + H_0 + H_{int}) \right\}, \\ H_0 &= \int \mathrm{d}^2 r \frac{\rho_s}{2\hbar^2} \left(\hbar\nabla\theta - \frac{2e}{c}\vec{A}_{ext} - \frac{2e}{c}\vec{A} \right)^2 \\ &+ \frac{1}{4\pi}\int \mathrm{d}^3 r \vec{B}^2, \\ H_{int} &= \int \mathrm{d}^2 r \int \mathrm{d}^2 r' \frac{1}{2}\rho(r)V(r-r')\rho(r'). \end{aligned} \tag{3.40}$$

Here, ρ and θ are the density and phase fluctuation of the Cooper pair field, respectively, $\vec{A}$ is the fluctuating electromagnetic field, and $\vec{A}_{ext}$ is the applied external electromangetic field, typically a perpendicular magnetic field. $V(r) = (2e)^2/r$ (whose 2d Fourier transform would be $2\pi(2e)^2/k$) is the Coulomb interaction between Cooper pairs. ρ_s is the bare stiffness for phase fluctuations. The value of ρ_s can be determined approximately by the zero-field Kosterlitz-Thouless temperature T_{KT}:

$$T_{KT} = \frac{\pi}{2}\rho_s. \tag{3.41}$$

The 2d number current of Cooper pairs is

$$\vec{j} = \frac{\rho_s}{\hbar^2}\left(\hbar\nabla\theta - \frac{2e}{c}\vec{A}_{ext} - \frac{2e}{c}\vec{A} \right). \tag{3.42}$$

One can introduce the dynamical field $\vec{j}$ by Hubbard-Stratonavich transformation (or Villain transformation in the lattice version of this derivation) and transform $\mathcal{Z}$ to be

$$\mathcal{Z} = \int \mathcal{D}\rho\mathcal{D}\theta\mathcal{D}\vec{j}\mathcal{D}\vec{A}e^{-S}, \tag{3.43}$$

where

$$\begin{aligned} S &= \sum_{\omega,\vec{q}} \left\{ -i\hbar\omega\rho\theta + \frac{1}{2}\rho V\rho + \frac{\hbar^2}{2\rho_s}\vec{j}^2 \right. \\ &+ i\vec{j}\cdot\left(\hbar(\nabla\theta)_q - \frac{2e}{c}\vec{A}_{ext} - \frac{2e}{c}\vec{A}(\vec{q}, z=0)\right) \\ &+ \left. \int \frac{dk_z}{2\pi}\frac{q^2+k_z^2}{4\pi}\vec{A}^2(\vec{q},k_z)\right\}. \end{aligned} \tag{3.44}$$

Here, i is the imaginary number unit, $\vec{q}$ is the in-plane 2d wave vector, while k_z is the 3rd wave vector component perpendicular to the plane, and subscripts $\vec{q}$ mean Fourier transformed variables. Next we split the θ field into a smooth part θ_s and a vortex part θ_v: $\theta = \theta_s + \theta_v$. Afterwards one can integrate out θ_s to obtain the continuity constraint:

$$\mathcal{Z} = \int \mathcal{D}\rho\mathcal{D}\vec{j}\mathcal{D}\theta_v\mathcal{D}\vec{A}\delta(\partial_t\rho + \nabla\cdot\vec{j})e^{-S}, \tag{3.45}$$

where

$$\begin{aligned} S = \sum_{\omega,\vec{q}} &\left\{ -i\hbar\omega\rho\theta_v + \frac{1}{2}\rho V\rho + \frac{\hbar^2}{2\rho_s}\vec{j}^2 \right. \\ &+ i\vec{j}\cdot\left(\hbar(\nabla\theta_v)_q - \frac{2e}{c}\vec{A}_{ext} - \frac{2e}{c}\vec{A}(\vec{q}, z=0)\right) \\ &+ \left. \int \frac{dk_z}{2\pi}\frac{q^2+k_z^2}{4\pi}\vec{A}^2(\vec{q},k_z)\right\}. \end{aligned}$$

Furthermore, noting that $\vec{A}(\vec{q}, z=0) = \int \frac{dk_z}{2\pi} \vec{A}(\vec{q}, k_z)$, one can integrate out $\vec{A}$ in its transverse gauge, and the action S now reads

$$\begin{aligned} S &= \sum_{\omega,\vec{q}} \left\{ -i\hbar\omega\rho\theta_v + \frac{1}{2}\rho V \rho + i\vec{j} \cdot \left(\hbar(\nabla\theta_v)_q - \frac{2e}{c}\vec{A}_{ext} \right) \right. \\ &+ \left. \frac{\hbar^2}{2\rho_s} \left(1 + \frac{q_c}{q} \right) \vec{j}^2 \right\}, \end{aligned} \tag{3.46}$$

where q_c is the inverse of the 2d Pearl screening length[193], and typically it is much smaller than $1/L$, where L is the sample size.

The continuity constraint is solved by defining a new gauge field $a_\mu = (a_0, \vec{a})$ such that

$$j_\mu = \frac{1}{\eta} \epsilon_{\mu\nu\eta} \partial_\nu a_\eta, \tag{3.47}$$

where $j_\mu = (c^*\rho, \vec{j})$ and $\partial_\mu = (\frac{1}{c^*}\partial_\tau, \nabla)$, and the value of constant η and the "speed of light" c^* are to be determined. Writing in components, (3.47) is

$$\vec{e} = \eta \vec{j} \times \hat{z}, \qquad b = \eta c^* \rho, \tag{3.48}$$

where $\vec{e}$ and b are the dual "electric field" and "magnetic field" associated with α, respectively. To fix η and c^*, we require

$$\frac{1}{4\pi}\vec{e}^2 = \frac{\hbar^2}{2\rho_s} \left(1 + \frac{q_c}{q} \right) \vec{j}^2, \qquad \frac{1}{4\pi} b^2 = \frac{1}{2}\rho V \rho, \tag{3.49}$$

thus

$$\eta \equiv \sqrt{\frac{2\pi\hbar^2}{\rho_s} \frac{q+q_c}{q}}, \qquad c^* = \sqrt{\frac{2\pi(2e)^2\rho_s}{(q+q_c)\hbar^2}}. \tag{3.50}$$

Using (3.47), we express the partition function $\mathcal{Z}$ as

$$\mathcal{Z} = \int \mathcal{D}\vec{a}\mathcal{D}a_0\mathcal{D}\theta_v e^{-S}, \tag{3.51}$$

where

$$\begin{aligned} S &= \sum_{\omega,\vec{q}} \left\{ \frac{1}{\eta} \epsilon_{\mu\nu\eta} q_\nu a_\eta \left(\hbar(\partial_\mu \theta_v)_q - \frac{2e}{c} A_\mu^{ext} \right) \right. \\ &+ \left. \frac{1}{4\pi} (\omega^2 - c_*^2 q^2) \left(\frac{\vec{a}}{c_*} \right)^2 + \frac{q^2}{4\pi} a_0^2 \right\}. \end{aligned} \tag{3.52}$$

Integrating by parts, and noting the definition of the vortex current density

$$j_\mu^v = \frac{1}{2\pi} \epsilon_{\mu\nu\eta} \partial_\nu \partial_\eta \theta^v, \tag{3.53}$$

we obtain

$$\begin{aligned} S &= \sum_{\omega,\vec{q}} \left\{ -e^* i a_0 \left(\rho_v - \frac{B_{ext}}{\Phi_0} \right) + i e^* \vec{j}^v \cdot \frac{\vec{a}}{c^*} \right. \\ &+ \left. \frac{1}{4\pi} (\omega^2 - c_*^2 q^2) \left(\frac{\vec{a}}{c_*} \right)^2 + \frac{q^2}{4\pi} a_0^2, \right\}. \end{aligned} \tag{3.54}$$

where $\Phi_0 = hc/(2e)$, and the "dual charge" of vortices is

$$e^* = \frac{2\pi\hbar}{\eta} = \sqrt{2\pi\rho_s} \sqrt{\frac{q}{q+q_c}}. \tag{3.55}$$

In the above, we have assumed that the only external electromagnetic field is a perpendicular magnetic field B_{ext}.

The magnitude of the Magnus force, which now appears as the electric force, can be easily verified:

$$F = e^* \times |\vec{e}| = \frac{2\pi\hbar}{\eta} \times \eta j = hj, \tag{3.56}$$

as expected.

Introducing a vortex field ψ_v and making the action explicitly gauge-invariant, we

write the action as

$$S = \sum_{\vec{q},\omega} \left\{ \delta\rho_v(-\hbar i\omega\phi - ie^* a_0) + \frac{1}{2m_v}\left[\left(\hbar\vec{q} - e^*\frac{\vec{a}}{c_*}\right)\psi_v\right]^2 + \frac{1}{4\pi}(\omega^2 - c_*^2 q^2)\left(\frac{\vec{a}}{c_*}\right)^2 + \frac{q^2}{4\pi}a_0^2 \right\}, \tag{3.57}$$

where $\delta\rho_v = \rho_v - \frac{B_{ext}}{\Phi_0}$, and we have introduced the vortex mass m_v. Integrating out a_0, one obtains

$$\begin{aligned} S &= \sum_{\vec{q},\omega} \left\{ -\delta\rho_v \hbar i\omega\phi + \frac{1}{2}\delta\rho_v U \delta\rho_v \right. \\ &+ \frac{1}{2m_v}\left[(\hbar\vec{q} - e^*\frac{\vec{a}}{c_*})\psi_v\right]^2 \\ &+ \left. \frac{1}{4\pi}(\omega^2 - c_*^2 q^2)\left(\frac{\vec{a}}{c_*}\right)^2 \right\}, \end{aligned} \tag{3.58}$$

where

$$U(q) = \frac{\Phi_0^2 q_c}{2\pi}\frac{1}{q(q+q_c)} \tag{3.59}$$

is the well-known Pearl interaction potential[193].

In the insulating phase, i.e., the vortex condensed phase with vortex superfluid stiffness ρ_{vs}, we have

$$\begin{aligned} S &= \sum_{\vec{q},\omega} \left\{ -\delta\rho_v \hbar i\omega\phi + \frac{\rho_{vs}}{2\hbar^2}\left(i\hbar\vec{q}\phi - e^*\frac{\vec{a}}{c_*}\right)^2 \right. \\ &+ \left. \frac{1}{2}\delta\rho_v U\delta\rho_v + \frac{1}{4\pi}(\omega^2 - c_*^2 q^2)\left(\frac{\vec{a}}{c_*}\right)^2 \right\}. \end{aligned} \tag{3.60}$$

Due to the Higgs mechanism in this "symmetry broken phase", the gap of the two modes in the vortex superfluid phase coincide to be

$$E_{gap} = \sqrt{2\pi\rho_{vs}e_*^2} \approx 2\pi\sqrt{\rho_{vs}\rho_s} \tag{3.61}$$

for $q_c \ll L^{-1}$. Roughly speaking the two modes correspond to a density fluctuation

of the vortices, or of the underlying Cooper-pairs Deep in the insulating phase, i.e., near the peak of the magnetoresistance, the vortex stiffness is simply

$$\rho_{vs} = \hbar^2 \frac{n_v}{m_v}, \tag{3.62}$$

where the vortex density $n_v \equiv B/\Phi_0$. Therefore, in this regime we have

$$E_{gap} = 2\pi\hbar\sqrt{\frac{n_v}{m_v}\rho_s}. \tag{3.63}$$

Since the gauge field a_μ is actually the fluctuation of Cooper pairs, we conjecture that its gap E_{gap} can be identified with the activation gap observed in the experiments of Ref. [35, 19] near the insulating peak. Ref.[35, 19] have also found that with increasing disorder strength, the ratio E_{gap}/T_{KT} is enhanced. This is natural from our expression (3.63): dividing (3.63) by (3.41), we have

$$\frac{E_{gap}}{T_{KT}} = 4\hbar\sqrt{\frac{n_v}{m_v}\frac{1}{\rho_s}}; \tag{3.64}$$

increasing disorder makes vortices more mobile and thereby suppresses the vortex mass m_v [17]; it also suppresses the superfluid stiffness ρ_s. Therefore, E_{gap}/T_{KT} is larger for more disordered sample.

Since there is still controversy over its theoretical value, we chose to use the experimental value of E_{gap} as an input to deduce the vortex mass from (3.63). Combining (3.41), we can express the vortex mass m_v as a function of observable quantities:

$$m_v = \frac{8\pi n_v T_{KT}}{E_{gap}^2}. \tag{3.65}$$

Again, the vortex density $n_v = B/\Phi_0$. For the InO film of Ref. [35], $T_{KT} \approx 0.5$K, and $E_{gap} \approx 1.6$K at $B = 9$T. Plugging these into (3.65), we obtain $m_v \approx 19m_e$ where m_e is the bare electron mass. For comparison, this value is not far from that of the so-called core mass of dirty superconductors[211, 212, 213, 214] $m \sim (k_F d)m_e \sim 49m_e$ if we use carrier density $\sim 5 \times 10^{20}\text{cm}^{-3}$ and $d \sim 20$nm (see Ref. [35, 19]).

3.B Field theory derivation of the vortex interaction potentials

For identical bilayer superconducting thin films separated by a (center-to-center) distance a, we have the following partition function for Cooper pairs:

$$\mathcal{Z} = \int \mathcal{D}\rho_1 \mathcal{D}\rho_2 \mathcal{D}\theta_1 \mathcal{D}\theta_2 \mathcal{D}\vec{A} e^{-S}, \tag{3.66}$$

where

$$\begin{aligned}
S &= \int_0^\beta \mathrm{d}\tau \left\{ \int \mathrm{d}^2 r \sum_{n=1,2} \hbar \rho_n \partial_\tau \theta_n + H_0 + H_{int} \right\}, \\
H_0 &= \int \mathrm{d}^2 r \sum_{n=1,2} \frac{\rho_s}{2\hbar^2} \left(\hbar \nabla \theta_n - \frac{2e}{c} \vec{A}_{ext} - \frac{2e}{c} \vec{A} \right)^2 \\
&+ \frac{1}{4\pi} \int \mathrm{d}^3 r \vec{B}^2, \\
H_{int} &= \int \mathrm{d}^2 r \int \mathrm{d}^2 r' \frac{1}{2} \sum_{n=1,2} \rho_n(r) V_i(r-r') \rho_n(r') \\
&+ \rho_1(r) V_e(r-r') \rho_2(r'),
\end{aligned}$$

where ρ_n and θ_n are the density and phase fluctuation of the $n-$th layer Cooper pair field, respectively, A and A_{ext} are the fluctuating and external part of the electromagnetic field, respectively. The intralayer Coulomb interaction $V_i(r) = (2e)^2/r$ (whose 2d Fourier transform would be $2\pi(2e)^2/q$), and the interlayer Coulomb interaction $V_e(r) = (2e)^2/\sqrt{r^2+a^2}$ (whose 2d Fourier transform is $2\pi(2e)^2/qe^{-qa}$). ρ_s is the superfluid phase stiffness of each layer.

Similar to the single layer case in Appendix 3.A, we can again introduce Hubbard-Stratonavich fields $\vec{j}_{1,2}$, split θ's into smooth parts θ_s and vortex parts θ_v, integrate out θ_s and $\vec{A}$, and obtain

$$\begin{aligned}
\mathcal{Z} &= \int \mathcal{D}\rho_1 \mathcal{D}\rho_2 \mathcal{D}\theta_1^v \mathcal{D}\theta_2^v \mathcal{D}\vec{j}_1 \mathcal{D}\vec{j}_2 \\
&\times \delta(\partial_t \rho_1 + \nabla \cdot \vec{j}_1) \delta(\partial_t \rho_2 + \nabla \cdot \vec{j}_2) e^{-S}
\end{aligned} \tag{3.67}$$

where

$$\begin{aligned} S &= \sum_{\omega,\vec{q}} \Big\{ -i\hbar\omega\rho_1\theta_1^v + i\vec{j}_1 \cdot \left(\hbar(\nabla\theta_1^v)_q - \frac{2e}{c}\vec{A}_{ext} \right) \\ &- i\hbar\omega\rho_2\theta_2^v + i\vec{j}_2 \cdot \left(\hbar(\nabla\theta_2^v)_q - \frac{2e}{c}\vec{A}_{ext} \right) \\ &+ \frac{1}{2}\rho_1 V_i \rho_1 + \frac{1}{2}\rho_2 V_i \rho_2 + \rho_1 V_e \rho_2 \\ &+ \frac{\hbar^2}{2\rho_s}\left(1 + \frac{q_c}{q}\right)\vec{j}_1^2 + \frac{\hbar^2}{2\rho_s}\left(1 + \frac{q_c}{q}\right)\vec{j}_2^2 \\ &+ \frac{\hbar^2}{\rho_s}\frac{q_c}{q}e^{-qa}\vec{j}_1 \cdot \vec{j}_2 \Big\}. \end{aligned} \tag{3.68}$$

The difference from the single layer case is that now the continuity constraint is solved by introducing two new gauge fields $\alpha_\mu = (\alpha_0, \vec{\alpha})$ and $\beta_\mu = (\beta_0, \vec{\beta})$ such that

$$\begin{aligned} j_{1\mu} + j_{2\mu} &= \frac{1}{\eta_1}\epsilon_{\mu\nu\eta}\partial_\nu\alpha_\eta, \\ j_{1\mu} - j_{2\mu} &= \frac{1}{\eta_2}\epsilon_{\mu\nu\eta}\partial_\nu\beta_\eta; \end{aligned}$$

Denoting the electric field and the magnetic field associated with $\alpha_\mu(\beta_\mu)$ are $\vec{e}_1$ and b_1 ($\vec{e}_2$ and b_2), respectively, we have

$$\begin{aligned} \vec{e}_1 &= \eta_1(\vec{j}_1 + \vec{j}_2) \times \hat{z}, \qquad b_1 = \eta_1 c_{*1}(\rho_1 + \rho_2) \\ \vec{e}_2 &= \eta_2(\vec{j}_1 - \vec{j}_2) \times \hat{z}, \qquad b_2 = \eta_2 c_{*2}(\rho_1 - \rho_2). \end{aligned} \tag{3.69}$$

To fix $\eta_{1,2}$ and the "speeds of light" $c_{*1,2}$, we require

$$\begin{aligned} &\frac{1}{4\pi}(\vec{e}_1^2 + \vec{e}_2^2) = \frac{\hbar^2}{2\rho_s}\left(1 + \frac{q_c}{q}\right)(\vec{j}_1^2 + \vec{j}_2^2) + \frac{\hbar^2}{\rho_s}\frac{q_c}{q}e^{-qa}\vec{j}_1 \cdot \vec{j}_2; \\ &\frac{1}{4\pi}(b_1^2 + b_2^2) = \frac{1}{2}\rho_1 V_i \rho_1 + \frac{1}{2}\rho_2 V_i \rho_2 + \rho_1 V_e \rho_2, \end{aligned}$$

thus for $n = 1, 2$,

$$\eta_n = \sqrt{\frac{\pi\hbar^2}{\rho_s}\left(1 + \frac{q_c}{q}\left(1 - (-1)^n e^{-qa}\right)\right)}, \tag{3.70}$$

$$c_{*n} = c\sqrt{\frac{q_c(1 - (-1)^n e^{-qa})}{q + q_c(1 - (-1)^n e^{-qa})}}. \tag{3.71}$$

Using (3.69) and (3.53), we can again integrate by parts and express the partition function $\mathcal{Z}$ as

$$\mathcal{Z} = \int \mathcal{D}\alpha\mathcal{D}\beta\mathcal{D}\theta_{v1}\mathcal{D}\theta_{v2}e^{-S}, \tag{3.72}$$

where

$$\begin{aligned} S &= \sum_{\omega,\vec{q}} i\left\{-(e_1^*\alpha_0 + e_2^*\beta_0)\left(\rho_{v1} - \frac{B_{ext}}{\Phi_0}\right)\right. \\ &- i(e_1^*\alpha_0 - e_2^*\beta_0)\left(\rho_{v2} - \frac{B_{ext}}{\Phi_0}\right) \\ &+ i\vec{j}_{v1}\cdot(e_1^*\frac{\vec{\alpha}}{c_{*1}} + e_2^*\frac{\vec{\beta}}{c_{*2}}) + i\vec{j}_{v2}\cdot(e_1^*\frac{\vec{\alpha}}{c_{*1}} - e_2^*\frac{\vec{\beta}}{c_{*2}}) \\ &+ \frac{1}{4\pi}(\omega^2 - c_{*1}^2q^2)\left(\frac{\vec{\alpha}}{c_{*1}}\right)^2 + \frac{q^2}{4\pi}\alpha_0^2 \\ &+ \left.\frac{1}{4\pi}(\omega^2 - c_{*2}^2q^2)\left(\frac{\vec{\beta}}{c_{*2}}\right)^2 + \frac{q^2}{4\pi}\beta_0^2\right\}, \end{aligned} \tag{3.73}$$

and for $n = 1, 2$, the dual "charges" of the vortices are

$$e_n^* = \frac{\pi\hbar}{\eta_n} = \sqrt{\pi\rho_s}\sqrt{\frac{q}{q + q_c(1 - (-1)^n e^{-qa})}}, \tag{3.74}$$

When a (number) current bias $\vec{j}_1$ is applied in layer 1, the force on a vortex in this layer is

$$\begin{aligned} F &= e_1^* \times |\vec{e}_1| + e_2^* \times |\vec{e}_2| = e_1^*\eta_1|\vec{j}_1| + e_2^*\eta_2|\vec{j}_1| \\ &= h|\vec{j}_1|, \end{aligned}$$

and the force on a vortex in the other layer is

$$\begin{aligned} F &= e_1^* \times |\vec{e}_1| - e_2^* \times |\vec{e}_2| = e_1^* \eta_1 |\vec{j}_1| - e_2^* \eta_2 |\vec{j}_1| \\ &= 0, \end{aligned}$$

as expected.

Again, introducing vortex fields ψ_{v1} and ψ_{v2} for each layer and making the action explicitly gauge-invariant, we can write the action as in

$$\begin{aligned} S = \sum_{\vec{q},\omega} \Bigg\{ \sum_{n=1,2} \Bigg[& \frac{\left(\left(\hbar \vec{q} - e_1^* \frac{\vec{\alpha}}{c_1^*} + (-1)^n e_2^* \frac{\vec{\beta}}{c_2^*} \right) \psi_{vn} \right)^2}{2m_v} \\ & + \delta\rho_{vn} \left(-i\hbar\omega\phi_n - ie_1^*\alpha_0 + (-1)^n i e_2^* \beta_0 \right) \Bigg] \\ & + \frac{1}{4\pi}(\omega^2 - c_{*1}^2 q^2) \left(\frac{\vec{\alpha}}{c_1^*} \right)^2 + \frac{1}{4\pi}(\omega^2 - c_{*2}^2 q^2) \left(\frac{\vec{\beta}}{c_2^*} \right)^2 \\ & + \frac{q^2}{4\pi}\alpha_0^2 + \frac{q^2}{4\pi}\beta_0^2 \Bigg\}. \end{aligned} \tag{3.75}$$

Integrating out α_0 and β_0, one obtains the intralayer vortex interaction potential

$$U_i(q) = \frac{\Phi_0^2 q_c}{2\pi} \frac{q + q_c}{q(q^2 + 2q_c q + q_c^2(1 - e^{-2qa}))}, \tag{3.76}$$

and interlayer vortex interaction potential

$$U_e(q) = -\frac{q_c}{q + q_c} e^{-qa} U_i. \tag{3.77}$$

Which concludes the field-theory derivation of the interaction potential.

3.C Classical derivation of the vortex interaction potential

In this appendix, we present an alternative way of deriving the vortex interaction potential between two vortices in a single superconducting thin film and in bilayer thin films.

First, consider the current and electromagnetic field configuration of a single vortex at $r = 0$ in a single superconducting thin film with thickness d located at $z = 0$. Combining the expression for the 3d current density of the vortex

$$\vec{j} = \frac{c}{4\pi\lambda^2}\left(\frac{\Phi_0}{2\pi r}\hat{\theta} - \vec{A}\right)\delta(z)d \tag{3.78}$$

where d is the thickness, and the Maxwell's equation, we have

$$\nabla^2\vec{A} = -\frac{4\pi}{c}\vec{j} = \frac{d}{\lambda^2}\left(\vec{A} - \frac{\Phi_0}{2\pi r}\hat{\theta}\right)\delta(z). \tag{3.79}$$

Next, we Fourier transform both sides of Eqn. (3.79):

$$-\vec{A}(\vec{q}, k_z) = \frac{1}{(\vec{q}^2 + k_z^2)}\frac{d}{\lambda}^2\left(\vec{A}(\vec{q}, z=0) - \frac{\Phi_0}{iq}\hat{\theta}_q\right), \tag{3.80}$$

where $\vec{q}$ is the $2d$ wave vector, k_z is the wave vector in $z-$direction, and $\hat{\theta}_q$ is the azimuthal unit vector in $q-$space. Defining the inverse 2d screening length $q_c = d/(2\lambda^2)$ and integrating both sides $\int_{-\infty}^{\infty}\mathrm{d}k_z$, one obtains

$$\vec{A}(\vec{q}, z=0) = \frac{q_c}{q+q_c}\frac{\Phi_0}{iq}\hat{\theta}_q. \tag{3.81}$$

From (3.78), we have

$$\vec{j}(\vec{q}) = \frac{q_c}{q+q_c}\frac{c\Phi_0}{2\pi i}\hat{\theta}_q. \tag{3.82}$$

Now, we calculate the interaction potential between two vortices in a single superconducting thin film. The first vortex is located at $r = 0$, whose current distribution

is given by (3.82):

$$\vec{j}_1(\vec{q}) = \frac{q_c}{q+q_c}\frac{c\Phi_0}{2\pi i}\hat{\theta}_q. \tag{3.83}$$

The second one is located at $\vec{R}$ away from the origin:

$$\begin{aligned}\vec{j}_2(\vec{q}) &= \int \mathrm{d}^2 r \vec{j}_2(\vec{r}) e^{-i\vec{q}\cdot\vec{r}} = \int \mathrm{d}^2 r \vec{j}_1(\vec{r}+\vec{R}) e^{-i\vec{q}\cdot\vec{r}} \\ &= \vec{j}_1(\vec{q}) e^{i\vec{q}\cdot\vec{R}}.\end{aligned} \tag{3.84}$$

Their interaction potential is given by

$$U(\vec{R}) = \frac{2\pi}{c^2}\int \frac{\mathrm{d}^2 q}{(2\pi)^2}\left(\frac{1}{q_c}+\frac{1}{q}\right)\vec{j}_1(-\vec{q})\vec{j}_2(\vec{q}), \tag{3.85}$$

where the first term is the kinetic energy contribution, while the second the term is from the magnetic energy B^2 term. Using (3.83) and (3.84), we have

$$\begin{aligned}U(\vec{R}) &= \frac{2\pi}{c^2}\int \frac{\mathrm{d}^2 q}{(2\pi)^2}\left(\frac{1}{q_c}+\frac{1}{q}\right)\vec{j}_1(-\vec{q})\vec{j}_1(\vec{q}) e^{i\vec{q}\cdot\vec{R}} \\ &= \int \frac{\mathrm{d}^2 q}{(2\pi)^2}\frac{\Phi_0^2 q_c}{2\pi}\frac{1}{q(q+q_c)} e^{i\vec{q}\cdot\vec{R}} \\ &\equiv \int \frac{\mathrm{d}^2 q}{(2\pi)^2} U(q) e^{i\vec{q}\cdot\vec{R}},\end{aligned} \tag{3.86}$$

where the vortex interaction potential

$$U(q) = \frac{\Phi_0^2 q_c}{2\pi}\frac{1}{q(q+q_c)} \tag{3.87}$$

is exactly the same as what we obtained earlier in Appendix 3.A with field theory formalism.

For the case of bilayer thin films with interlayer separation a, we can proceed in the same way. But there is one subtlety in that case. A vortex in layer 1, characterized by a phase singularity in layer 1, will also induce a circulating screening current in layer 2. Suppose the two identical layers are located at $z = 0$ and $z = -a$, respectively,

the one-vortex configuration is given by

$$\begin{aligned}
\vec{j}_1 &= \frac{c}{4\pi\lambda^2}\left(\frac{\Phi_0}{2\pi r}\hat{\theta} - \vec{A}(z=0)\right)\delta(z)d, \\
\vec{j}_1' &= \frac{c}{4\pi\lambda^2}\left(-\vec{A}(z=-a)\right)\delta(z+a)d, \\
\nabla^2\vec{A} &= -\frac{4\pi}{c}\left(\vec{j}_1 + \vec{j}_1'\right).
\end{aligned} \tag{3.88}$$

Performing Fourier transform, one obtains

$$\begin{aligned}
\vec{A}(\vec{q}, k_z) = &\frac{2q_c}{q^2 + k_z^2} \\
&\times \left(\frac{\Phi_0}{iq}\hat{\theta}_q - \vec{A}(\vec{q}, z=0) - e^{ik_z a}\vec{A}(\vec{q}, z=-a)\right).
\end{aligned}$$

Integrating over k_z, one obtains two equations for $\vec{A}(\vec{q}, z=0)$ and $\vec{A}(\vec{q}, z=-a)$, whose solution is given by

$$\begin{aligned}
\vec{A}(\vec{q}, z=0) &= \frac{q_c[q + q_c(1 - e^{-2qa})]}{(q+q_c)^2 - q_c^2 e^{-2qa}} \times \frac{\Phi_0}{iq}\hat{\theta}_q, \\
\vec{A}(\vec{q}, z=-a) &= \frac{q_c q e^{-qa}}{(q+q_c)^2 - q_c^2 e^{-2qa}} \times \frac{\Phi_0}{iq}\hat{\theta}_q.
\end{aligned} \tag{3.89}$$

Thus, one can obtain $\vec{j}_1$ and $\vec{j}_1'$ from (3.88)

$$\begin{aligned}
\vec{j}_1 &= \frac{q_c(q+q_c)}{(q+q_c)^2 - q_c^2 e^{-2qa}} \frac{c\Phi_0}{2\pi i}\hat{\theta}_q, \\
\vec{j}_1' &= -\frac{q_c^2 e^{-qa}}{(q+q_c)^2 - q_c^2 e^{-2qa}} \frac{c\Phi_0}{2\pi i}\hat{\theta}_q.
\end{aligned} \tag{3.90}$$

Next, one put in the currents $\vec{j}_2$ and $\vec{j}_2'$ of another vortex either in the same layer or the other layer, and calculate the intralayer and interlayer vortex interaction potential U_i and U_e in the same way as we did for the single layer case. For example, to calculate the vortex interlayer interaction U_e, we put in another vortex with its core at the second layer, and it has a current $\vec{j}_2$ in the second layer, and a circulating

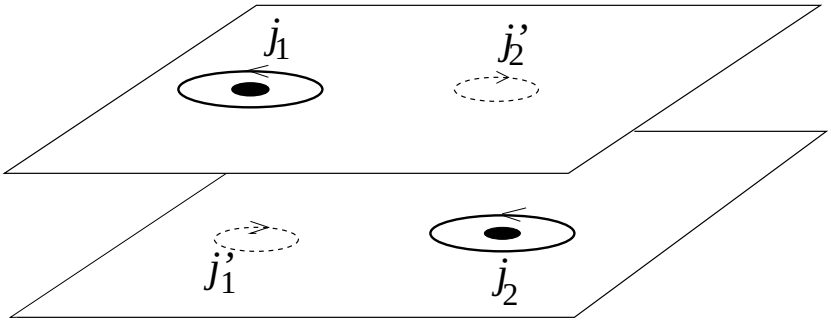

Figure 3.4: The setup for calculating vortex interlayer interaction potential U_e. A phase singularity in layer 1 leads to current $\vec{j}_1$ and $\vec{j}_1'$ in laye 1 and 2, respectively, and similarly a phase singularity in layer 2 leads to current $\vec{j}_2$ and $\vec{j}_2'$ in layer 2 and 1, respectively.

screening current $\vec{j}_2'$ in the first layer (see FIG. 3.4). Thus,

$$U_e(\vec{R}) = \frac{2\pi}{c^2}\int \frac{\mathrm{d}^2q}{(2\pi)^2}\left[\left(\frac{1}{q_c}+\frac{1}{q}\right)(\vec{j}_1\vec{j}_2'+\vec{j}_2\vec{j}_1') + \frac{e^{-qa}}{q}(\vec{j}_1\vec{j}_2+\vec{j}_1'\vec{j}_2')\right]. \tag{3.91}$$

The final results are exactly the same as what we found in the field theory formalism in Sec. 3.2.1 and Appendix 3.B:

$$\begin{aligned} U_i(q) &= \frac{\Phi_0^2 q_c}{2\pi}\frac{q+q_c}{q(q^2+2q_cq+q_c^2(1-e^{-2qa}))}, \\ U_e(q) &= -\frac{q_c}{q+q_c}e^{-qa}U_i. \end{aligned} \tag{3.92}$$

3.D Hard-disc liquid description of the vortex metal phase

As explained in Sec. 3.2.2, we expect that our results for the vortex drag do not depend sensitively on the microscopic model we use for the vortices. In Sec. 3.2.2 we used the fermionic vortex response function to determine the drag resistance in the intermediate metallic regime. Here we demonstrate the robustness of this result by reproducing the drag resistance results while modeling the vortex liquid in this regime as a classical hard-disc liquid.

The density response function $\chi(k,z)$ for a liquid of hard-core disks in the hydrodynamical limit is[205, 206, 215]

$$\chi(k,z) = \chi(k) + i\frac{z}{T}C(k,z), \tag{3.93}$$

where z is the frequency, T is the temperature, $\chi(k)$ is the static compressibility, and

$$\begin{aligned} C(k,z) = iT\chi(k) \Bigg[& \frac{1}{\gamma}\frac{z + ik^2(\Gamma + D(\gamma-1))}{z^2 - c^2k^2 + izk^2\Gamma} \\ & + \left(1 - \frac{1}{\gamma}\right)\frac{1}{z + ik^2D}\Bigg], \end{aligned} \tag{3.94}$$

showing a diffusive mode with weight $1 - \frac{1}{\gamma}$, and a propagating mode with velocity c, weight $1/\gamma$ and life time $1/(\Gamma k^2)$. Thus

$$\frac{\chi(k,z)}{\chi(k)} = \left(1 - \frac{1}{\gamma}\right)\frac{Dk^2}{Dk^2 - iz} + \frac{1}{\gamma}\frac{c^2k^2 - izDk^2(\gamma-1)}{c^2k^2 - z^2 - i\Gamma k^2 z}, \tag{3.95}$$

which satisfies the defining property of χ:

$$\chi(k) = \lim_{z\to 0}\chi(k,z). \tag{3.96}$$

Here, $\gamma = C_p/C_v$, $C_v = 1$ is the constant volume specific heat, and

$$C_p = C_v + T\chi_T\beta_V^2/n \tag{3.97}$$

is the constant pressure specific heat, where n is the vortex density, $\chi_T = \frac{1}{nT}\lim_{k\to 0} S(k)$ is the isothermal compressibility, and $S(k)$ is the structure factor of the vortex liquid; $\beta_V \equiv n(1+y)$, where $y \equiv \frac{\pi}{2}n\sigma^2 g(\sigma)$,

$$g(\sigma) \equiv \frac{1 - 7\zeta/16}{(1-\zeta)^2} - \frac{\zeta^3/64}{(1-\zeta)^4}, \tag{3.98}$$

$\zeta = \frac{\pi n\sigma^2}{4}$ is the packing fraction, and σ is the diameter of the hard-disc vortex which we take to be the core size of the vortex, which in turn is approximately supercon-

ducting coherence length $\sim$ 10nm.

In addition, $\Gamma = a\left(\frac{\gamma-1}{\gamma}\right) + b$, and the diffusion coefficient $D = \frac{a}{\gamma}$, where

$$\begin{aligned} a &= \frac{\nu\sigma^2}{4} + \frac{2}{\nu}(1+3y/4)^2 v_0^2, \\ b &= 3\nu\sigma^2/8 + v_0^2(1+y/2)^2/\nu, \end{aligned} \tag{3.99}$$

$\nu = 2\sqrt{\pi}n\sigma g(\sigma)v_0$ is called the Enskog collision frequency, and the thermal velocity $v_0 = \sqrt{\frac{T}{m}}$, m is the vortex mass. Finally, the speed of sound is

$$c = \sqrt{\frac{C_p}{C_v}}\frac{v_0}{nT\chi_T}. \tag{3.100}$$

The static compressibility $\chi(k)$ is related to the structure factor $S(k)$ (strictly speakly, the Ursell function [216]) by

$$\chi(k) = \frac{n}{T}S(k), \tag{3.101}$$

and the structure factor $S(k)$ of a hard disk liquid is determined by following the so-called Percus-Yevick approximation of Ref. [217, 218]:

$$S(k) = 1/(1-nh(k)), \tag{3.102}$$

where

$$h(k) = 2\pi\int_0^\infty \mathrm{d}RRJ_0(kR)h(R), \tag{3.103}$$

$$h(R) = \begin{cases} h(0) + \frac{\zeta h(1)^2 S(R)}{2\mu_D}, & 0 \le R < 1 \\ 0, & R \ge 1 \end{cases}. \tag{3.104}$$

Here, $\mu_D = \pi/16$, $\zeta = \frac{\pi n\sigma^2}{4}$ is the packing fraction,

$$h(1) = \frac{\sqrt{(1-4\zeta)^2 - 4(\alpha-\beta)} - (1-4\zeta)}{2(\alpha-\beta)}, \tag{3.105}$$

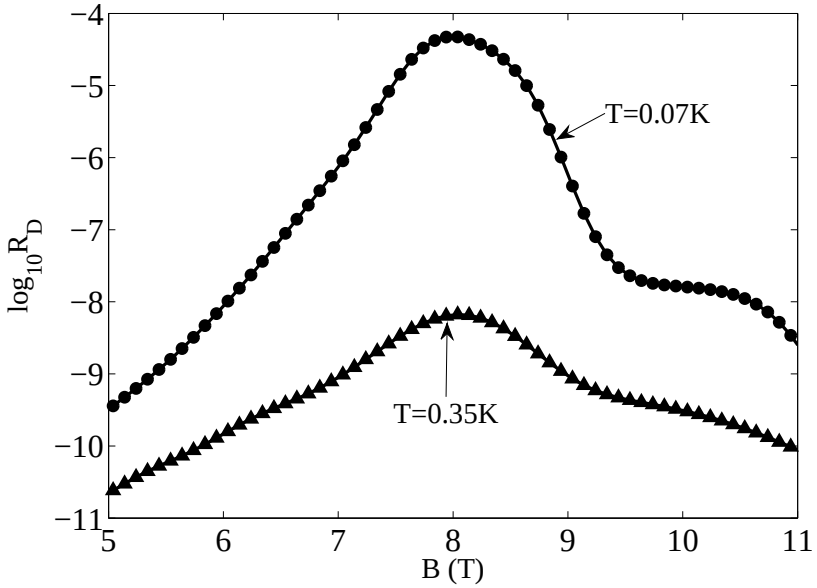

Figure 3.5: Drag resistance in the vortex paradigm at $T = 0.07$K, with the metallic phase modeled as classical hard-disc liquid. Everything else is the same those in FIG. 2.

$$h(0) = h(1) - \beta h(1)^2, \tag{3.106}$$

$$\beta = \frac{\zeta S(R=1)}{2\mu_D}, \qquad \alpha = 2\zeta^2 A, \tag{3.107}$$

$$A = \frac{1}{\mu_D}\left(\frac{2}{\tilde{a}}\right)^3 \int_0^{\frac{\tilde{a}}{2}} \mathrm{d}z z^2 (1-z^2)^{1/2}, \tilde{a} = 1+\zeta, \tag{3.108}$$

$$S(R) = \frac{1}{\tilde{a}}\left\{\arcsin\left(\frac{\tilde{a}R}{2}\right) + \frac{\tilde{a}R}{2}\left[1-\left(\frac{\tilde{a}R}{2}\right)^2\right]^{1/2}\right\}. \tag{3.109}$$

Putting these formulae together, we can compute the vortex density response function in (3.93) and insert it into the drag resistance formula (3.15). The drag resistance is shown in FIG. 3.5. One can see that it is remarkably close to our results obtained in Sec. (3.2.2), and thereby demonstrating that the scale of the drag resistance in the metallic regime is mainly set by the factors dR/dB and is not sensitive to the statistics of the vortex particles.

3.E Coulomb Drag for disordered electron glass

In this section, we calculate the drag resistance due to Coulomb interaction between two disordered electron glasses with finite thickness. This calculation is related to the work of Ref. [219], but in our case the screening of the interlayer Coulomb interaction is important (see below), and we take into account the effect of finite film thickness.

The general formula for Coulomb drag resistance in d dimensions is[198, 199]

$$\rho_D^{ij} = \frac{\hbar^2}{e^2}\frac{1}{2\pi n^2 T}\frac{1}{\Omega}\sum_{\vec{k}} k^i k^j \int_0^\infty \frac{\mathrm{d}\omega}{\sinh\frac{\hbar\omega}{2T}} |U|^2 \operatorname{Im}\chi_1 \operatorname{Im}\chi_2. \tag{3.110}$$

For the quasi-2d film we are considering, we can break the wavevector summation into two summations: one over k_z, another over the 2d wavevector $\vec{q}$. The k_z summation is dominated by the term with $k_z = 0$ component, which physically corresponds to the configuration with constant density along z-direction. In this case, we can use the quasi-2d form of the intralyer and interlayer Coulomb interaction potentials

$$U_i(\vec{q}, k_z = 0) = \frac{2\pi e^2 d}{q}, \qquad U_e(\vec{q}, k_z = 0) = \frac{2\pi e^2 d}{q} e^{-qa},$$

where d is the film thickness, and a is the center-to-center layer separation. The real and imaginary parts of the density response function for a localized electron gas is[220, 221, 222]

$$\begin{aligned}
\operatorname{Re}\chi(\vec{q}, k_z = 0, \omega) &= \nu(q^2 + k_z^2)\xi^2\Big|_{k_z=0} = \nu q^2 \xi^2, \\
\operatorname{Im}\chi(\vec{q}, k_z = 0, \omega) &= \nu\frac{(q^2 + k_z^2)\omega\xi^4}{D}\Big|_{k_z=0} = \nu\frac{q^2\omega\xi^4}{D},
\end{aligned}$$

where ν is the 3d density of states at the Fermi energy, and ξ is the localization length, and D is the diffusion constant in the conducting phase. The above expression is valid so long as $\operatorname{Im}\chi \ll \operatorname{Re}\chi$, which is straightforward to verify in our case recalling that ω is cut off by the temperature T in (3.110).

Thus, in the screened interlayer interaction we can neglect $\operatorname{Im}\chi$ compared to $\operatorname{Re}\chi$:

$$\begin{aligned} U &= \frac{U_i e^{-qa}}{(1+U_i\chi_1)(1+U_i\chi_2)-(U_i e^{-qa}\chi_1)(U_i e^{-qa}\chi_2)} \\ &\approx \frac{1}{2U_i \operatorname{Re}\chi_1 \operatorname{Re}\chi_2 \sinh(qa)}, \end{aligned} \tag{3.111}$$

where in the last line we have made an approximation that $U_i \operatorname{Re}\chi \gg 1$, i.e.,

$$qa \gg x_0 \equiv \frac{a}{\nu\xi^2 2\pi e^2 d}. \tag{3.112}$$

We have verified that the contribution from $0 < qa < x_0$ is negligible compared to that from $qa > x_0$. Therefore,

$$\begin{aligned} R_D &= \frac{\rho_D^{xx}}{d} \\ &= \frac{1}{8\pi^2(nd)^2 T}\frac{\hbar^2}{e^2}\int_{x_0}^{\infty} q^3 \mathrm{d}q \\ &\times \int_0^{\infty} \frac{\mathrm{d}\omega}{\sinh^2\frac{\hbar\omega}{2T}} \frac{\operatorname{Im}\chi_1 \operatorname{Im}\chi_2}{4U_i^2(\operatorname{Re}\chi_1)^2(\operatorname{Re}\chi_2)^2\sinh^2(qa)} \\ &= \frac{T^2}{128\pi^4\hbar e^2(nda)^2(D_1 e^2 d\nu)(D_2 e^2 d\nu)} \\ &\times \int_{x_0}^{\infty} \frac{x\mathrm{d}x}{\sinh^2 x}\int_0^{\infty}\frac{x^2\mathrm{d}x}{\sinh^2(x/2)} \\ &= \frac{T^2}{128\pi^4\hbar e^2(nda)^2(D_1 e^2 d\nu)(D_2 e^2 d\nu)}\log\frac{1}{2x_0}\frac{4\pi^2}{3} \\ &= \frac{T^2}{96\pi^2\hbar e^2(nda)^2(D_1 e^2 d\nu)(D_2 e^2 d\nu)}\log\frac{1}{2x_0}. \end{aligned}$$

Note that

$$De^2 d\nu = \frac{1}{R}, \tag{3.113}$$

we have

$$\begin{aligned} R_D &= \frac{T^2 R_1 R_2}{96\pi^2\hbar e^2(nda)^2}\log\frac{1}{2x_0} \\ &= \frac{1}{96\pi^2}\frac{R_1 R_2}{\hbar/e^2}\left(\frac{T}{e^2 nda}\right)^2\log\frac{1}{2x_0}. \end{aligned} \tag{3.114}$$

Since D is the diffusion constant in the conducting phase, R in the above expression should also be the resistance of the conducting phase. Thus this expression gives a slight overestimate of the drag resistance in the percolation paradigm if we use the value of R_{NN} of the insulating phase for simplicity.

Note that our derivation relied on momentum summations. There are concerns that such an approach, although quite common in the literature, is incorrect when attempting to describe drag in strongly disordered systems. For our purposes, the derivation based on Eq. 3.110 is sufficient; this issue is taken up, however, in Ref. [223].

3.F No drag resistance for a genuine superconductor

In this section, we show that a genuine superconducting link (i.e., without mobile vortices) has no measurable drag effect in a resistor network.

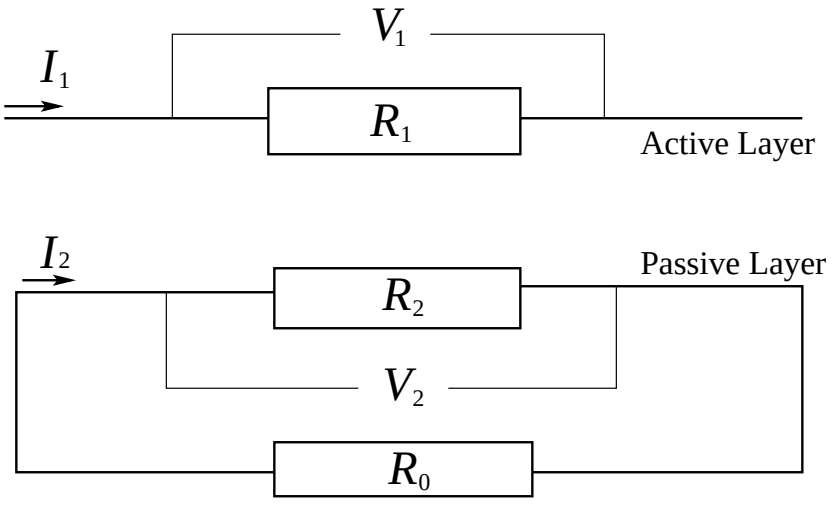

Figure 3.6: The typical setup for a drag effect experiment: in the active layer, a driving current I_1 flows through a resistor R_1 (normal or superconducting) with a voltage drop $V_1 = I_1 R_1$. In the passive layer, certain interaction effect takes place in a resistor R_2 (normal or superconducting), which may result in a drag current I_2 and a voltage drop V_2 across R_2. R_2 is also connected to another resistor R_0, which can be of any value.

FIG. 3.6 illustrates the typical setup for a drag effect experiment: in the active layer, a driving current I_1 flows through a resistor R_1 (normal or superconducting) with a voltage drop $V_1 = I_1 R_1$. In the passive layer, certain interaction effects take place in a resistor R_2 (normal or superconducting), which may result in a drag current I_2 and a voltage drop V_2 across R_2. R_2 is also connected to another resistor R_0, which might represent a voltmeter, an open circuit ($R_0 = \infty$), or something else.

When one talks about the drag effect, there are two different concepts one needs to distinguish. The first one is the "intrinsic" effect, which manifests itself by the appearance of a drag current I_D in the passive layer *if* $R_0 = 0$. Generically, we have

$$I_D \equiv I_2|_{R_0=0} = \eta I_1. \tag{3.115}$$

For example, for the case of $R_1, R_2 > 0$, i.e., both R_1 and R_2 are non-superconducting, $I_2|_{R_0=0} = \sigma_D V_1 = \sigma_D I_1 R_1$ (e.g., Coulomg drag between two 2DEGs), thus $\eta = \sigma_D R_1$; for $R_1 = R_2 = 0$ (superconductor), we have the Cooper pair version of the supercurrent drag effect Eqn. (3.32), thus η is finite in this case as well. For the case of $R_1 > 0$ (normal) and $R_2 = 0$ (superconducting), it would be unphysical to have $\eta = \infty$, thus we have $\eta < \infty$ and $\sigma_{D,NS} = \eta/R_1 < \infty$. From Kubo formula for the drag conductance, we expect that $\sigma_{D,SN} = \sigma_{D,NS} < \infty$, and hence for the case of $R_1 = 0$ and $R_2 > 0$ we have $\eta = \sigma_{D,SN} R_1 = 0$.

In contrast, the second drag effect is the drag current I_2 in the presence of R_0, in which case he drag current at $R_0 = 0$ may or may not survive. In a large-size resistor network we are considering for the percolation picture, when we focus on the drag effect of one specific link R_2, we can simplify the circuit of the passive layer to be of the form in FIG. 3.6, in which case R_0 representing the rest of the circuit is almost always larger than 0. If the drag effect survives the presence of the nonzero R_0, it will manifest itself as the appearance of a non-zero drag emf ε_D on R_2. To see this, first consider the case $R_2 > 0$, and R_1 can be either 0 or > 0. I_2 receives contribution

from both Ohm's law and the drag effect:

$$I_2 = \frac{V_2}{R_2} + \eta I_1 = -\frac{I_2 R_0}{R_2} + \eta I_1, \tag{3.116}$$

thus

$$I_2 = \frac{(\eta R_2) I_1}{R_0 + R_2} \equiv \frac{R_D I_1}{R_0 + R_2} \equiv \frac{\varepsilon_D}{R_0 + R_2}, \tag{3.117}$$

where $\varepsilon_D = R_D I_1$ is the drag emf, and $R_D = \eta R_2$ is the drag resistance. If $R_1 = 0$ (superconducting) and $R_2 > 0$ (normal), we argued earlier that $\eta = 0$, and thus $\varepsilon_D = R_D = 0$ and there is no drag effect.

If $R_2 = 0$ (superconductor), no matter if $R_1 = 0$ (superconducting) or > 0 (normal), it is straightforward to see from Kirchoff's Law that we have only one steady-state solution $I_2|_{R_0>0} = 0$. More insight into this case can be gained by considering what happens in real time. Suppose at time $t = 0$, the drag effect takes place, a drag supercurrent $I_2(R_0 = 0)$ starts to flow in the circuit. But due to the presence of the normal resistor R_0, a voltage $I_2 R_0$ now exist on the supercondutor, which will crank up the phase winding of the superconductor and degrade the drag supercurrent, until a steady state is reached where the total supercurrent is zero. Thus, we see that for the case $R_2 = 0$ and $R_0 > 0$, there is no observable drag effect, i.e., $I_2|_{R_0>0} = 0$, $\varepsilon_D = I_2(R_2 + R_0) = 0$, $R_D = \varepsilon_D / I_1 = 0$, although there is nonzero "intrinsic" drag effect η.

We can also understand this result $R_D = 0$ for $R_2 = 0$ by examining the expression $R_D = \eta R_2$. For both the case of $R_1 = R_2 = 0$ and the case of $R_1 > 0$ and $R_2 = 0$, we found earlier that $\eta < \infty$, and thus the drag resistance $R_D = \eta R_2$ and the drag emf ε_D are 0 for $R_2 = 0$.

In conclusion, we have shown that when connected with a nonzero resistor, as typically true in a resistor network, a genuine superconducting link has no measurable drag effect at all, no matter whether it is vertically aligned with a normal link or another superconducting link.

Chapter 4

First Order Phase Transitions in Bilayer Quantum Hall Systems

4.1 Introduction

As discussed in Chapter 1, we assume that the transition tuned by d/l is a thermodynamic first-order transition between spin-polarized coherent $\nu_{tot} = 1$ quantum Hall state and partially-polarized composite Fermi liquid state, and derive the Clausius-Clapeyron relations for this system. The Clausius-Clapeyron relations will allow us to obtain the phase boundary shapes for the transition; a comparison of these boundaries with experiments presents a stringent consistency test of the first order transition scenario. The first-order scenario was invoked by Ref. [138] to explain the strongly enhanced longitudinal Coulomb drag for intermediate d/l, and it also has some support from exact-diagonalization study[137]. Note that we will only consider the case of negligible interlayer tunneling.

The Clausius-Clapeyron relations are the results of matching the free energies of the two phases along the phase boundary. To be more specific, we denote the free energy density of the coherent and the incoherent phases to be E_c and E_i, and define

$$f(\delta, B_{tot}, \Delta n, T) = E_c(\delta, B_{tot}, \Delta n, T) - E_i(\delta, B_{tot}, \Delta n, T),$$

where $\delta \equiv d/l$, B_{tot} is the total magnetic field coupled to electrons' physical spin, $\Delta n = (n_1 - n_2)/2$ is the density imbalance, T is the temperature. At any point along

the phase boundary, we must have

$$f(\delta_c, B_{tot}, \Delta n, T) = 0. \tag{4.1}$$

This equation can be viewed as defining the δ_c at which the transition occurs. When one changes the total field by $\mathrm{d}B_{tot}$, the critical $\delta_c(B_{tot}, \Delta n, T)$ also changes by $\mathrm{d}\delta_c$ when the filling factor is kept fixed at $\nu_{tot} = 1$. Their relation is determined by

$$0 = \frac{\partial f}{\partial \delta}\mathrm{d}\delta_c + \frac{\partial f}{\partial B_{tot}}\mathrm{d}B_{tot}, \tag{4.2}$$

therefore the slope of the phase boundary is determined by the following ODE:

$$\frac{\mathrm{d}\delta_c}{\mathrm{d}B_{tot}} = -\frac{\frac{\partial f}{\partial B_{tot}}}{\frac{\partial f}{\partial \delta}} = \frac{\frac{\partial E_i}{\partial B_{tot}} - \frac{\partial E_c}{\partial B_{tot}}}{\frac{\partial f}{\partial \delta}}. \tag{4.3}$$

A crucial assumption of our work is that

$$\frac{\partial f}{\partial \delta} = \eta \frac{e^2}{\epsilon l^3}, \tag{4.4}$$

where $e^2/(\epsilon l^3)$ not only gives the correct units, but is the only energy scale that exists in this problem if we neglect the Landau Level mixing. η is a universal positive dimensionless constant. It is positive because f should be an increasing function of $\delta = d/l$, since the incoherent phase should be more and more energetically favorable with increasing d/l. In general, η could be a function of $\delta = d/l$, i.e., $\eta(\delta) \approx \eta(\delta_0) + \mathcal{O}[(\delta - \delta_0)/\delta_0]$, but since in experiments δ does not change much (ranging from 1.7 to 2), $(\delta - \delta_0)/\delta_0 \ll 1$, we will assume η to be a constant for simplicity.

Similar analysis also applies to finite temperature transitions:

$$\frac{\mathrm{d}\delta_c}{\mathrm{d}T} = \frac{\frac{\partial E_i}{\partial T} - \frac{\partial E_c}{\partial T}}{\eta \frac{e^2}{\epsilon l^3}}. \tag{4.5}$$

For density imbalance experiments, we will focus on the phase boundary near $\Delta n = 0$.

First, note that by symmetry

$$\frac{\partial f}{\partial \Delta n} = 0. \tag{4.6}$$

Thus, we need to expand f to second order in Δn:

$$0 = \frac{\partial f}{\partial \delta} \mathrm{d}\delta_c + \frac{1}{2} \frac{\partial^2 f}{\partial \Delta n^2} (\Delta n)^2, \tag{4.7}$$

and therefore

$$\frac{\mathrm{d}\delta_c}{\mathrm{d}(\Delta n^2)} = \frac{\frac{1}{2}\frac{\partial^2 E_i}{\partial \Delta n^2} - \frac{1}{2}\frac{\partial^2 E_c}{\partial \Delta n^2}}{\eta \frac{e^2}{\epsilon l^3}}. \tag{4.8}$$

The above equations constitute the Clausius-Clapeyron relations for the bilayer quantum Hall systems. In the following sections, we will investigate whether the phase boundary shapes implied by Clausius-Clapeyron relations are consistent with experiments, and whether a single universal parameter η can explain all available experimental results. To obtain the detailed forms of free energy of both phases, we will primarily work with the pseudospin ferromagnet description for the coherent quantum Hall phase and the Chern-Simons approach for the incoherent composite Fermi liquid phase. Spin transitions, finite temperature transitions, and density imbalance experiments are studied in Sec. 4.2, 4.3, and 4.4, respectively. Finally, we summarize and discuss our results in Sec. 4.5. Some theoretical details are relegated to Appendices. This chapter is adapter from our work Ref. [224].

4.2 Spin transition experiments

Ref. [121] and Ref. [125] have studied the effect of NMR/heat pulse and parallel magnetic field on the transition tuned by d/l, respectively. In the experiment of Ref. [125], since the interlayer tunneling is negligible, the main effect of the parallel field is on the spins of electrons. Similarly, in the experiment of Ref. [121], NMR/heat pulse acts to depolarize the nuclei and therefore also changes the Zeeman field on the electrons through the hyperfine coupling. Thus, these two experiments can be analyzed in a similar fashion. Since we assume the coherent phase is spin polarized,

the spin part of the coherent phase free energy is simply the Zeeman energy:

$$E_c = -\frac{1}{2}N_T|g|\mu_B B_{tot} = -\frac{e|g|\mu_B B_\perp B_{tot}}{4\pi\hbar}, \tag{4.9}$$

where N_T is the total electron density of the two layers, $B_\perp$ is the perpendicular magnetic field, B_{tot} is the total magnetic field coupled to electron spin, $g = -0.44$ is the g-factor of the GaAs two dimensional electron gas, and μ_B is the Bohr magneton.

For the partially spin-polarized incoherent phase, the single layer free energy is

$$\frac{E_i}{2} = \frac{1}{2\chi}M^2 - MB_{tot}, \tag{4.10}$$

where the magnetization

$$M = \frac{1}{2}|g|\mu_B(n_\uparrow - n_\downarrow) \equiv |g|\mu_B\Delta n, \tag{4.11}$$

and χ is the single layer spin susceptibility. The steady state is obtained by minimizing E_i with respect to M:

$$\chi = \frac{M}{B_{tot}}, \tag{4.12}$$

therefore

$$\frac{E_i}{2} = \begin{cases} -\frac{1}{2}\chi B_{tot}^2, & B_{tot} < B_{tot,p} \\ \frac{1}{2\chi}M_{max}^2 - M_{max}B_{tot}, & B_{tot} > B_{tot,p} \end{cases}, \tag{4.13}$$

where the maximum magnetization M_{max} and the field for full polarization $B_{tot,p}$ are given by

$$\begin{aligned} M_{max} &= \frac{1}{2}|g|\mu_B n = \frac{e|g|\mu_B B_\perp}{8\pi\hbar}, \\ B_{tot,p} &= \frac{M_{max}}{\chi}. \end{aligned} \tag{4.14}$$

Plugging these forms of free energy into (4.3), we obtain an equation

$$\frac{\mathrm{d}\delta_c}{\mathrm{d}B_{tot}} = \begin{cases} \frac{-2\chi B_{tot} + \frac{e|g|\mu_B B_\perp}{4\pi\hbar}}{\eta\frac{e^2}{\epsilon l^3}}, & B_{tot} < B_{tot,p} \\ 0, & B_{tot} > B_{tot,p} \end{cases}. \tag{4.15}$$

Note that the RHS also depends on δ_c through $B_\perp$ which determines ℓ. Eqn. (4.15) can be solved numerically to yield the $\delta_c - B_{tot}$ curve. For typical experimental parameters, $\mathrm{d}\delta_c/dB_{tot}$ starts out to be positive when B_{tot} is small, and continuously decreases to zero when

$$-2\chi B_{tot} + \frac{e|g|\mu_B B_\perp}{4\pi\hbar} = 0, \tag{4.16}$$

this is nothing but Eqn. (4.14) which determines the magnetic field at which all composite fermions get polarized.

It remains to determine the value of the composite fermion spin susceptibility χ. This can be done if B_{tot} and $B_\perp$ at which full polarization occurs are known, because from Eqn. (4.14) or (4.16) we have

$$\chi = \frac{|g|\mu_B B_{\perp,p}}{4B_{tot,p}\phi_0}, \tag{4.17}$$

where the subscript p denotes the point of full polarization. In experimental and exact-diagonalization studies, one often parametrize χ with the form of non-interacting Fermi gas with a "polarization mass" m_p[225, 109]:

$$\chi = \frac{m_p}{4\pi\hbar^2}(|g|\mu_B)^2. \tag{4.18}$$

In the lowest-Landau-level approximation, $\frac{e^2}{\epsilon l}$ is the only relevant energy scale, and thus

$$\frac{\hbar^2}{l^2 m_p} \propto \frac{e^2}{\epsilon l}. \tag{4.19}$$

Therefore, presumably m_p scales as $\sqrt{B_\perp}$:

$$m_p = x m_e \sqrt{B_\perp}, \tag{4.20}$$

where m_e is the vacuum electron mass, x is a dimensionless number, $B_\perp$ is in units of Tesla. It is worth noting that unlike free electrons spin-susceptibility which is proportional to $1/m_e$, the susceptibility of composite fermions is proportional to m_p and therefore to $\sqrt{B}$. The reason for this is that the Bohr magneton μ_B depends on

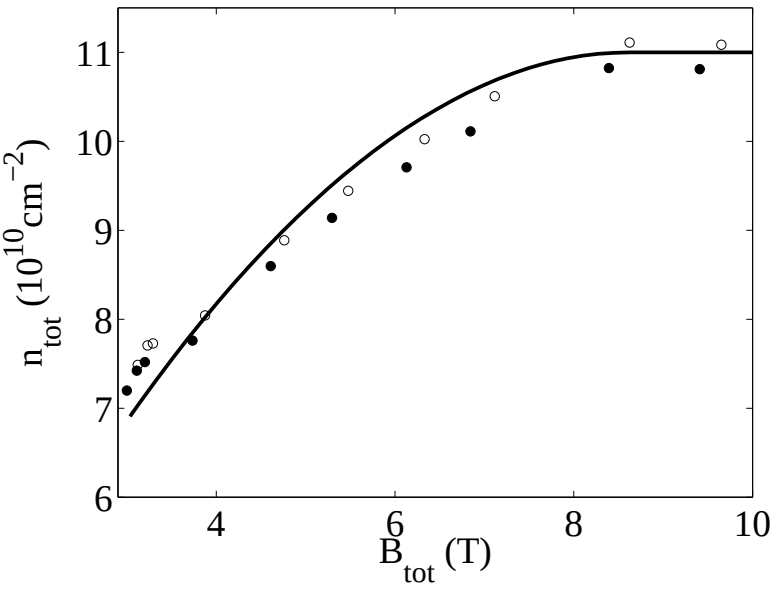

Figure 4.1: Total electron density deduced from the critical $d/l = \delta_c$ vs. the total magnetic field for the parallel magnetic field experiments. Open and solid circles are experimental results of Giudici *et al.* [125] (c.f. FIG. 4a there). Solid line is our theoretical calculation with the fitting parameter $\eta = 0.8 \cdot 10^{-3}$. The boundary condition in our calculation is chosen as $n_{tot} = 11 \cdot 10^{10}\text{cm}^{-2}$ when $B = 10\text{T}$.

the bare mass of the electron, and therefore does not overturn the proportionality to effective mass in the density of states factor of the susceptibility.

For the parallel field experiment of Ref. [125], composite fermions get polarized at total density $n_{tot} = 11 \cdot 10^{10}\text{cm}^{-2}$, tilting angle $\theta = 58^\circ$, which corresponds to $B_{tot,p} = 8.60\text{T}$, $B_{\perp,p} = 4.56\text{T}$, $x = 0.56$ if we parametrize χ in terms of the polarization mass m_p. Then we solve the ODE (4.15) with the boundary condition at the high field endpoint ($B_{tot} = 10\text{T}$, $n_{tot} = 11 \cdot 10^{10}\text{cm}^{-2}$), and plot the n_{tot} deduced from δ_c vs. B_{tot} in FIG .4.1. To tune the result to resemble the experimental results in FIG. 4a of Ref. [125], we get

$$\eta = (0.8 \pm 0.2) \cdot 10^{-3}, \tag{4.21}$$

where the error mainly comes from fitting errors, meaning a finite range of η's make the $\delta_c - B_{tot}$ curve resemble the experimental result.

For the NMR and heat pulse experiments of Ref. [121], the phase boundary before any perturbation is $\delta_{c0} = 1.967$, which correspond to $B_\perp = 3.26\text{T}$. Ref. [121]

has estimated the effective nuclear magnetic field to be $B_N = -0.17$T, therefore the total effective magnetic field felt by electronic spin is $B_{tot} = B_\perp + B_N$. After a heat pulse, nuclear spins are depolarized, and B_N is set to zero. B_{tot} is strengthened to $B_\perp$, and the phase boundary changes to $\delta_c = 1.983$. We can not determine the spin susceptibility or the polarization mass directly from experimental information, and therefore we use the numerical and experimental results from the literature $m_p = (0.7 \pm 0.2) m_e \sqrt{B_\perp}$ with B in units of Tesla [225, 226, 227, 228, 114]. In this way, we obtain

$$\eta \approx (1.3 \pm 0.4) \cdot 10^{-3}, \tag{4.22}$$

where the error mainly comes from uncertainty in the value of the polarization mass m_p.

Note that our calculations in this section do not rely on the Chern-Simons description of composite fermions.

4.3 Finite temperature transition experiments

Ref. [126] has studied the changes in critical $\delta_c = d/l$ as a function of the temperature T. They found that the phase boundary moves to smaller d/l with higher T. When analyzing the temperature dependence of the transition, one needs to include the entropy contributions to the free energy associated with various low energy excitations for both phases. In the interlayer-coherent quantum Hall phase, the only gapless excitation is the linearly dispersing Goldstone mode, which corresponds to in-plane spin wave in the pseudospin language. Therefore, this mode dominates the temperature dependence of the free energy of the coherent phase. Denoting its velocity to be v, we have the free energy

$$E_c(T) = \sum_k T \ln(1 - e^{-\hbar v k/T}) \approx \frac{-1.2}{2\pi} \frac{T^3}{(\hbar v)^2}, \tag{4.23}$$

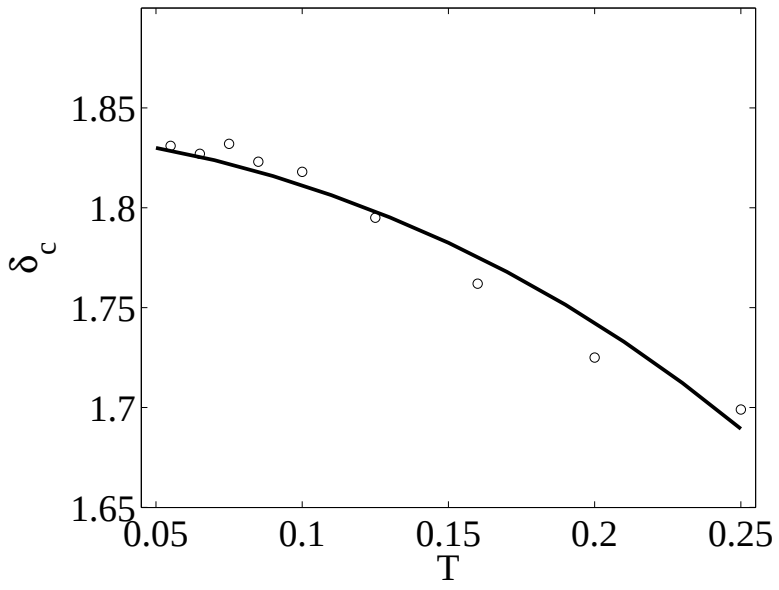

Figure 4.2: The phase boundary d/l vs. the temperature T (in Kelvin) for the finite temperature experiments. Circles are experimental results of Champagne *et al.* [126] (c.f. FIG. 2c there). Solid line is our theoretical calculation with the fitting parameter $\eta = 0.7 \cdot 10^{-3}$. The boundary condition in our calculation is chosen as $\delta_c = 1.83$ when $T = 50$mK.

and therefore

$$\frac{\partial E_c}{\partial T} = -\frac{1.8}{\pi}\frac{T^2}{(\hbar v)^2}. \tag{4.24}$$

We use the experimental result of Ref. [92] to estimate the value of v (which we assume to be a constant independent of δ):

$$v = 1.4 \cdot 10^4 m \cdot s^{-1} \tag{4.25}$$

For the incoherent phase, working in the Chern-Simons framework, we have contributions from composite fermions as well as Chern-Simons gauge fields. The free energy is

$$E_i = -T \ln Z, \tag{4.26}$$

where the partition function Z contains both composite fermion fields and Chern-Simons gauge fields of the two layers. Integrating out the composite fermions, we

obtain[100, 229] (see Appendix 4.A for details)

$$Z = Z_0 Z_+ Z_-, \tag{4.27}$$

where Z_0 is the partition function for free fermions, and

$$Z_\pm = \int \mathcal{D}a_\pm e^{-\int \mathrm{d}\tau \mathrm{d}^2x (a_\pm D_\pm^{-1} a_\pm/2)}, \tag{4.28}$$

where $a_\pm$ are the in-phase and out-of-phase combinations of Chern-Simons gauge fields of the two layers, and the polarizations $D_\pm^{-1}$ in the Coulomb gauge have the following form

$$D_\pm^{-1} = \frac{1}{2} \begin{pmatrix} \Pi_{00}^0 & \frac{iq}{4\pi} \\ \frac{-iq}{4\pi} & \Pi_{11}^0 + \frac{2V_\pm q^2}{(4\pi)^2} \end{pmatrix}, \tag{4.29}$$

where the index 0 and 1 denote time and transverse component, respectively.

$$V_\pm(q) = \frac{1}{2} \left[\frac{2\pi e^2}{q} (1 \pm e^{-qd}) \right] F(q) \tag{4.30}$$

is linear combinations of intralayer and interlayer Coulomb interactions, $F(q)$ is the finite thickness form factor[230, 231], and Π_{00}^0 and Π_{11}^0 are the fermion density and transverse current correlations functions, respectively:

$$\begin{aligned} \Pi_{00}^0 &\approx \frac{m_*}{\pi} \left(1 + i \frac{\omega}{v_F q} \right), \\ \Pi_{11}^0 &\approx -\frac{q^2}{12\pi m_*} + i \frac{2n\omega}{k_F q}. \end{aligned} \tag{4.31}$$

m^* is the activation mass of the composite fermions, and, as we discuss below is different from the polarization mass m_p used in the previous section. Continuing the derivation,

$$E_i = -T \ln Z = -T \ln Z_0 - T \ln Z_+ - T \ln Z_-, \tag{4.32}$$

where the free fermion part gives

$$\frac{\partial E_{i,fermion}}{\partial T} = -\frac{\partial(T \ln Z_0)}{\partial T} = -\frac{2\pi}{3} T \frac{m_*}{\hbar^2}, \tag{4.33}$$

and the gauge field parts give[81, 100]

$$\frac{\partial E_{i,\pm}}{\partial T} = -\int_0^\infty \frac{\omega \mathrm{d}\omega}{\pi T^2} \frac{e^{\beta\omega}}{(e^{\beta\omega}-1)^2} \int_0^\infty \frac{q\mathrm{d}q}{2\pi} \operatorname{Im} \ln \det D_\pm^{-1}, \tag{4.34}$$

A straightforward calculation following Ref. [100] shows that in the zero-thickness approximation (form factor $F(q)$ set to 1),

$$\frac{\partial E_{i,\pm}}{\partial T} = -\frac{1.917}{4\pi} \cdot \frac{5}{3} C_1^{2/3} T^{2/3} - \frac{1.645 C_2}{2\pi^2} T \ln \frac{\omega_0}{T}, \tag{4.35}$$

where

$$C_1 = \frac{16\pi n}{k_F d e^2/\epsilon}, C_2 = \frac{8\pi n}{k_F e^2/\epsilon}, \omega_0 = \frac{(2k_F)^2}{C_2},$$

n is the single layer density of composite fermions, and $k_F = \sqrt{2\pi n}$.

Finite thickness corrections to the form of Coulomb interaction is found to have negligible effect on the value of η, partly because it only affects the gauge field contribution which is itself dominated by the free composite-fermion-quasiparticle contribution for experimentally relevant temperatures and for the choice of m_* discussed below.

The value of the composite fermion mass m_* is believed to be close to the value determined by the activation gaps of fractional quantum Hall phases away from $\nu = 1/2$ [100, 102, 229, 104]. Therefore, we use the experimental value of this activation mass determined from gap measurements in Refs. [110, 232], which is

$$\frac{m_*}{m_e\sqrt{B_\perp}} = 0.2 \pm 0.02. \tag{4.36}$$

Note that in numerical calculations the activation mass is typically smaller than experimental value by about a factor of 2[100, 233, 234], but it is believed that the theoretical value should approach experimental value once finite thickness effect, dis-

order and Landau level mixing are taken into account[235, 234, 236, 237]. Therefore, we feel the use of experimental value stated above is more appropriate. Also note that the polarization mass m_p we used in the previous section is different from the mass we use here. Conceptually, within the Landau Fermi liquid theory, the two masses are related by $m_p = m_*/(1 + F_0^a)$, F_0^a being the zeroth spin-asymmetric Landau parameter.

Using this value of the mass along with the forms of free energy in Clausius-Clapeyron equation (4.5) , we get an ODE, which can be solved with the boundary condition that $\delta_c = 1.83$ when $T = 50$mK to yield the $\delta_c - T$ curve plotted in FIG. 4.2. To make this curve resemble the experimental result of Ref. [126], we have set

$$\eta = (0.7 \pm 0.2) \cdot 10^{-3}, \tag{4.37}$$

where the error mainly comes from the uncertainty in the value of the activation mass m_* and also the fitting error, meaning a finite range of η's make the $\delta_c - T$ curve resemble the experimental result.

In the above calculation, we assumed that the composite Fermi liquid is spin-unpolarized, and one might wonder how partial spin-polarization would affect the result. Because the free fermion contribution dominates $\partial E_i/\partial T$ and it is proportional to the density of states of composite fermions, our results would stay the same for partially-polarized composite Fermi liquid.

4.4 Density imbalance experiments

Refs. [119, 127] have studied the dependence of the critical $\delta_c = d/l$ on the density imbalance between the layers. They observed that at small imbalance, the phase boundary has a quadratic dependence on the density imbalance, and the coherent quantum Hall phase survives at higher d/l with larger imbalance.

Denoting the density of the two layers $n_{1,2}$, a density imbalance between the layers,

$$\Delta n \equiv \frac{n_1 - n_2}{2} \tag{4.38}$$

costs an energy which includes a dominating geometrical capacitance term and quantum mechanical corrections. This is true for both phases. For the coherent phase, we follow Ref. [95] to obtain the free energy density to be

$$\begin{aligned} E_c &= \left(\frac{2\pi e^2 d}{\epsilon} + \beta_{m,E}\right)(\Delta n)^2, \\ \beta_{m,E} &= \int_0^\infty \frac{qdq}{2\pi} V^z(q) h(q) \end{aligned} \tag{4.39}$$

where $2\pi e^2 d/\epsilon$ is the geometrical capacitance term, while $\beta_{m,E}$ is the exchange contribution which tends to offset the geometrical capacitance term. Here, $V^z(q) = V(q) - U(q)$, $V(q) = \frac{2\pi e^2}{\epsilon q} F(q)$ is the intralayer Coulomb interaction, $F(q)$ is the finite thickness form factor[230, 231], $U(q) = V(q)e^{-qd}$ is the interlayer Coulomb interaction, and $h(q) = -2\pi l^2 \exp(-q^2 l^2/2)$ is the pair distribution function of the Halperin (1,1,1) wavefunction.

The free energy density of the incoherent phase is (see Appendix 4.B for details)

$$E_i = \frac{(\Delta n)^2}{\tilde{K} - \tilde{K}'}, \tag{4.40}$$

where

$$\begin{aligned} \tilde{K} &\equiv \frac{1}{\beta A} \lim_{\vec{q}\to 0} \lim_{\omega \to 0} \langle \rho_{1,\vec{q},\omega} \rho_{1,-\vec{q},-\omega} \rangle, \\ \tilde{K}' &\equiv \frac{1}{\beta A} \lim_{\vec{q}\to 0} \lim_{\omega \to 0} \langle \rho_{1,\vec{q},\omega} \rho_{2,-\vec{q},-\omega} \rangle, \end{aligned} \tag{4.41}$$

where β is the inverse of temperature, A is the area of the sample, $\rho_{1,2}$ are the composite fermion density of each layer. Treating the Coulomb interaction within RPA, we obtain (see Appendix 4.B for details)

$$\tilde{K} = -\tilde{K}' = \frac{\kappa}{2\left(1 + \frac{2\pi e^2 d}{\epsilon} \cdot \kappa\right)}, \tag{4.42}$$

where κ is the $\omega \to 0, q \to 0$ limit of the 1-particle-irreducible density response function, namely compressibility, of a single-layer composite Fermi liquid. Plugging (4.42) into (4.40), one obtains the energy cost of uniform density imbalance in the incoherent phase:

$$E_i = \left(\frac{1}{\kappa} + \frac{2\pi e^2 d}{\epsilon}\right) \Delta n^2. \tag{4.43}$$

From the Clausius-Clapeyron equation (4.8), the geometrical capacitance term of the two phases cancels out, and we have

$$\eta = \frac{\kappa^{-1} - \beta_{m,E}}{\frac{\mathrm{d}\delta_c}{d(\Delta n^2)} \frac{e^2}{\epsilon l^3}}. \tag{4.44}$$

Since κ is the single layer compressibility, it is connected to the ground state energy per area of the composite Fermi liquid E_{GS} via

$$\kappa^{-1} = \frac{\partial^2 E_{GS}}{\partial n^2}. \tag{4.45}$$

Note that our definition of the compressibility is slightly different from some literature where $\kappa^{-1} = n^2 \frac{\partial^2 E_{GS}}{\partial n^2}$ are used instead.

Alternatively, treating the Chern-Simons interaction within RPA (see Appendix 4.B for details), we obtain

$$\kappa^{-1} = \kappa_0^{-1} - 16\pi^2 \chi_d, \tag{4.46}$$

where

$$\kappa_0 = \frac{m_*}{\pi(1 + F_0^s)} \tag{4.47}$$

is the compressibility without the Chern-Simons interaction, F_0^s is the zeroth Landau parameter in the spin-symmetric channel, and

$$\chi_d = -\frac{1}{12\pi m_*} \tag{4.48}$$

is the Landau diamagnetic susceptibility. Therefore

$$E_i = \left(\frac{\pi}{m_*} + \frac{\pi F_0^s}{m_*} + \frac{4\pi}{3m_*} + \frac{2\pi e^2 d}{\epsilon} \right) \Delta n^2. \tag{4.49}$$

Clearly, we can identify the four terms as free fermion contribution, exchange/correlation effect, Landau diamagnetism for Chern-Simons flux[127], and geometric capacitance term, respectively.

Although the Chern-Simons expression of κ Eqn. (4.49) offers valuable physical insight into its structure, the precise value of the parameters m_*, χ_d, and especially F_0^s are not very well understood. The best way to estimate κ is to use its connection with ground state energy density E_{GS} of composite Fermi liquid (4.45). In the zero-thickness approximation, Park *et al.* [238] have estimated the value of E_{GS} for spin unpolarized composite Fermi liquid to be

$$E_{GS} = -0.4695 \frac{e^2}{\epsilon l} n, \tag{4.50}$$

thus

$$\kappa^{-1} = -0.4695 \cdot 3\pi \frac{e^2}{\epsilon} l, \tag{4.51}$$

where n is the single layer density of composite fermions, and l is the magnetic length.

Using this value of κ^{-1} and the zero-thickness form of Coulomb interaction to calculate the coherent phase exchange term $\beta_{m,E}$ (because the numerical result for E_{GS} of the incoherent phase quoted above from Ref. [238] was also done with zero thickness), and extracting the curvature $\frac{\mathrm{d}\delta_c}{d(\Delta n^2)}$ from experiments, we readily obtain the value of η. This result does not depend on the Chern-Simons description of composite fermions. We have plotted in FIG. 4.3 the values of η extracted from density imbalance experiments as well as those determined from spin transition and finite temperature transition experiments. The error bars for the density imbalance experiments mainly come from fitting errors.

Note that the main effect of the finite thickness correction to the form of Coulomb interaction is to reduce the exchange terms of both phases. Since the value of η

is related to the difference between the exchange term of the two phases, we do not expect the result of η to sensitively depend on this effect. Nevertheless, we can include it in the Chern-Simons treatment of κ. We use the activation mass $m_* = 0.2m_e\sqrt{B_\perp}$ estimated in Sec. 4.3 as the value of m_*, set $\chi_d = -1/(12\pi m_*)$, and use the Hubbard approximation to estimate F_0^s. In the Hubbard approximation, the exchange effect is taken into account by introducing a many-body local field factor $G(q) = q/(2\sqrt{q^2 + k_F^2})$, and $F_0^s = -\frac{m_*}{\pi}\lim_{q\to 0} V(q)G(q)$. Thus, we obtain from Eqn. (4.46)

$$\kappa^{-1} = \frac{7}{3}\frac{\pi\hbar^2}{m_*} - \frac{\pi e^2}{\epsilon k_F}. \tag{4.52}$$

Using this value of κ^{-1} and the finite-thickness form of Coulomb interaction to calculate the coherent phase exchange term $\beta_{m,E}$, we have calculated the values of η from density imbalance experiments which turned out to be extremely close to the results obtained earlier in FIG. 4.3.

Comments about the value of the compressibility in the composite Fermi liquid phase are in order. First, In Ref. [239], the compressibility of a single layer 2DEG at zero field was studied in detail, and it was found that aside from the well-known density-of-states contribution and exchange contribution to the compressibility, there is a third contribution coming from the so-called Hartree band-bending effect due to the influence of the finite quantum well width on the out-of-plane direction of electron wavefunction. For the bilayer system studied here, we expect a similar effect on the composite Fermi liquid compressibility κ^{-1} in the incoherent phase and on $\beta_{m,E}$ for the coherent quantum Hall phase as well. A quantitative analysis of this effect and its impact on the density imbalance experiments is beyond the scope of this chapter, and we simply note that the Hartree band-bending effect is essentially a single-particle effect[239], and therefore it will contribute equally to κ^{-1} and $\beta_{m,E}$. To obtain the value of η from Eqn. (4.44), we only need the difference between κ^{-1} and $\beta_{m,E}$, and therefore we do not expect the Hartree band-bending effect to modify our results. Second, quenched disorder acts to broaden the Landau levels and therefore adds a positive contribution to the compressibility. This could account for the close-to-zero

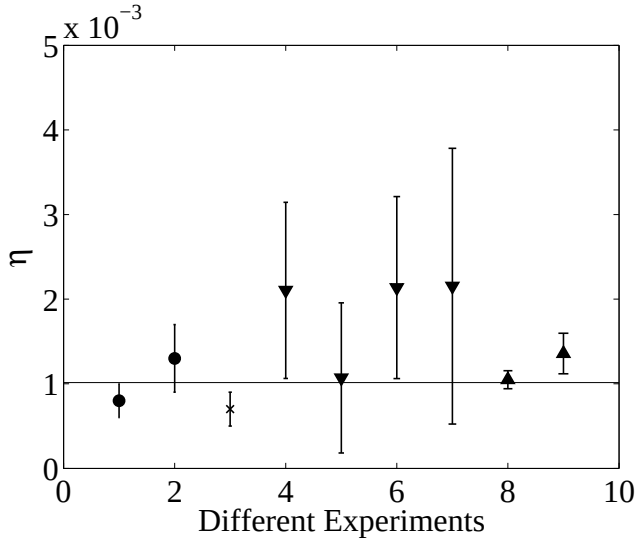

Figure 4.3: Summary of the value of η extracted from various experiments. Experiment 1: parallel field experiment of Ref. [125]. Experiment 2: NMR/heat pulse experiment of Ref. [121]. Experiment 3: finite temperature transition experiment of Ref. [126]. Experiment 4 to 7: density imbalance experiments of Ref. [127], with T = 55mK, 85mK, 125mK, 200mK. Experiment 8 and 9: density imbalance experiments of Ref. [119] with phase boundary determined by Hall drag and tunneling. To obtain this result we used the numerical result of Ref. [238] for unpolarized composite Fermi liquid ground state energy to estimate κ^{-1}. The horizontal line is the average value of η weighted by inverse of error square, which is $\sim (1 \pm 0.1) \times 10^{-3}$.

compressibility measured by Ref. [239]. Again, this effect is likely to be similar for both phases, and we do not expect disorder to affect the difference between κ^{-1} and $\beta_{m,E}$ appreciably. Nevertheless, disorder is important in smearing the first order transition into a continuous one (see discussion in Sec. 4.5).

We assumed that the composite Fermi liquid is unpolarized above, but again we do not expect partial polarization to affect our results strongly. For (4.51), Park *et al.*[238] also reported the ground state energy for polarized composite Fermi liquid to be very close to the unpolarized one quoted above:

$$E_{polarized} = -0.4656\frac{e^2}{\epsilon l}n, \tag{4.53}$$

and therefore our results would also stay very close. In the Chern-Simons treatment (4.49) and(4.52), since the Chern-Simons fields couple to both spins and the density and current response function stays the same for partially-polarized and unpolarized composite Fermi liquids, our calculation also remains valid (see Appendix 4.B).

4.5 Summary and discussion

To summarize, we derived the Clausius-Clapeyron relations [Eqn. (4.3, 4.5, 4.8)] for the phase transition tuned by d/l in bilayer $\nu_{tot} = 1$ quantum Hall system, assuming that it is a first-order transition between spin-polarized coherent quantum Hall state and spin partially-polarized composite-fermion Fermi liquid state. In Sec. 4.2, we studied the changes of phase boundary $(d/l)_c$ when the magnetic field coupled to spin is changed by either NMR/heat pulse or parallel magnetic field. The phase boundary as a function of temperature was studied in Sec. 4.3. The temperature dependence of free energy in the coherent quantum Hall phase is dominated by the linearly-dispersing Goldstone mode, while the incoherent composite Fermi liquid phase has contributions from both fermions and gauge fields. In Sec. 4.4, we investigated the changes of phase boundary when there is density imbalance between the two layers. We use the result of Ref. [95] for the free energy cost of density imbalance in the

coherent quantum Hall phase. The free energy for the incoherent phase is shown to be connected to the compressibility of single layer composite Fermi liquid.

Our main goal was to check the consistency of the Clausius-Clapeyron relation with the observed transition. Each experiment which observes the change in $(d/\ell)_c$ due to changing another parameter in the system indicates a value for η, as defined in Eq. (4.4); all values should agree.

In FIG. 4.3, we have plotted the values of η determined from spin transition, finite temperature transition, and density imbalance transition experiments. The horizontal line is the average value of η weighted by inverse of error square, i.e., the maximum likelihood estimator of η. One can see that, indeed, all nine values of η extracted from various experiments roughly lie in the range $1 \sim 2 \times 10^{-3}$, and the weighted average value of $\eta = (1 \pm 0.1) \cdot 10^{-3}$ is roughly within all the error bars. Our analysis, therefore, confirms the consistency for the scenario of a direct first-order phase transition between coherent quantum-Hall phase and incoherent composite Fermi-liquid phase. Furthermore, the analysis provides a unified framework within which we can understand the observed phase boundaries for several distinct experiments.

In Sec. 4.4, we also worked in the Chern-Simons description of composite fermions [i.e. Eq. (4.52)] in addition to our treatment [i.e. Eq. (4.51)] using the numerical results of Ref. [238], and we obtained extremely similar results. Stepping back a little from that analysis with the Chern-Simons treatment, one can pretend ignorance of any knowledge of the parameters including the effective mass m_* and the exchange contribution to κ^{-1}, and ask what values of them would give good agreement between the values of η extracted from experiments. We have plotted the standard deviation of η extracted from various experiments divided by the their average value in FIG. 4.4 as a function of the composite fermion mass (in units of $m_e\sqrt{B_\perp}$) and the exchange contribution to κ^{-1}, which is $F_0^s \pi/m_*$ (in units of $e^2 l/\epsilon$). The finite thickness form of the Coulomb interaction is used in calculating the coherent-phase exchange term when producing this plot. Grey color denotes the region where at least one of the η's becomes negative, thus unphysical, while dark blue denotes parameter regimes which give rise to good agreement among η's extracted from different experiments. The

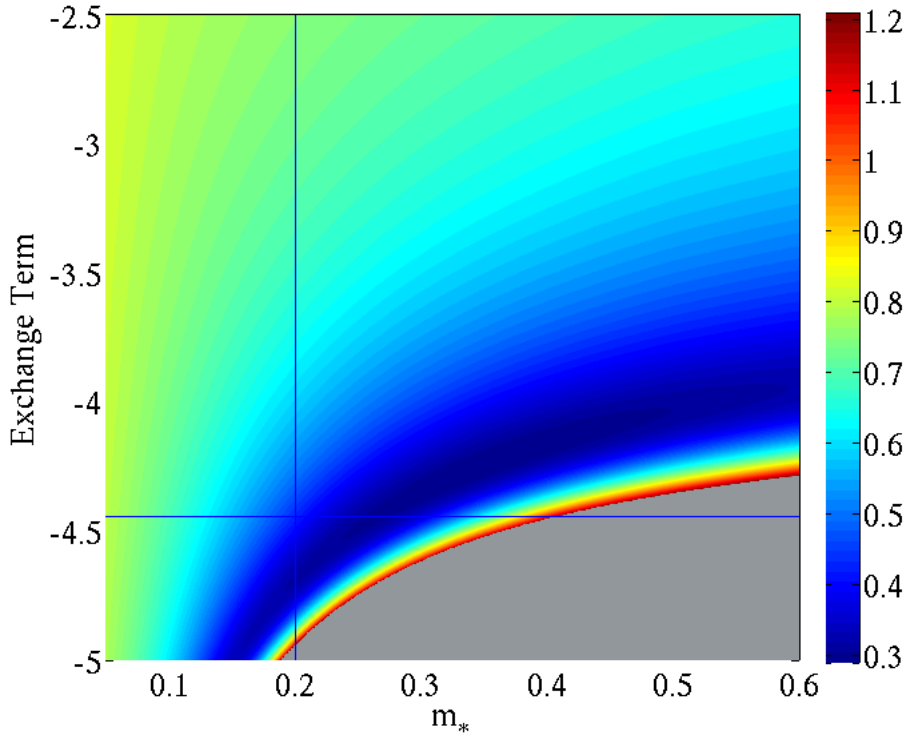

Figure 4.4: (Color online.) Standard deviation of η among various experiments divided by their average value (which measures the goodness of agreement between ηs) within the Chern-Simons framework as a function of the composite fermion mass and the exchange contribution to κ^{-1} [see Eq. (4.52)]. Horizontal axis: composite fermion mass in units of $m_e\sqrt{B_\perp}$, m_e being the vacuum electron mass, $B_\perp$ is in units of Tesla. Vertical axis: exchange contribution to κ^{-1}, which is $F_0^s\pi/m_*$ (in units of e^2l/ϵ, l being the magnetic length). Grey color denotes the region where at least one of the η's becomes negative, thus unphysical. The horizontal line denotes the Hubbard approximation to the exchange effect ($-\sqrt{2}\pi$). The vertical line denotes the experimental value of the activation mass $m_* \approx 0.2m_e\sqrt{B_\perp}$, which is the value of composite fermion mass we used in calculations for FIG. 4.2 and FIG. 4.3.

horizontal line denotes the Hubbard approximation to the exchange effect ($\sqrt{2}\pi$), while he vertical line denotes the experimental value of the activation mass $m_* \approx 0.2 m_e \sqrt{B_\perp}$.

We have not explicitly discuss the role of disorder, which is always present in the samples. Disorder will bring spatial fluctuations into some variables in the Clausius-Clapeyron equations we have derived, and therefore smear the first order transition into a continuous one, as observed in experiments. Roughly speaking, the analysis we have performed in this work applies to the spatially averaged quantities. For example, with disorder, the RHS of the Clausius-Clapeyron equation for spin transitions (4.15) will acquire spatial dependence most likely through a spatially fluctuating spin susceptibility χ:

$$\frac{\mathrm{d}\delta_c(\vec{x})}{\mathrm{d}B_{tot}} = \frac{-2\chi(\vec{x})B_{tot} + \frac{eg\mu_B B_\perp}{4\pi\hbar}}{\eta \frac{e^2}{\epsilon l^3}} \tag{4.54}$$

Thus, one can take the spatial average of both sides and study how the averaged critical δ_c changes with B_{tot}, as we did in this work. Furthermore, one can also take the standard deviation of both sides of (4.54), and conclude that the width of the phase transition, which is the standard deviation of δ_c, grows with B_{tot} assuming the standard deviation of $\chi(\vec{x})$ does not change appreciably with B_{tot}. One can also study the finite temperature transition in a similar way. Because there the free fermion term (4.33) dominates, one can conclude that the transition becomes wider at higher temperature, if one assumes the composite fermion mass m_* has some temperature-independent spatial variation. This is in accord with the experimental observation of Ref. [126].

A major question which is not directly addressed in our analysis is the possibility of a continuous quantum crossover between the coherent and incoherent phases (see, e.g., Refs. [142, 143]). If indeed no real thermodynamic singularity exists even in the clean case, then there is no reason for the Clausius-Clapeyron relations to hold as well as we find they do. Nonetheless, there is also no contradiction in them holding where no first-order transition exists. In this case, however, we can draw the conclusion that the crossover region between the two phases must be very narrow, such that

it approximates a smeared thermodynamic singularity (just as disorder would widen a thermodynamic singularity) and therefore follows the Clausius-Clapeyron relations we presented here for the unmixed phases. In other words, a good agreement with the relations indicates that already at regions in parameter space close to the transition, the thermodynamic functions of the pure coherent and pure incoherent phases apply, and they indicate a smeared phase transition line.

Additional outstanding questions which we did not address, but are noteworthy are as follows. First, a thermodynamic phase transition between the coherent and incoherent phases does not have to be first order at high Zeeman fields when both phases are spin-polarized; a second-order phase transition is not ruled out *a priori*. Future experiments should clarify this issue (see the recent experiments of Refs. [129, 130]). In addition, for the density imbalance transitions, we have mainly focused on the regime of small imbalance, while the experiments of Ref. [127] have studied the case of large imbalance, e.g., $\Delta\nu = \nu_1 - \nu_2 \leq 0.4$. The interlayer incoherent phase in that regime could be two decoupled single-layer fractional quantum Hall phase. It would be very interesting to see if a similar Clausius-Clapeyron equation can describe the phase transition in that case. Finally, although our assumption (4.4) is very natural on qualitative ground, a microscopic derivation of this quantity would be very useful.

4.A Temperature dependence of the incoherent phase free energy

Within the Chern-Simons description of the composite-fermion Fermi liquid at $\nu = 1/2$, we have the following partition function of the system:

$$Z = \int \mathcal{D}a_1 \mathcal{D}a_2 \mathcal{D}\psi_{1\sigma} \mathcal{D}\psi_{2\sigma} e^{-\int \mathrm{d}\tau d^2x \mathcal{L}}, \tag{4.55}$$

where

$$\begin{aligned}\mathcal{L} = \sum_{n=1,2} \Big\{ & \psi^\dagger_{n\sigma}(\partial_\tau - \mu_n - i a_{n,0})\psi_{n\sigma} - \frac{i}{8\pi} a_{n\mu}\epsilon^{\mu\nu\lambda}\partial_\nu a_{n\lambda} \\ & + \frac{1}{2m}\psi^\dagger_{n\sigma}\left(-i\nabla - \vec{a}_n\right)^2 \psi_{n\sigma} \\ & + \frac{1}{2}\int \mathrm{d}^2x' \psi^\dagger_{n\sigma}(x)\psi_{n\sigma}(x) V(x-x')\psi^\dagger_{n\sigma'}(x')\psi_{n\sigma'}(x') \Big\} \\ & + \int \mathrm{d}^2x' \psi^\dagger_{1\sigma}(x)\psi_{1\sigma}(x) U(x-x')\psi^\dagger_{2\sigma'}(x')\psi_{2\sigma'}(x'),\end{aligned} \tag{4.56}$$

where $\psi_{n\sigma}$ is the composite fermion fields in the n'th layer with spin σ, V and U are the intralayer and interlayer Coulomb interaction, respectively. Here, $a_{n\mu}$ are the fluctuations of the Chern-Simons gauge fields in the n'th layer from its saddle point value which cancels the external magnetic field exactly, and $\mu = 0, 1, 2$ are the time and two spatial coordinates, respectively. Integrating out $a_{n,0}$, one obtains the expected constraints

$$\nabla \times \vec{a}_n = 4\pi \psi^\dagger_{n\sigma}\psi_{n\sigma}. \tag{4.57}$$

Following Ref. [100], we make use of this constraint and replace $\psi^\dagger_{n\sigma}\psi_{n\sigma}$ in Coulomb interaction terms by $\nabla \times \vec{a}_n/(4\pi)$. Next, we define

$$\begin{aligned} a_{\pm\mu} &= a_{1\mu} \pm a_{2\mu}, \\ V_\pm &= \frac{V \pm U}{2}, \end{aligned} \tag{4.58}$$

and reorganize $\mathcal{L}$ as

$$\begin{aligned}
\mathcal{L} &= \mathcal{L}_f + \mathcal{L}_{CS}, \\
\mathcal{L}_f &= \psi_{1\sigma}^\dagger \left(\partial_\tau - \mu_1 - i\frac{a_{+0} + a_{-0}}{2} \right) \psi_{1\sigma} \\
&\quad + \psi_{2\sigma}^\dagger \left(\partial_\tau - \mu_2 - i\frac{a_{+0} - a_{-0}}{2} \right) \psi_{2\sigma} \\
&\quad + \psi_{1\sigma}^\dagger \frac{\left(-i\nabla - (\vec{a}_+ + \vec{a}_-)/2\right)^2}{2m} \psi_{1\sigma} \\
&\quad + \psi_{2\sigma}^\dagger \frac{\left(-i\nabla - (\vec{a}_+ - \vec{a}_-)/2\right)^2}{2m} \psi_{2\sigma} \\
\mathcal{L}_{CS} &= -\frac{i}{16\pi} a_{+\mu} \epsilon^{\mu\nu\lambda} \partial_\nu a_{+\lambda} - \frac{i}{16\pi} a_{-\mu} \epsilon^{\mu\nu\lambda} \partial_\nu a_{-\lambda} \\
&\quad + \frac{1}{2} \frac{1}{(4\pi)^2} \int \mathrm{d}^2x' [\nabla \times \vec{a}_+(x)] V_+(x - x') [\nabla \times \vec{a}_+(x')] \\
&\quad + \frac{1}{2} \frac{1}{(4\pi)^2} \int \mathrm{d}^2x' [\nabla \times \vec{a}_-(x)] V_-(x - x') [\nabla \times \vec{a}_-(x')].
\end{aligned} \tag{4.59}$$

Denoting the free fermion partition function to be

$$Z_0 = \int \mathcal{D}\psi_{1\sigma} \mathcal{D}\psi_{2\sigma} \exp\left(- \int \mathrm{d}\tau \mathrm{d}^2x \mathcal{L}_f(a_\pm = 0) \right), \tag{4.60}$$

and following standard methods[100] to integrate out composite fermion fields $\psi_{n\sigma}$, we obtain

$$Z = Z_0 Z_+ Z_-, \tag{4.61}$$

where Z_0 is the partition function for free fermions, and

$$Z_\pm = \int \mathcal{D}a_\pm e^{-\int \mathrm{d}\tau \mathrm{d}^2x (a_\pm D_\pm^{-1} a_\pm / 2)}, \tag{4.62}$$

In Coulomb gauge, one can treat the polarizations $D_\pm^{-1}$ as 2×2 matrices, with index 0 and 1 to be the time and transverse component, respectively. Thus, $D_\pm^{-1}$ take the following form:

$$D_\pm^{-1} = \frac{1}{2} \begin{pmatrix} \Pi_{00}^0 & \frac{iq}{4\pi} \\ \frac{-iq}{4\pi} & \Pi_{11}^0 + \frac{2V_\pm q^2}{(4\pi)^2} \end{pmatrix}, \tag{4.63}$$

where Π^0_{00} and Π^0_{11} are the density and transverse current correlation functions of free fermions resulted from integrating out composite fermion fields. Thus, the free energy is given by

$$E_i = -T \ln Z = -T \ln Z_0 - T \ln Z_+ - T \ln Z_-, \tag{4.64}$$

and the rest of the steps are given in Section 4.3.

4.B Density imbalance dependence of the incoherent phase free energy

Starting from action (4.55) or any other action for composite fermions, we integrate out all fluctuating fields and obtain

$$\begin{aligned} Z = \exp \Bigg\{ \frac{1}{2\beta A} \sum_{\vec{q},\omega} \big[& K_{\vec{q},\omega} \phi_{1,\vec{q},\omega} \phi_{1,-\vec{q},-\omega} \\ & + K_{\vec{q},\omega} \phi_{2,\vec{q},\omega} \phi_{2,-\vec{q},-\omega} + 2K'_{\vec{q},\omega} \phi_{1,\vec{q},\omega} \phi_{2,-\vec{q},-\omega} \big] \Bigg\}, \end{aligned} \tag{4.65}$$

where

$$\begin{aligned} K_{\vec{q},\omega} &= \frac{1}{\beta A} \langle \rho_{1,\vec{q},\omega} \rho_{1,-\vec{q},-\omega} \rangle = \frac{1}{\beta A} \langle \rho_{2,\vec{q},\omega} \rho_{2,-\vec{q},-\omega} \rangle, \\ K'_{\vec{q},\omega} &= \frac{1}{\beta A} \langle \rho_{1,\vec{q},\omega} \rho_{2,-\vec{q},-\omega} \rangle, \end{aligned} \tag{4.66}$$

ρ_j is the composite fermion density of the j'th layer, β is the inverse of the temperature, A is the area of the sample, and $\phi_{j,\vec{q},\omega}$ is the Fourier-transformed potential in the j'th layer. For a constant potential ϕ_j $(j = 1, 2)$, we have

$$\phi_{j,\vec{q},\omega} = \phi_j \cdot \beta A \delta_{\vec{q},0} \delta_{\omega,0}, \tag{4.67}$$

and the grand potential Ω is

$$\Omega = -T \ln Z = -\frac{A}{2} \left(\tilde{K} \phi_1^2 + \tilde{K} \phi_2^2 + 2\tilde{K}' \phi_1 \phi_2 \right), \tag{4.68}$$

where

$$\tilde{K} \equiv \lim_{\vec{q}\to 0}\lim_{\omega\to 0} K_{\vec{q},\omega}, \tilde{K}' \equiv \lim_{\vec{q}\to 0}\lim_{\omega\to 0} K'_{\vec{q},\omega}. \tag{4.69}$$

The density in each layer is

$$\begin{aligned} n_1 &= -\frac{1}{A}\frac{\partial\Omega}{\partial\phi_1} = \tilde{K}\phi_1 + \tilde{K}'\phi_2, \\ n_2 &= -\frac{1}{A}\frac{\partial\Omega}{\partial\phi_2} = \tilde{K}\phi_2 + \tilde{K}'\phi_1. \end{aligned} \tag{4.70}$$

Finally, the free energy is obtained via a Legendre transformation

$$\begin{aligned} F &= \Omega + \phi_1 n_1 A + \phi_2 n_2 A \\ &= \frac{A}{4}\left(\frac{(n_1-n_2)^2}{\tilde{K}-\tilde{K}'} + \frac{(n_1+n_2)^2}{\tilde{K}+\tilde{K}'}\right). \end{aligned} \tag{4.71}$$

Within the RPA treatment of the Coulomb interaction, the full density response function K is related to its one-particle-irreducible (1PI) counterpart Π (which neglects the long range Coulomb interaction) by

$$K^{-1} = \Pi^{-1} + \tilde{V}, \tag{4.72}$$

where K, Π, and $\tilde{V}$ are 2×2 matrices in the layer-index space:

$$\tilde{V} = \begin{pmatrix} V & U \\ U & V \end{pmatrix}, \qquad \Pi = \begin{pmatrix} \Pi_{00} & 0 \\ 0 & \Pi_{00} \end{pmatrix}. \tag{4.73}$$

Here, V and U are intralayer and interlayer Coulomb interaction potential, respectively, and Π_{00} in the static uniform limit gives the single layer compressibility κ:

$$\kappa \equiv \lim_{q\to 0}\lim_{\omega\to 0} \Pi_{00}. \tag{4.74}$$

Solving (4.72), we have

$$K_{11} = K_{22} = \frac{\Pi_{00}(1+\Pi_{00}V)}{(1+\Pi_{00}V)^2 - \Pi_{00}^2 U^2},$$
$$K_{12} = \frac{-(\Pi_{00})^2 U}{(1+\Pi_{00}V)^2 - \Pi_{00}^2 U^2}.$$

Given the form of Coulomb interactions

$$V(q) = \frac{2\pi e^2}{q} F(q), \qquad U(q) = V(q) e^{-qd}, \tag{4.75}$$

and the fact that the finite thickness form factor $F(q) \to 1$ as $q \to 0$, in the limit $\omega \to 0$ and $q \to 0$, the denominators of K_{11}, K_{22}, and K_{12} become

$$\begin{aligned} &(1+\Pi_{00}V)^2 - (\Pi_{00})^2 U^2 \\ &\to \frac{4\pi e^2 \kappa}{\epsilon q}\left(1 + \frac{2\pi e^2 \kappa d}{\epsilon}\right), \text{ as } \omega \to 0, q \to 0. \end{aligned} \tag{4.76}$$

Therefore in this limit

$$\begin{aligned} \tilde{K} &\equiv \lim_{q\to 0}\lim_{\omega\to 0} K_{11} = \frac{\kappa}{2\left(1 + 2\pi e^2 \kappa d/\epsilon\right)}, \\ \tilde{K}' &\equiv \lim_{q\to 0}\lim_{\omega\to 0} K_{12} = -\frac{\kappa}{2\left(1 + 2\pi e^2 \kappa d/\epsilon\right)}, \end{aligned} \tag{4.77}$$

and the imbalance part of the free energy density is

$$\begin{aligned} E_i &= \lim_{\vec{q}\to 0}\lim_{\omega\to 0} \frac{\Delta n^2}{\tilde{K} - \tilde{K}'} \\ &= \left(\frac{1}{\kappa} + \frac{2\pi e^2 d}{\epsilon}\right)\Delta n^2, \end{aligned} \tag{4.78}$$

as shown in Section 4.4. This result does not depend on the Chern-Simons description of composite fermions. Note also that the total compressibility $\tilde{K} + \tilde{K}'$ vanishes linearly in q as $q \to 0$ due to the long-range nature of the Coulomb interaction, similar to the single layer case as analyzed by Halperin *et al.* [100].

To calculate the single layer compressibility κ within the Chern-Simons framework,

we have the following RPA equation:

$$(\Pi)^{-1} = (\Pi^0)^{-1} + C, \tag{4.79}$$

where C is the propagator of the Cherns-Simons field, and Π^0 is the correlation functions without the Chern-Simons interaction. We work in the Coulomb gauge and treat Π, Π^0, and C as 2×2 matrices in the space of density and transverse current. In the static and long wavelength limit, we have

$$\Pi^0 = \begin{pmatrix} \kappa_0 & 0 \\ 0 & \chi_d q^2 \end{pmatrix}, \qquad C = \frac{4\pi}{q} \begin{pmatrix} 0 & i \\ -i & 0 \end{pmatrix}. \tag{4.80}$$

where $\kappa_0 = m_*/[\pi\hbar^2(1+F_0^s)]$ is the density response function neglecting Chern-Simons interaction, and χ_d is the Landau diamagnetic susceptibility. Hence,

$$\kappa^{-1} = \kappa_0^{-1} - 16\pi^2\chi_d, \tag{4.81}$$

as shown in Section. 4.4. Note that these results are the same for unpolarized and partially-polarized composite Fermi liquids, because (4.79) is valid in any case since Chern-Simons fields couple to both spins, and the value of κ_0 and χ_d in (4.80) stays the same for partially-polarized composite Fermi liquid. The value of F_0^s in the Hubbard approximation treatment is also roughly the same for partially-polarized and unpolarized composite Fermi liquids.

Chapter 5

Achieving Random Hopping Model In Optical Lattices

5.1 Introduction

As we discussed in Chapter 1, in analogy to the dynamical localization phenomena, we expect to obtain the random hopping model by fast-modulating the disordered potential energies of an Anderson insulator. However, as we will see later sections, if the modulating frequency ω is much larger than typical potential energy, this randomness in effective hopping amplitude is suppressed, and we obtain a uniform-hopping tight-binding model. Therefore, the random hopping model behavior surivives when the frequency ω is comparable to the typical potential energy. In summary, as the oscillation frequency of the potential energy is gradually increased from zero to infinity, one can tune a non-interacting system from an Anderson insulator to a random hopping model with diverging localization length at the band center, and eventually to a uniform-hopping tight-binding model (see FIG. 5.1). Some interesting but puzzling results when ω is much smaller than γ but larger than 0 is also presented.

In the remaining of this chapter, we will support these claims by analyzing the

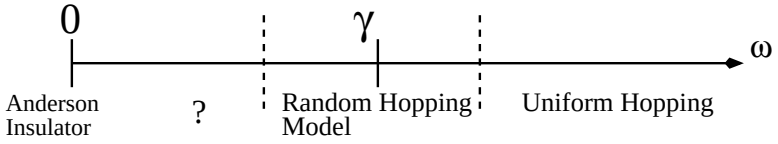

Figure 5.1: Phase diagram of the model (5.1) studied in this work. At zero frequency, the system is an Anderson insulator; when the frequency ω is comparable to the disorder width γ, the system behaves as a random hopping model; when ω is much larger than γ, the system enters the uniform-hopping tight-binding regime. Some interesting but puzzling results when ω is much smaller than γ but larger than 0 is also presented.

following model:

$$\begin{aligned} H &= H_0 + 2V\cos(\omega t), \\ H_0 &= -J\sum_{n=1}^{N-1}(c_n^\dagger c_{n+1} + c_{n+1}^\dagger c_n), \\ V &= \sum_{n=1}^{N} v_n c_n^\dagger c_n, \end{aligned} \tag{5.1}$$

where N is the system size, and we assume the onsite potential v_n obeys a uniform distribution between $[-\gamma/2, \gamma/2]$. We will obtain the localization length and the density of states of this model mainly by directly working with this time-dependent Hamiltonian using Floquet technique, but but we will also compare the results with those obtained from the transformed effective Hamiltonian in the high frequency regime. Note also the related but different model studied by Ref. [162, 163]. This chapter is adapted from our unpublished work Ref. [240].

5.2 Computation of the density of states and the localization length

To obtain the density of states, first we recall that in Floquet systems the concept of energy is replaced by quasienergies. By Floquet theorem, which is the analog of the Bloch theorem for time-periodic systems, the wavefunctions of a time-dependent

system with period $T = 2\pi/\omega$ have the form of

$$\psi(t) = e^{-iEt}\phi(t), \tag{5.2}$$

where E is the quasienergy defined up to modulo ω, and $\phi(t+T) = \phi(t)$. It is also well-known that e^{-iET} and $\phi(T)$ are the eigenvalue and eigenstates of the Floquet operator

$$\mathcal{F} = \mathcal{T}\exp\left(-i\int_0^T \mathrm{d}t H(t)\right), \tag{5.3}$$

where $\mathcal{T}$ is the time-ordering operator. Thus to obtain the density of states, we first compute the Floquet operator $\mathcal{F}$ by numerical Trotterization procedure. Next we diagonalize it to find the quasienergies which we define to be in the "first Brillouin zone" $-\omega/2 \leq E \leq \omega/2$. Then, we obtain the cumulative distribution function of the quasienergies, average it over many realization of disorder, numerically differentiate it with respect to quasienergy, and finally obtain the density of states.

We would also like to obtain the localization length of this model for arbitrary frequency ω. For one-dimensional non-interacting time-independent Hamiltonian, we recall that the localization length of a state with energy E is given by [147]

$$\frac{1}{\lambda(E)} = -\lim_{N\to\infty}\frac{1}{N}\ln|G_{1N}(E)|, \tag{5.4}$$

where the Green's function

$$G(E) = (EI - H)^{-1}, \tag{5.5}$$

I is the identity matrix.

For Floquet system, one instead has the Floquet Hamiltonian[241]

$$H_F = H - i\partial t \tag{5.6}$$

in the augmented Hilbert space $\mathcal{H}\times\mathcal{T}$, where $\mathcal{H}$ is the original Hilbert space, and $\mathcal{T}$

is the frequency space. And we also define the Floquet Green's function as

$$G_F(E) = (EI - H_F)^{-1}. \tag{5.7}$$

Following Ref. [242, 163], we generalize the concept of localization length of a time-periodic system by defininng it as the localization length of the time-averaged wavefunction. In terms of the Green's function, it is

$$\frac{1}{\lambda(E)} = -\lim_{N\to\infty} \frac{1}{N} \ln |G_{1N}(E)| \tag{5.8}$$

where

$$G = \langle \Omega = 0 | G_F(E) | \Omega = 0 \rangle. \tag{5.9}$$

For a Hamiltonian of the form

$$H = H_0 + 2V \cos(\omega t), \tag{5.10}$$

from

$$(EI - H_F) G_F = I, \tag{5.11}$$

we insert the resolve of identity in the frequency space and obtain

$$\sum_p \langle m | (EI - H_F) | p \rangle \langle p | G_F | n \rangle = I \langle m | n \rangle, \tag{5.12}$$

thus

$$\left[(E + m\omega) I - H_0 \right] G_{mn} - V G_{m+1,n} - V G_{m-1,n} = I \delta_{mn},$$

where

$$G_{mn} \equiv \langle m | G | n \rangle. \tag{5.13}$$

To solve $G_{00}(E)$ from this system of equations, we follow Ref. [163] to obtain

$$G_{00}(E) = (EI - H_0 - V_{eff}^{+} - V_{eff}^{-})^{-1}, \tag{5.14}$$

where

$$V_{eff}^{\pm} = V \frac{1}{E \pm 1\omega - H_0 - V \frac{1}{E \pm 2\omega - H_0 - V \frac{1}{\vdots} V} V} V, \tag{5.15}$$

and the number of iterations needed to ensure the convergence of $V_{eff}^{\pm}$ is roughly proportional to γ/ω.

Finally, it would be interesting to mathematically check if the Thouless relation[147] between the density of states and the localization length holds for a Floquet system.

5.3 Effective Hamiltonian in the fast oscillation limit

In this section, we show that if the oscillation frequency ω is comparable or larger than the disorder width γ, the original Schrodinger equation of a time-dependent Hamiltonian can be transformed to that of a time-independent effective Hamiltonian. For the original Schrodinger equation

$$i\partial_t \psi = H\psi, \qquad H = H_0 + 2V\cos(\omega t), \tag{5.16}$$

we define

$$\psi = U\tilde{\psi}, \qquad U = e^{-2i\sin(\omega t)V/\omega}. \tag{5.17}$$

Then the schrodinger equation becomes

$$i\partial_t \tilde{\psi} = H_{eff}\tilde{\psi}, \qquad H_{eff} = U^{\dagger}HU - 2V\cos(\omega t).$$

Using

$$e^{i\eta c_n^{\dagger}c_n} c_n e^{-iEc_n^{\dagger}c_n} = c_n e^{-i\eta}, \tag{5.18}$$

we have

$$\begin{aligned} H_{eff} = -J \sum_n \Big[& (c_n^\dagger c_{n+1} + c_{n+1}^\dagger c_n) \\ & \times \sum_{m=-\infty}^{\infty} (-1)^m \mathcal{J}_m \left(\frac{2(v_n - v_{n+1})}{\omega} \right) \cos(m\omega t) \\ & + i(c_n^\dagger c_{n+1} - c_{n+1}^\dagger c_n) \\ & \times \sum_{m=-\infty}^{\infty} (-1)^{m+1} \mathcal{J}_m \left(\frac{2(v_n - v_{n+1})}{\omega} \right) \sin(m\omega t) \Big] . \end{aligned}$$

For ω larger than or comparable to γ, the argument of the Bessel functions is comparable or smaller than 1, and $\mathcal{J}_0$ dominates other Bessel functions, and

$$H_{eff}^{(0)} \approx -J \sum_n \left(c_n^\dagger c_{n+1} + c_{n+1}^\dagger c_n \right) \mathcal{J}_0 \left(\frac{2(v_n - v_{n+1})}{\omega} \right), \tag{5.19}$$

which is a random hopping model. When ω is not too large, the model should exhibit behaviors such as logrithmically diverging localization length at the band center. We can compute the localization length of this effective Hamiltonian by using (5.4) and compare with the exact calculation using (5.8):

$$\begin{aligned} \frac{1}{\lambda(E)} &= -\lim_{N\to\infty} \frac{1}{N} \ln |G_{1N}(E)|, \\ G_{eff}(E) &= (EI - H_{eff}^{(0)})^{-1}. \end{aligned} \tag{5.20}$$

However when $\omega \gg \gamma$,

$$\mathcal{J}_0 \left(\frac{2(v_n - v_{n+1})}{\omega} \right) \approx 1 \tag{5.21}$$

regardless of the value of v_n, and therefore in this limit the system behaves like a uniform-hopping tight-binding model (see FIG. 5.1).

5.4 Numerical results

We analyze the case of fixed $\gamma \gg J$ and a wide range of ω. The inverse of localization length and the inverse of density of states computed both from the Floquet technique (5.8) and from the effective Hamiltonian are plotted in FIG. 5.2. One can see that

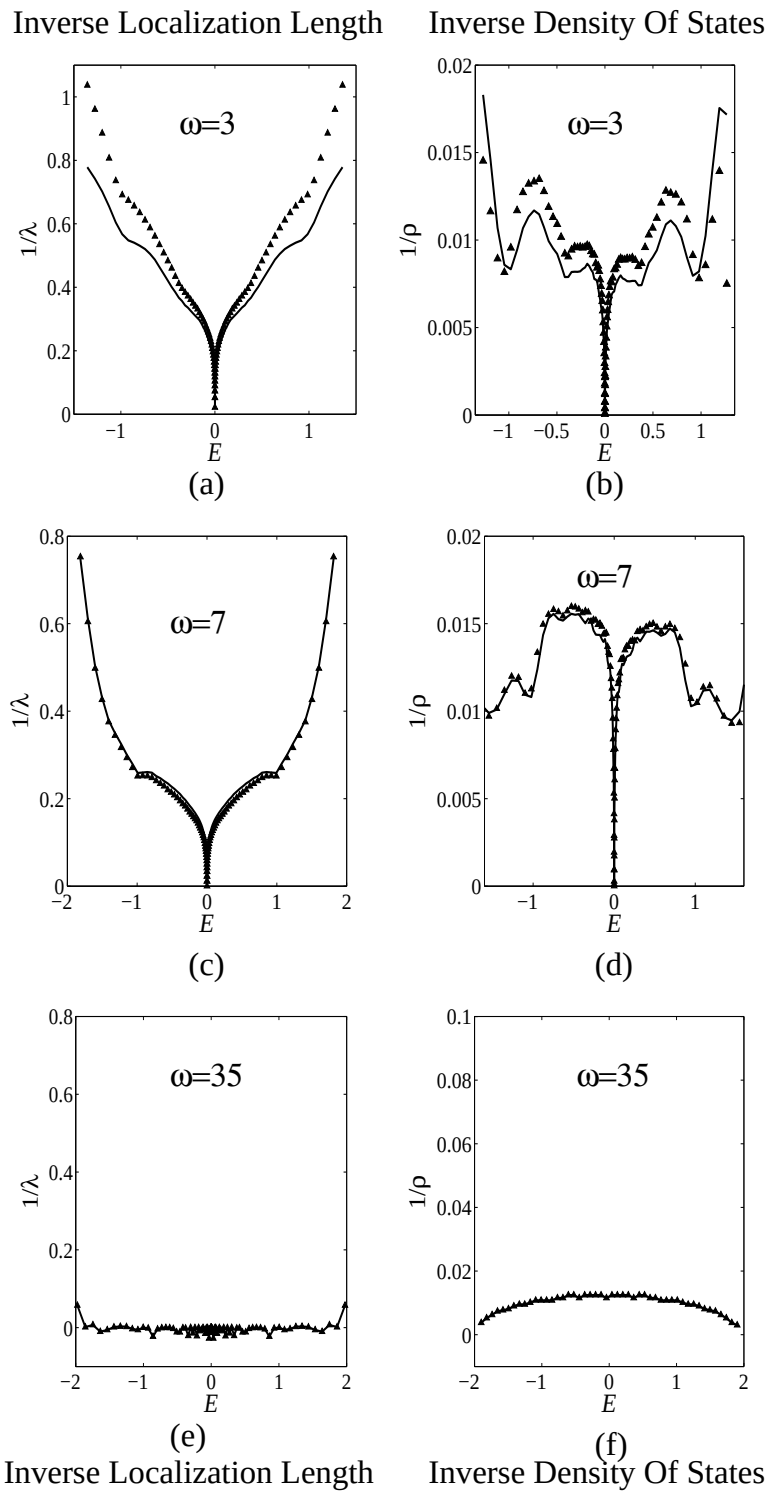

Figure 5.2: Inverse of localization length (a,c,e) and inverse of density of states (b,d,f) vs. energy E (in units of the hopping J).$\gamma = 10J$, $\omega = 3J, 7J, 35J$. Solid line are the exact results of directly calculation from model (5.1); triangles are from the effective Hamiltonian $H^{(0)}_{eff}$.

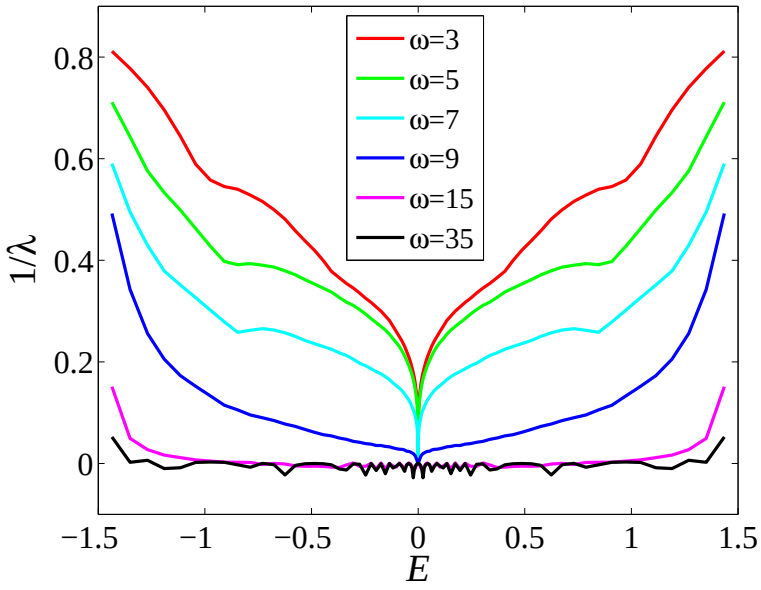

Figure 5.3: (Color online.) Inverse of localization length λ (in units of 1 / lattice constant) vs. energy E (in units of the hopping J). Number of sites $N = 100$, averaged over 50 realizations of disorder. $\gamma = 10J$, $\omega = 3J, 5J, 7J, 9J, 15J, 35J$.

when $\omega = 7$ which is comparable to the disorder width $\gamma = 10$ and when $\omega = 35$ which is much larger than γ, the results from the exact Floquet calculation and those from the effective Hamiltonian calculation agree quite well, as expected. At $\omega = 35 \gg \gamma = 10$, the localization length diverges for all states, and the density of states diverges at the band edge, as expected for a uniform-hopping tight-binding model. At $\omega = 7$ which is comparable to γ, the localiztion length and the density of states diverge only at the band center, as expected for a random hopping model. The case of $\omega = 3$ is slightly more surprising: although the effective Hamiltonian is not expected to work well (indeed as we see in FIG. 5.2a,b), it still exhibits a diverging localization length and diverging density of states at the bandcenter, which are characteristic of a random hopping model. In FIG. 5.3, we plot the localization length for more values of ω from 3 to 35, and the trend from random hopping model behavior to uniform-hopping tight-binding model behavior is clearly seen.

Near the bandcenter, we fit the results of localization and the density of states to

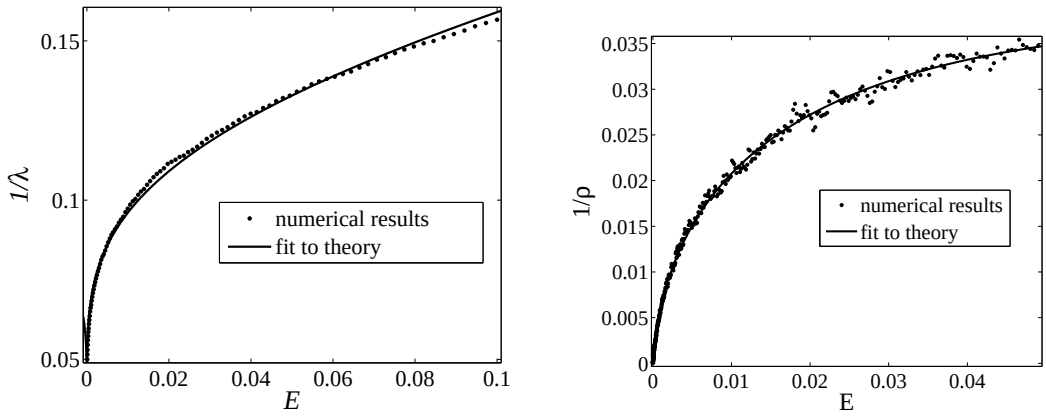

Figure 5.4: Fitting λ^{-1} and ρ^{-1} to their analytical form $\rho(E) = N \cdot \frac{2\sigma^2}{|E(\ln(E/E_0)^2)^3|}$ and $\lambda(E) = \frac{2\ln(E/E_0)^2}{\sigma^2}$. $\sigma_{theory} = \mathrm{Std}(\ln J_{eff}^2) = 1.535$; $\sigma_{fit,\lambda} = 1.495$ $\sigma_{fit,\rho} = 1.677$. $J = 1$, $\omega = 7$, $\gamma = 10$.

known analytical results[149] (see FIG. 5.4)

$$\begin{aligned} \rho(E) &= N \cdot \frac{2\sigma^2}{|E(\ln(E/E_0)^2)^3|}, \\ \lambda(E) &= \frac{2\ln(E/E_0)^2}{\sigma^2}, \end{aligned} \tag{5.22}$$

where σ is the standard deviation of the logarithm of the effective hopping amplitude square $\ln J_{eff}^2$, with

$$J_{eff,n} = J\mathcal{J}_0\left[\frac{2(v_n - v_{n+1})}{\omega}\right]. \tag{5.23}$$

We can easily evaluate σ numerically to be 1.535 given $\omega = 7$, $\gamma = 10$. Fitting numerical results of localization length and density of states, we obtain

$$\sigma_{fit,\lambda} = 1.495, \qquad \sigma_{fit,\rho} = 1.677, \tag{5.24}$$

which are quite close to the theoretical value 1.535 obtained above, further confirming our expectation that random hopping model behavior can be achieved by fast-modulating the onsite energy of Anderson insulators.

At frequencies much smaller than γ and the original hopping strength J, interestingly, the system has quite large localization length in this regime. In FIG. 5.5,

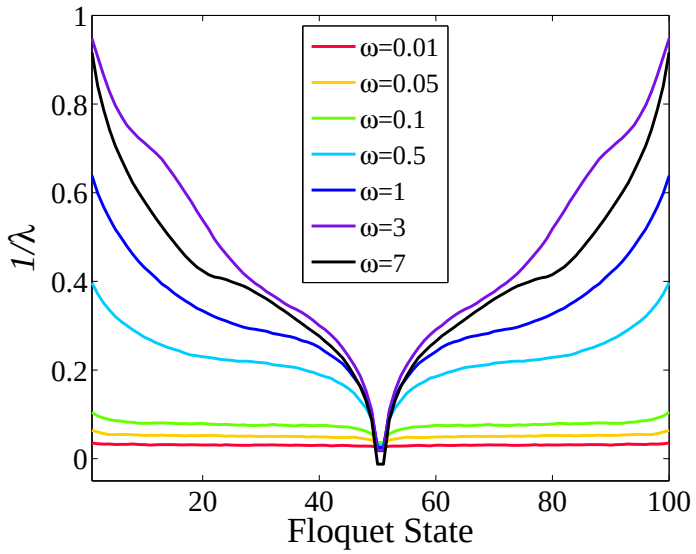

Figure 5.5: (Color online.) Inverse of localization length λ plotted for every Floquet eigenstate for $\omega = 0.05, 0.1, 0.5, 1, 3, 7$, system sizee $N = 100$.

we plot the inverse of the localization length vs. the label (e.g., 1st, 2nd,...) of every Floquet eigenstate for $\omega = 0.05, 0.1, 0.5, 1, 3, 7$ with system sizee $N = 100$ (the total number of Floquet states equals the system size N). One can see that from $\omega = 7$, when ω is lowered, first the localization length decreases (inverse of the localization increases), but around $\omega = 3$ this trend is reversed, and all the states become more and more delocalized at smaller frequencies. At $\omega = 0.05$ and 0.1, all the states have almost equally large localization length. We do not yet have a good understanding about this trend of delocalization at small frequencies.

5.5 Discussions on experimental feasibility

Currently, the application of a disorder potential to ultracold atomic systems, and the resulting localization phenomena is being intensely investigated [243]. Experiments have relied on two methods to introduce disorder into such systems. The first involves using two incommensurate optical lattice potentials, providing an effective realization of the Aubrey Andre model which has been shown to give localization [244]. The second method uses a speckle potential produced by passing a laser through a diffusing

plate which directly imprints a disorder potential [245].

The main challenge in realizing the phenomena introduced in this work is producing time-dependent disorder potentials which periodically attract and repel the atoms in the optical lattice system. The most direct way to achieve this is to periodically change the detuning of the disorder potential potential from red to blue. That is, the disorder potential is given by

$$V(r) = \frac{3\pi c^2}{2\omega_0^2}\left(\frac{\Gamma}{\Delta}\right) I(r), \tag{5.25}$$

where c is the speed of light, ω_0 is the atomic resonance frequency, $\Delta = \omega - \omega_0$ is the detuning frequency. Thus, the sign of the disorder potential can be periodically changed by periodically changing the detuning. This can be achieved by using an acousto-optic modulator to continuously vary the laser frequency. However, sweeping through the responance can produce undesirable atomic losses. Thus it might be best to periodically alternate two laser beams (one red and the other blue detuned) through the same speckle potential.

The main experimental probe to detect Anderson localization in cold atom system has been time-of-flight spectroscopy [244, 245]. In particular, for weak disorder when the condensate occupies a delocalized state, the condensate ballistically expands when the confining potential is removed. On the other hand for strong disorder potentials, the condensate occupies localized states and ceases to expand at a characteristic time after released from the trap. As we have seen, in the random hopping model some of the states are localized while others are delocalized (near the band center). Thus disentangling such behavior using time-of-flight spectroscopy alone might prove to be an experimental challenge. On the other hand, the well-developed technique of Bragg spectroscopy [246, 247] allows the access to the spectral function and therefore the density of states of quantum gas. Thus, perhaps the most promising way of detecting the Dyson delocalized state is through its distinct single single-particle density of states near the band center given by Eq. (5.22) measured through Bragg spectroscopy.

Bibliography

[1] H. Onnes, Leiden Comm. (1911) 120b.

[2] W. Meissner, R. Ochsenfeld, Naturwissenschaften 21 (1933) 787.

[3] J. Bardeen, L. N. Cooper, J. R. Schrieffer, Phys. Rev. 108 (1957) 1175.

[4] M. Tinkham, Introduction to Superconductivity, Dover, 1996.

[5] R. Shankar, Rev. Mod. Phys. 66 (1994) 129.

[6] M. K. Wu, J. R. Ashburn, C. J. Torng, P. H. Hor, R. L. Meng, L. Gao, Z. J. Huang, Y. Q. Wang, C. W. Chu, Superconductivity at 93 k in a new mixed-phase y-ba-cu-o compound system at ambient pressure, Phys. Rev. Lett. 58 (9) (1987) 908–910.

[7] Z. X. Zhao, L. Q. Chen, Q. S. Yang, Y. Z. Huang, G. H. Chen, Kexue Tongbao 33 (1987) 661.

[8] Y. Kamihara, T. Watanabe, M. Hirano, H. Hosono, J. Am. Chem. Soc. 130 (2008) 3296.

[9] J. P. Carbotte, Properties of boson-exchange superconductors, Rev. Mod. Phys. 62 (4) (1990) 1027–1157.

[10] P. W. Anderson, J. Phys. Chem. Solids 11 (1959) 26.

[11] A. A. Abrikosov, L. P. Gorkov, Sov. Phys. JETP 9 (1959) 220.

[12] M. Vershinin, S. Misra, S. Ono, Y. Abe, Y. Ando, A. Yazdani, Local Ordering in the Pseudogap State of the High-T_c Superconductor $Bi_2Sr_2CaCu_2O_{8+\delta}$, Vol. 303, Oxford University Press, 2004.

[13] J. M. Kosterlitz, D. J. Thouless, Ordering, metastability and phase transitions in two-dimensional systems, J. Phys. C 6 (1973) 1181.

[14] J. E. Mooij, in: A. M. Goldman, S. A. Wolf (Eds.), Percolation, Localization, and Superconductivity, Plenum Press, 1984.

[15] B. I. Halperin, D. R. Nelson, J. Low. Temp. Phys. 36 (1979) 599.

[16] A. L. Fetter, J. D. Walecka, Quantum Theory of Many-Particle Systems, Dover, 2003.

[17] M. Wallin, E. S. Sorensen, S. M. Girvin, A. P. Young, Phys. Rev. B 49 (1994) 12115.

[18] D. B. Haviland, Y. Liu, A. M. Goldman, Onset of superconductivity in the two-dimensional limit, Phys. Rev. Lett. 62 (18) (1989) 2180–2183.

[19] M. A. Steiner, G. Boebinger, A. Kapitulnik, Possible field-tuned superconductor-insulator transition in high-t[sub c] superconductors: Implications for pairing at high magnetic fields, Phys. Rev. Lett. 94 (10) (2005) 107008.

[20] M. P. A. Fisher, D. H. Lee, Correspondence between two-dimensional bosons and a bulk superconductor in a magnetic field, Phys. Rev. B 39 (4) (1989) 2756–2759.

[21] M. P. A. Fisher, Quantum phase transitions in disordered two-dimensional superconductors, Phys. Rev. Lett. 65 (7) (1990) 923–926.

[22] X. G. Wen, A. Zee, Int. J. Mod. Phys. B 4 (1990) 437.

[23] M. P. A. Fisher, G. Grinstein, S. M. Girvin, Presence of quantum diffusion in two dimensions: Universal resistance at the superconductor-insulator transition, Phys. Rev. Lett. 64 (5) (1990) 587–590.

[24] M. C. Cha, M. P. A. Fisher, S. M. Girvin, M. Wallin, A. P. Young, Phys. Rev. B 44 (1991) 6883.

[25] A. F. Hebard, M. A. Paalanen, Magnetic-field-tuned superconductor-insulator transition in two-dimensional films, Phys. Rev. Lett. 65 (7) (1990) 927–930.

[26] M. A. Paalanen, A. F. Hebard, R. R. Ruel, Low-temperature insulating phases of uniformly disordered two-dimensional superconductors, Phys. Rev. Lett. 69 (10) (1992) 1604–1607.

[27] J. M. Valles, R. C. Dynes, J. P. Garno, Phys. Rev. Lett. 69 (1992) 3567.

[28] Y. Liu, D. B. Haviland, B. Nease, A. M. Goldman, Insulator-to-superconductor transition in ultrathin films, Phys. Rev. B 47 (10) (1993) 5931–5946.

[29] S. Y. Hsu, J. A. Chervenak, J. M. Valles, Phys. Rev. Lett. 75 (1995) 132.

[30] J. M. Valles, S. Y. Hsu, R. C. Dynes, J. P. Garno, Physica B 197 (1994) 522.

[31] A. Yazdani, A. Kapitulnik, Superconducting-insulating transition in two-dimensional a-moge thin films, Phys. Rev. Lett. 74 (15) (1995) 3037–3040.

[32] S. Y. Hsu, J. A. Chervenak, J. M. Valles, J. Phys. Chem. Solids 59 (1998) 2065.

[33] A. M. Goldman, N. Markovic, Phys. Today 51 (1998) 39.

[34] A. M. Goldman, Physica E 18 (2003) 1.

[35] G. Sambandamurthy, L. W. Engel, A. Johansson, D. Shahar, Superconductivity-related insulating behavior, Phys. Rev. Lett. 92 (10) (2004) 107005.

[36] A. M. Finkel'stein, JETP lett. 45 (1987) 46.

[37] A. M. Finkel'stein, Physica B 197 (1994) 636.

[38] A. Larkin, Ann. Phys. (Leipzig) 8 (1999) 785.

[39] C. Dasgupta, B. I. Halperin, Phase transition in a lattice model of superconductivity, Phys. Rev. Lett. 47 (21) (1981) 1556–1560.

[40] M. V. Feigelman, V. B. Geshkenbein, L. B. Ioffe, A. I. Larkin, Two-dimensional bose liquid with strong gauge-field interaction, Phys. Rev. B 48 (22) (1993) 16641–16661.

[41] N. Nagaosa, Quantum Field Theory in Condensed Matter Physics, Springer, 1999.

[42] L. Balents, L. Bartosch, A. Burkov, S. Sachdev, K. Sengupta, arXiv:cond-mat/0504692.

[43] E. Simanek, Inhomogeneous Superconductors: Granular and Quantum Effects, Vol. 422, Oxford University Press, 2005.

[44] A. E. White, R. C. Dynes, J. P. Garno, Phys. Rev. B 33 (1986) 3549.

[45] R. C. Dynes, A. E. White, J. M. Graybeal, J. P. Garno, Phys. Rev. Lett 57 (1986) 2195.

[46] J. M. Valles, R. C. Dynes, J. P. Garno, Phys. Rev. B 40 (1989) 6680.

[47] L. Merchant, J. Ostrick, R. P. Barber, R. C. Dynes, Crossover from phase fluctuation to amplitude-dominated superconductivity: A model system, Phys. Rev. B 63 (13) (2001) 134508.

[48] Z. Long, M. D. Stewart., T. Kouh, J. M. Valles., Subgap density of states in superconductor-normal metal bilayers in the cooper limit, Phys. Rev. Lett 93 (2004) 257001.

[49] Z. Long, M. D. Stewart., J. M. Valles., Super-weakly coupled superconductivity in ultrathin superconductor17cnormal-metal bilayers, Phys. Rev. B 73 (2006) 140507(R).

[50] L. N. Cooper, Superconductivity in the neighborhood of metallic contacts, Phys. Rev. Lett 6 (1961) 689.

[51] P. G. de Gennes, Boundary effects in superconductors, Rev. Mod. Phys. 36 (1964) 225.

[52] Y. V. Fominov, M. V. Feigel'man, Superconductive properties of thin dirty superconductor-normal-metal bilayers, Phys. Rev. B 63 (2001) 094518.

[53] Y. Qin, C. L. Vicente, J. Yoon, Magnetically induced metallic phase in superconducting tantalum films, Phys. Rev. B 73 (10) (2006) 100505(R).

[54] D. Ephron, A. Yazdani, A. Kapitulnik, M. R. Beasley, Phys. Rev. Lett. 76 (1996) 1529.

[55] N. Mason, A. Kapitulnik, Dissipation effects on the superconductor-insulator transition in 2d superconductors, Phys. Rev. Lett. 82 (26) (1999) 5341–5344.

[56] N. Mason, A. Kapitulnik, True superconductivity in a two-dimensional superconducting-insulating system, Phys. Rev. B 64 (6) (2001) 060504(R).

[57] Y. Seo, Y. Qin, C. L. Vicente, K. S. Choi, J. Yoon, Origin of nonlinear transport across the magnetically induced superconductor-metal-insulator transition in two dimensions, Phys. Rev. Lett. 97 (2006) 057005.

[58] Y. Li, C. L. Vicente, J. Yoon, Transport phase diagram for superconducting thin films of tantalum with homogeneous disorder, Phys. Rev. B 81 (2) (2010) 020505.

[59] T. I. Baturina, D. R. Islamov, J. Bentner, C. Strunk, M. R. Baklanov, A. Satta, JETP Lett. 79 (2004) 337.

[60] V. Gantmakher, V. Dolgopolov, Physics-Uspekhi 53 (2010) 3.

[61] L. Balents, M. P. A. Fisher, Phys. Rev. B 71 (2005) 085119.

[62] V. M. Galitski, G. Refael, M. P. A. Fisher, T. Senthil, Vortices and quasiparticles near the superconductor-insulator transition in thin films, Phys. Rev. Lett. 95 (7) (2005) 077002.

[63] Y. Dubi, Y. Meir, Y. Avishai, Phys. Rev. B 73 (2006) 054509.

[64] E. Shimshoni, A. Auerbach, A. Kapitulnik, Transport through quantum melts, Phys. Rev. Lett. 80 (1998) 3352.

[65] A. Ghosal, M. Randeria, N. Trivedi, Phys. Rev. B 65 (2001) 014501.

[66] Y. Dubi, Y. Meir, Y. Avishai, Nature 449 (2007) 876.

[67] B. Spivak, P. Oreto, S. A. Kivelson, Phys. Rev. B 77 (2008) 214523.

[68] D. Dalidovich, P. Phillips, Phase glass is a bose metal: A new conducting state in two dimensions, Phys. Rev. Lett. 89 (2) (2002) 027001.

[69] J. Wu, P. Phillips, Vortex glass is a metal: Unified theory of the magnetic-field and disorder-tuned bose metals, Phys. Rev. B 73 (2006) 214507.

[70] R. Ikeda, J. Phys. Soc. Jpn. 76 (2007) 064709.

[71] A. Johansson, N. Stander, E. Peled, G. Sambandamurthy, D. Shahar, arXiv:cond-mat/0602160.

[72] R. Crane, N. P. Armitage, A. Johansson, G. Sambandamurthy, D. Shahar, G. Gruner, Survival of superconducting correlations across the two-dimensional superconductor-insulator transition: A finite-frequency study, Phys. Rev. B 75 (2007) 184530.

[73] P. Spathis, H. Aubin, A. Pourret, K. Behnia, Europhys. Lett. 83 (2008) 57005.

[74] B. Sacepe, C. Chapelier, T. I. Baturina, V. M. Vinokur, M. R. Baklanov, M. Sanquer, Phys. Rev. Lett. 101 (2008) 157006.

[75] Stormer, Physica B 177 (1992) 401.

[76] K. v. Klitzing, G. Dorda, M. Pepper, New method for high-accuracy determination of the fine-structure constant based on quantized hall resistance, Phys. Rev. Lett. 45 (6) (1980) 494–497.

[77] D. C. Tsui, H. L. Stormer, A. C. Gossard, Two-dimensional magnetotransport in the extreme quantum limit, Phys. Rev. Lett. 48 (22) (1982) 1559–1562.

[78] Y. Zhang, Y. W. Tan, H. L. Stormer, P. Kim, Nature 438 (2005) 201.

[79] S.Girvin, The quantum hall effect: Novel excitations and broken symmetries, in: A. Comtet, T. Jolicoeur, S. Ouvry, F. David (Eds.), Topological Aspects of Low Dimensional Systems, Springer-Verlag, 2000.

[80] G. Murthy, R. Shankar, Hamiltonian theories of the fractional quantum hall effect, Rev. Mod. Phys. 75 (4) (2003) 1101–1158.

[81] X. G. Wen, Quantum Field Theory of Many-body Systems: From the Origin of Sound to an Origin of Light and Electrons, Oxford University Press, 2007.

[82] R. B. Laughlin, Anomalous quantum hall effect: An incompressible quantum fluid with fractionally charged excitations, Phys. Rev. Lett. 50 (18) (1983) 1395–1398.

[83] S. C. Zhang, T. H. Hansson, S. Kivelson, Effective-field-theory model for the fractional quantum hall effect, Phys. Rev. Lett. 62 (1) (1989) 82–85.

[84] D.-H. Lee, S.-C. Zhang, Collective excitations in the ginzburg-landau theory of the fractional quantum hall effect, Phys. Rev. Lett. 66 (9) (1991) 1220–1223.

[85] J. K. Jain, Composite-fermion approach for the fractional quantum hall effect, Phys. Rev. Lett. 63 (2) (1989) 199–202.

[86] A. Lopez, E. Fradkin, Fractional quantum hall effect and chern-simons gauge theories, Phys. Rev. B 44 (10) (1991) 5246–5262.

[87] C. Nayak, S. H. Simon, A. Stern, M. Freedman, S. Das Sarma, Non-abelian anyons and topological quantum computation, Rev. Mod. Phys. 80 (3) (2008) 1083–1159.

[88] A. Kitaev, Ann. Phys. 303 (2) (2003) 30.

[89] B. I. Halperin, Statistics of quasiparticles and the hierarchy of fractional quantized hall states, Phys. Rev. Lett. 52 (18) (1984) 1583–1586.

[90] J. P. Eisenstein, A. H. MacDonald, Nature 432 (2004) 691.

[91] I. B. Spielman, J. P. Eisenstein, L. N. Pfeiffer, K. W. West, Resonantly enhanced tunneling in a double layer quantum hall ferromagnet, Phys. Rev. Lett. 84 (25) (2000) 5808–5811.

[92] I. B. Spielman, J. P. Eisenstein, L. N. Pfeiffer, K. W. West, Observation of a linearly dispersing collective mode in a quantum hall ferromagnet, Phys. Rev. Lett. 87 (3) (2001) 036803.

[93] M. Kellogg, I. B. Spielman, J. P. Eisenstein, L. N. Pfeiffer, K. W. West, Observation of quantized hall drag in a strongly correlated bilayer electron system, Phys. Rev. Lett. 88 (12) (2002) 126804.

[94] M. Kellogg, J. P. Eisenstein, L. N. Pfeiffer, K. W. West, Vanishing hall resistance at high magnetic field in a double-layer two-dimensional electron system, Phys. Rev. Lett. 93 (3) (2004) 036801.

[95] K. Moon, H. Mori, K. Yang, S. M. Girvin, A. H. MacDonald, L. Zheng, D. Yoshioka, S.-C. Zhang, Spontaneous interlayer coherence in double-layer quantum hall systems: Charged vortices and kosterlitz-thouless phase transitions, Phys. Rev. B 51 (8) (1995) 5138–5170.

[96] X. G. Wen, A. Zee, Tunneling in double-layered quantum hall systems, Phys. Rev. B 47 (1993) 2265–2270.

[97] A. Stern, S. M. Girvin, A. H. MacDonald, N. Ma, Theory of interlayer tunneling in bilayer quantum hall ferromagnets, Phys. Rev. Lett. 86 (9) (2001) 1829–1832.

[98] Y. N. Joglekar, A. H. MacDonald, Is there a dc josephson effect in bilayer quantum hall systems?, Phys. Rev. Lett. 87 (19) (2001) 196802.

[99] H. A. Fertig, G. Murthy, Coherence network in the quantum hall bilayer, Phys. Rev. Lett. 95 (15) (2005) 156802.

[100] B. I. Halperin, P. A. Lee, N. Read, Theory of the half-filled landau level, Phys. Rev. B 47 (12) (1993) 7312–7343.

[101] S. H. Simon, B. I. Halperin, Finite-wave-vector electromagnetic response of fractional quantized hall states, Phys. Rev. B 48 (23) (1993) 17368–17387.

[102] A. Stern, B. I. Halperin, Singularities in the fermi-liquid description of a partially filled landau level and the energy gaps of fractional quantum hall states, Phys. Rev. B 52 (8) (1995) 5890–5906.

[103] S. H. Simon, A. Stern, B. I. Halperin, Composite fermions with orbital magnetization, Phys. Rev. B 54 (16) (1996) R11114–R11117.

[104] S. H. Simon, in: O. Heinonen (Ed.), Composite Fermions, World Scientific, 1998.

[105] R. Shankar, G. Murthy, Towards a field theory of fractional quantum hall states, Phys. Rev. Lett. 79 (22) (1997) 4437–4440.

[106] N. Read, Lowest-landau-level theory of the quantum hall effect: The fermi-liquid-like state of bosons at filling factor one, Phys. Rev. B 58 (24) (1998) 16262–16290.

[107] D.-H. Lee, Neutral fermions at filling factor $\nu = 1/2$, Phys. Rev. Lett. 80 (21) (1998) 4745–4748.

[108] A. Stern, B. I. Halperin, F. von Oppen, S. H. Simon, Half-filled landau level as a fermi liquid of dipolar quasiparticles, Phys. Rev. B 59 (19) (1999) 12547–12567.

[109] R. Shankar, Hamiltonian theory of gaps, masses, and polarization in quantum hall states, Phys. Rev. B 63 (8) (2001) 085322.

[110] R. R. Du, H. L. Stormer, D. C. Tsui, L. N. Pfeiffer, K. W. West, Experimental evidence for new particles in the fractional quantum hall effect, Phys. Rev. Lett. 70 (1993) 2944–2947.

[111] R. Willett, Adv. Phys. 46 (1997) 447.

[112] W. Kang, H. L. Stormer, L. N. Pfeiffer, K. W. Baldwin, K. W. West, How real are composite fermions?, Phys. Rev. Lett. 71 (23) (1993) 3850–3853.

[113] V. J. Goldman, B. Su, J. K. Jain, Detection of composite fermions by magnetic focusing, Phys. Rev. Lett. 72 (13) (1994) 2065–2068.

[114] L. A. Tracy, J. P. Eisenstein, L. N. Pfeiffer, K. W. West, Spin transition in the half-filled landau level, Phys. Rev. Lett. 98 (8) (2007) 086801.

[115] F. Schulze-Wischeler, U. Zeitler, C. v. Zobeltitz, F. Hohls, D. Reuter, A. D. Wieck, H. Frahm, R. J. Haug, Measurement of the specific heat of a fractional quantum hall system, Phys. Rev. B 76 (15) (2007) 153311.

[116] M. P. Lilly, J. P. Eisenstein, L. N. Pfeiffer, K. W. West, Coulomb drag in the extreme quantum limit, Phys. Rev. Lett. 80 (8) (1998) 1714–1717.

[117] M. Kellogg, J. P. Eisenstein, L. N. Pfeiffer, K. W. West, Bilayer quantum hall systems at $\nu t = 1$: Coulomb drag and the transition from weak to strong interlayer coupling, Phys. Rev. Lett. 90 (24) (2003) 246801.

[118] E. Tutuc, S. Melinte, E. P. De Poortere, R. Pillarisetty, M. Shayegan, Role of density imbalance in an interacting bilayer hole system, Phys. Rev. Lett. 91 (2003) 076802.

[119] I. B. Spielman, M. Kellogg, J. P. Eisenstein, L. N. Pfeiffer, K. W. West, Onset of interlayer phase coherence in a bilayer two-dimensional electron system: Effect of layer density imbalance, Phys. Rev. B 70 (8) (2004) 081303.

[120] W. R. Clarke, A. P. Micolich, A. R. Hamilton, M. Y. Simmons, C. B. Hanna, J. R. Rodriguez, M. Pepper, D. A. Ritchie, Evolution of the bilayer $\nu = 1$ quantum hall state under charge imbalance, Phys. Rev. B 71 (8) (2005) 081304.

[121] I. B. Spielman, L. A. Tracy, J. P. Eisenstein, L. N. Pfeiffer, K. W. West, Spin transition in strongly correlated bilayer two-dimensional electron systems, Phys. Rev. Lett. 94 (7) (2005) 076803.

[122] N. Kumada, K. Muraki, K. Hashimoto, Y. Hirayama, Spin degree of freedom in the $\nu = 1$ bilayer electron system investigated by nuclear spin relaxation, Phys. Rev. Lett. 94 (2005) 096802.

[123] S. Luin, V. Pellegrini, A. Pinczuk, B. S. Dennis, L. N. Pfeiffer, K. W. West, Observation of collapse of pseudospin order in bilayer quantum hall ferromagnets, Phys. Rev. Lett. 94 (2005) 146804.

[124] L. A. Tracy, J. P. Eisenstein, L. N. Pfeiffer, K. W. West, Resistively detected nmr in a two-dimensional electron system near nu = 1: Clues to the origin of the dispersive lineshape, Phys. Rev. B 73 (2006) 121306.

[125] P. Giudici, K. Muraki, N. Kumada, Y. Hirayama, T. Fujisawa, Spin-dependent phase diagram of the nu[sub t] = 1 bilayer electron system, Phys. Rev. Lett. 100 (10) (2008) 106803.

[126] A. R. Champagne, J. P. Eisenstein, L. N. Pfeiffer, K. W. West, Evidence for a finite-temperature phase transition in a bilayer quantum hall system, Phys. Rev. Lett. 100 (9) (2008) 096801.

[127] A. R. Champagne, A. D. K. Finck, J. P. Eisenstein, L. N. Pfeiffer, K. W. West, Charge imbalance and bilayer two-dimensional electron systems at nu[sub t] = 1, Phys. Rev. B 78 (20) (2008) 205310.

[128] B. Karmakar, V. Pellegrini, A. Pinczuk, L. N. Pfeiffer, K. W. West, First-order quantum phase transition of excitons in quantum hall bilayers, Phys. Rev. Lett. 102 (2009) 036802.

[129] A. D. K. Finck, J. P. Eisenstein, L. N. Pfeiffer, K. W. West, Quantum hall exciton condensation at full spin polarization, Phys. Rev. Lett. 104 (1) (2010) 016801.

[130] P. Giudici, K. Muraki, N. Kumada, T. Fujisawa, Intrinsic gap and exciton condensation in the $\nu t = 1$ bilayer system, Phys. Rev. Lett. 104 (5) (2010) 056802.

[131] R. Côté, L. Brey, A. H. MacDonald, Broken-symmetry ground states for the two-dimensional electron gas in a double-quantum-well system, Phys. Rev. B 46 (16) (1992) 10239–10250.

[132] L. Zheng, H. A. Fertig, Wigner-crystal states for the two-dimensional electron gas in a double-quantum-well system, Phys. Rev. B 52 (1995) 12282–12290.

[133] S. Narasimhan, T.-L. Ho, Wigner-crystal phases in bilayer quantum hall systems, Phys. Rev. B 52 (1995) 12291–12306.

[134] N. E. Bonesteel, I. A. McDonald, C. Nayak, Gauge fields and pairing in double-layer composite fermion metals, Phys. Rev. Lett. 77 (1996) 3009–3012.

[135] Y. B. Kim, C. Nayak, E. Demler, N. Read, S. Das Sarma, Bilayer paired quantum hall states and coulomb drag, Phys. Rev. B 63 (20) (2001) 205315.

[136] E. Demler, C. Nayak, S. Das Sarma, Bilayer coherent and quantum hall phases: Duality and quantum disorder, Phys. Rev. Lett. 86 (2001) 1853–1856.

[137] J. Schliemann, S. M. Girvin, A. H. MacDonald, Strong correlation to weak correlation phase transition in bilayer quantum hall systems, Phys. Rev. Lett. 86 (9) (2001) 1849–1852.

[138] A. Stern, B. I. Halperin, Strong enhancement of drag and dissipation at the weak- to strong-coupling phase transition in a bilayer system at a total landau level filling $\nu = 1$, Phys. Rev. Lett. 88 (10) (2002) 106801.

[139] S. H. Simon, E. H. Rezayi, M. V. Milovanovic, Coexistence of composite bosons and composite fermions in $\nu = 12 + 12$ quantum hall bilayers, Phys. Rev. Lett. 91 (2003) 046803.

[140] N. Shibata, D. Yoshioka, Ground state of $\nu = 1$ bilayer quantum hall systems, J. Phys. Soc. Jpn. 75 (2006) 043712.

[141] J. Ye, L. Jiang, Quantum phase transitions in bilayer quantum hall systems at a total filling factor nu[sub t] = 1, Phys. Rev. Lett. 98 (23) (2007) 236802.

[142] G. Möller, S. H. Simon, E. H. Rezayi, Paired composite fermion phase of quantum hall bilayers at nu = (1/2)+(1/2), Phys. Rev. Lett. 101 (2008) 176803.

[143] G. Möller, S. H. Simon, Paired composite-fermion wave functions, Phys.Rev. B 77 (7) (2008) 075319.

[144] M. V. Milovanović, Z. Papić, Nonperturbative approach to the quantum hall bilayer, Phys. Rev. B 79 (11) (2009) 115319.

[145] Y. Q. Li, V. Umansky, K. von Klitzing, J. H. Smet, Nature of the spin transition in the half-filled landau level, Phys. Rev. Lett. 102 (4) (2009) 046803.

[146] F. J. Dyson, The dynamics of a disordered linear chain, Phys. Rev. 92 (6) (1953) 1331–1338.

[147] D. J. Thouless, J. Phys. C 5 (1972) 77.

[148] G. Theodorou, M. H. Cohen, Extended states in a one-demensional system with off-diagonal disorder, Phys. Rev. B 13 (10) (1976) 4597–4601.

[149] T. P. Eggarter, R. Riedinger, Singular behavior of tight-binding chains with off-diagonal disorder, Phys. Rev. B 18 (2) (1978) 569–575.

[150] D. S. Fisher, Random antiferromagnetic quantum spin chains, Phys. Rev. B 50 (6) (1994) 3799–3821.

[151] L. Balents, M. P. A. Fisher, Delocalization transition via supersymmetry in one dimension, Phys. Rev. B 56 (20) (1997) 12970–12991.

[152] M. S. Foster, A. W. W. Ludwig, Metal-insulator transition from combined disorder and interaction effects in hubbard-like electronic lattice models with random hopping, Phys. Rev. B 77 (16) (2008) 165108.

[153] E. Altman, Y. Kafri, A. Polkovnikov, G. Refael, Phase transition in a system of one-dimensional bosons with strong disorder, Phys. Rev. Lett. 93 (15) (2004) 150402.

[154] E. Altman, Y. Kafri, A. Polkovnikov, G. Refael, Insulating phases and superfluid-insulator transition of disordered boson chains, Phys. Rev. Lett. 100 (17) (2008) 170402.

[155] D. H. Dunlap, V. M. Kenkre, Dynamic localization of a charged particle moving under the influence of an electric field, Phys. Rev. B 34 (6) (1986) 3625–3633.

[156] F. Grossmann, T. Dittrich, P. Jung, P. Hänggi, Coherent destruction of tunneling, Phys. Rev. Lett. 67 (4) (1991) 516–519.

[157] M. Holthaus, Collapse of minibands in far-infrared irradiated superlattices, Phys. Rev. Lett. 69 (2) (1992) 351–354.

[158] M. Holthaus, Towards coherent control of a bose-einstein condensate in a double well, Phys. Rev. A 64 (1) (2001) 011601.

[159] A. Eckardt, C. Weiss, M. Holthaus, Superfluid-insulator transition in a periodically driven optical lattice, Phys. Rev. Lett. 95 (26) (2005) 260404.

[160] A. Eckardt, T. Jinasundera, C. Weiss, M. Holthaus, Analog of photon-assisted tunneling in a bose-einstein condensate, Phys. Rev. Lett. 95 (20) (2005) 200401.

[161] C. E. Creffield, T. S. Monteiro, Tuning the mott transition in a bose-einstein condensate by multiple photon absorption, Phys. Rev. Lett. 96 (21) (2006) 210403.

[162] D. F. Martinez, R. A. Molina, Delocalization induced by low-frequency driving in disordered tight-binding lattices, Phys. Rev. B 73 (7) (2006) 073104.

[163] D. F. Martinez, R. A. Molina, Eur. Phys. J. B. 52 (2006) 281.

[164] A. Eckardt, M. Holthaus, Eur. Phys. Lett. 80 (2007) 50004.

[165] H. Lignier, C. Sias, D. Ciampini, Y. Singh, A. Zenesini, O. Morsch, E. Arimondo, Dynamical control of matter-wave tunneling in periodic potentials, Phys. Rev. Lett. 99 (22) (2007) 220403.

[166] E. Kierig, U. Schnorrberger, A. Schietinger, J. Tomkovic, M. K. Oberthaler, Single-particle tunneling in strongly driven double-well potentials, Phys. Rev. Lett. 100 (19) (2008) 190405.

[167] X. Luo, Q. Xie, B. Wu, Quasienergies and floquet states of two weakly coupled bose-einstein condensates under periodic driving, Phys. Rev. A 77 (5) (2008) 053601.

[168] N. Tsukada, H. Yoshida, T. Suzuki, Effective tunneling coefficient of a coupled double-well system modulated by anharmonic periodic potentials, Phys. Rev. A 77 (2) (2008) 022101.

[169] A. Eckardt, M. Holthaus, H. Lignier, A. Zenesini, D. Ciampini, O. Morsch, E. Arimondo, Exploring dynamic localization with a bose-einstein condensate, Phys. Rev. A 79 (1) (2009) 013611.

[170] A. A. Abrikosov, Fundamental Theory of Metals, North-Holland, 1988.

[171] I. Martin, D. Podolsky, S. A. Kivelson, Enhancement of superconductivity by local inhomogeneities, Phys. Rev. B 72 (2005) 060502(R).

[172] A. I. Larkin, Y. N. Ovchinnikov, Sov. Phys. JETP 34 (1972) 1144.

[173] J. S. Meyer, B. D. Simons, Gap fluctuations in inhomogeneous superconductors, Phys. Rev. B 64 (13) (2001) 134516.

[174] K. Aryanpour, E. R. Dagotto, M. Mayr, T. Paiva, W. E. Pickett, R. T. Scalettar, Effect of inhomogeneity on s-wave superconductivity in the attractive hubbard model, Phys. Rev. B 73 (10) (2006) 104518.

[175] K. Aryanpour, T. Paiva, W. E. Pickett, R. T. Scalettar, s-wave superconductivity phase diagram in the inhomogeneous two-dimensional attractive hubbard model, Phys. Rev. B 76 (18) (2007) 184521.

[176] Y. L. Loh, E. W. Carlson, Using inhomogeneity to raise superconducting critical temperatures, Phys. Rev. B 75 (2007) 132506.

[177] Y. Zou, I. Klich, G. Refael, Effect of inhomogeneous coupling on bcs superconductors, Phys. Rev. B 77 (14) (2008) 144523.

[178] K. D. Usadel, Generalized diffusion equation for superconducting alloys, Phys. Rev. Lett 25 (1970) 507.

[179] W. Belzig, F. Wilhelm, G. Schon, C. Bruder, A. Zaikin, Quasiclassical green's function approach to mesoscopic superconductivity, Superlattices and Microstructures 25 (1999) 1251.

[180] L. G. Aslamasov, A. I. Larkin, Phys. Lett. 26A (1968) 238.

[181] B. I. Haperin, D. R. Nelson, J. Low. Temp. Phys. 36 (1979) 599.

[182] A. F. Hebard, M. A. Paalanen, Phys. Rev. Lett. 54 (1985) 2155.

[183] A. M. Zagoskin, Quantum Theory of Many-Body Systems, Springer, 1998.

[184] F. Zhou, P. Charlat, B. Spivak, B. Pannetier, Density of states in superconductor-normal metal-superconductor junctions, Journal of Low Temperature Physics 110 (1998) 841.

[185] A. P. van Gelder, Energy gaps in the excitation spectrum of a superconductor, Phys. Rev. 181 (1969) 787.

[186] Z. Long, J. J. M. Valles, Early stage morphology of quench condensed ag, pb and pb/ag hybrid films, J. Low. Temp. Phys. 139 (2005) 429.

[187] I. Giaever, Phys. Rev. Lett. 15 (1965) 825.

[188] K. Michaeli, A. M. Finkel'stein, Metal-insulator transition in a system of superconducting vortices caused by a metallic gate, Phys. Rev. Lett. 97 (11) (2006) 117004.

[189] N. Mason, A. Kapitulnik, Superconductor-insulator transition in a capacitively coupled dissipative environment, Phys. Rev. B 65 (22) (2002) 220505.

[190] T. J. Gramila, J. P. Eisenstein, A. H. MacDonald, L. N. Pfeiffer, K. W. West, Phys. Rev. Lett. 66 (1991) 1216.

[191] Y. Zou, G. Refael, J. Yoon, Investigating the superconductor-insulator transition in thin films using drag resistance: Theoretical analysis of a proposed experiment, Phys. Rev. B 80 (2009) 180503.

[192] Y. Zou, G. Refael, J. Yoon, Theoretical analysis of drag resistance in amorphous thin films exhibiting superconductor-insulator-transition, in preparation.

[193] J. Pearl, Appl. Phys. Lett. 5 (1964) 65.

[194] A. De Col, V. B. Geshkenbein, G. Blatter, Dissociation of vortex stacks into fractional-flux vortices, Phys. Rev. Lett. 94 (9) (2005) 097001.

[195] M. D. Sherrill, Phys. Rev. B 7 (1973) 1908.

[196] M. D. Sherrill, Phys. Rev. B 11 (1975) 1066.

[197] A.-P. Jauho, H. Smith, Coulomb drag between parallel two-dimensional electron systems, Phys. Rev. B 47 (8) (1993) 4420–4428.

[198] L. Zheng, A. H. MacDonald, Phys. Rev. B 48 (1993) 8203.

[199] A. Kamenev, Y. Oreg, Phys. Rev. B 52 (1995) 7516.

[200] K. Flensberg, B. Hu, A. Jauho, J. M. Kinaret, Phys. Rev. B 52 (1995) 14761.

[201] F. von Oppen, S. H. Simon, A. Stern, Phys. Rev. Lett. 87 (2001) 106803.

[202] E. H. Hwang, S. D. Sarma, V. Braude, A. Stern, Phys. Rev. Lett. 90 (2003) 086801.

[203] G. D. Mahan, Many-Particle Physics, Plenum Press, New York, 1981.

[204] F. Stern, Phys. Rev. Lett. 18 (1967) 546.

[205] E. Leutheusser, J. Phys. C. 15 (1982) 2801.

[206] E. Leutheusser, S. Yip, B. J. Alder, W. E. Alley, J. Stat. Phys. 32.

[207] J. M. Duan, S. Yip, Phys. Rev. Lett. 70 (1993) 3647.

[208] S. V. Terenttjev, S. I. Shevchenko, Low Temp. Phys. 25 (1999) 493.

[209] D. V. Fil, S. I. Shevchenko, Low Temp. Phys. 30 (2004) 770.

[210] O. Narayan, J. Phys. A 36 (2003) L373.

[211] Kuprianov, Likharev, Sov. Phys. JETP 41 (1975) 755.

[212] G. Blatter, V. B. Geshkenbein, V. M. Vinokur, Quantum collective creep, Phys. Rev. Lett. 66 (25) (1991) 3297–3300.

[213] J.-M. Duan, A. J. Leggett, Inertial mass of a moving singularity in a fermi superfluid, Phys. Rev. Lett. 68 (8) (1992) 1216–1219.

[214] E. B. Sonin, V. B. Geshkenbein, A. van Otterlo, G. Blatter, Vortex motion in charged and neutral superfluids: A hydrodynamic approach, Phys. Rev. B 57 (1) (1998) 575–581.

[215] D. Forster, Hydrodynamic Fluctuations, Broken Symmetry, And Correlation Functions, Westview Press, 1995.

[216] P. M. Chaikin, T. C. Lubensky, Principles of condensed matter physics, Cambridge University Press, 1995.

[217] E. Leutheusser, J. Chem. Phys. 84 (1986) 1050.

[218] P. A. Whitlock, M. Bishop, J. L. Tiglias, J. Chem. Phys. 126 (2007) 224505.

[219] E. Shimshoni, Phys. Rev. B 56 (1997) 13301.

[220] D. Vollhardt, P. Wolfle, Phys. Rev. B 22 (1980) 4666.

[221] D. Vollhardt, P. Wolfle, in: W. Hanke, Y. V. Kopaev (Eds.), Electronic Phase Transitions, North-Holland, 1992.

[222] Y. Imry, Y. Gefen, D. J. Bergman, Phys. Rev. B 26 (1982) 3436.

[223] V. M. Apalkov, M. E. Raikh, Effective drag between strongly inhomogeneous layers: Exact results and applications, Phys. Rev. B 71 (2005) 245109.

[224] Y. Zou, G. Refael, A. Stern, J. P. Eisenstein, Clausius-clapeyron relations for first order phase transitions in bilayer quantum hall systems, Phys. Rev. B In press.

[225] K. Park, J. K. Jain, Phase diagram of the spin polarization of composite fermions and a new effective mass, Phys. Rev. Lett. 80 (19) (1998) 4237–4240.

[226] S. Melinte, N. Freytag, M. Horvatić, C. Berthier, L. P. Lévy, V. Bayot, M. Shayegan, Nmr determination of 2d electron spin polarization at $\nu = 1/2$, Phys. Rev. Lett. 84 (2000) 354–357.

[227] N. Freytag, M. Horvatić, C. Berthier, M. Shayegan, L. P. Lévy, Nmr investigation of how free composite fermions are at $\nu = 12$, Phys. Rev. Lett. 89 (2002) 246804.

[228] I. V. Kukushkin, K. v. Klitzing, K. Eberl, Spin polarization of composite fermions: Measurements of the fermi energy, Phys. Rev. Lett. 82 (1999) 3665–3668.

[229] Y. B. Kim, P. A. Lee, Specific heat and validity of the quasiparticle approximation in the half-filled landau level, Phys. Rev. B 54 (1996) 2715–2717.

[230] P. J. Price, Polar-optical-mode scattering for an ideal quantum-well heterostructure, Phys. Rev. B 30 (1984) 2234–2235.

[231] A. Gold, Electronic transport properties of a two-dimensional electron gas in a silicon quantum-well structure at low temperature, Phys. Rev. B 35 (1987) 723–733.

[232] R. R. Du, H. L. Stormer, D. C. Tsui, A. S. Yeh, L. N. Pfeiffer, K. W. West, Drastic enhancement of composite fermion mass near landau level filling $\nu = 12$, Phys. Rev. Lett. 73 (1994) 3274–3277.

[233] R. Morf, N. d'Ambrumenil, Morf1995, Phys. Rev. Lett. 74 (25) (1995) 5116–5119.

[234] K. Park, J. K. Jain, Activation gaps and mass enhancement of composite fermions, Phys. Rev. Lett. 81 (19) (1998) 4200–4203.

[235] D. Yoshioka, Excitation energies of the fractional quantum hall effect, J. Phys. Soc. Jpn. 55 (3) (1986) 885–896.

[236] R. H. Morf, Comment on ıactivation gaps and mass enhancement of composite fermionsȷ, Phys. Rev. Lett. 83 (7) (1999) 1485.

[237] K. Park, N. Meskini, J. K. Jain, Activation gaps for the fractional quantum hall effect: realistic treatment of transverse thickness, J. Phys.: Condensed Matter 11 (1999) 7283–7299.

[238] K. Park, V. Melik-Alaverdian, N. E. Bonesteel, J. K. Jain, Possibility of p-wave pairing of composite fermions at $\nu = 12$, Phys. Rev. B 58 (1998) R10167–R10170.

[239] J. P. Eisenstein, L. N. Pfeiffer, K. W. West, Compressibility of the two-dimensional electron gas: Measurements of the zero-field exchange energy and fractional quantum hall gap, Phys. Rev. B 50 (1994) 1760–1778.

[240] Y. Zou, R. Barnett, G. Refael, Particle-hole symmetric localization in optical lattices using time modulated random on-site potentials, in preparation.

[241] H. Sambe, Steady states and quasienergies of a quantum-mechanical system in an oscillating field, Phys. Rev. A 7 (6) (1973) 2203–2213.

[242] D. F. Martinez, J. Phys. A: Math. Gen. 36 (2003) 9827.

[243] L. Fallani, C. Fort, M. Inguscio, Bose-einstein condensates in disordered potentials, arXiv:0804.2888.

[244] G. Roati, C. D'Errico, L. Fallani, M. Fattori, C. Fort, M. Zaccanti, G. Modugno, M. Modugno, M. Inguscio, Nature 453 (2008) 895.

[245] J. Billy, V. Josse, Z. Zuo, A. Bernard, B. Hambrecht, P. Lugan, D. Clment, L. Sanchez-Palencia, P. Bouyer, A. Aspect, Nature 453 (2008) 891.

[246] J. Stenger, S. Inouye, A. P. Chikkatur, D. M. Stamper-Kurn, D. E. Pritchard, W. Ketterle, Bragg spectroscopy of a bose-einstein condensate, Phys. Rev. Lett. 82 (23) (1999) 4569–4573.

[247] D. M. Stamper-Kurn, A. P. Chikkatur, A. Görlitz, S. Inouye, S. Gupta, D. E. Pritchard, W. Ketterle, Excitation of phonons in a bose-einstein condensate by light scattering, Phys. Rev. Lett. 83 (15) (1999) 2876–2879.